Measurement, Data Analysis and Prediction of Pyrotechnic Shock

V. H. Neubert

M. J. Evans

L. J. Bement

Final Report

NASA Grant NAG 1-543 #4

January, 1987

TABLE OF CONTENTS

List of Figures

6.47 Theoretical Hopkinson bar force, with pin-puller adaptor and end-caps.

6.48 Theoretical Hopkinson bar force, tapered plate adaptor, 1/2 inch grid, 100 μs impulse.

6.49 Force vs. time, Hopkinson bar with separation joint, tapered plate adaptor.

6.50 Compare acceleration vs. time: experimental and finite element solution at x = L, with endcap.

6.51 Shock spectrum from force, spherical impactor, cap on input end.

6.52 Shock spectrum from force, spherical impactor, separation joint tapered plate adaptor on input end.

6.53 Shock spectrum from force, separation joint test 17.

6.54 Experimental force vs. time, Hopkinson bar, spherical impactor, 15" pull-back, on 3" separation joint adaptor. (Adaptor in inset).

6.55 Experimental force vs. time, Hopkinson bar, 3" long separation joint with 7 grain/foot off-center.

1.0 SUMMARY

The ability to quantify the effects of pyrotechnic shock through measurement and analysis is of considerable importance. Pyrotechnics are used in many devices on spacecraft. The output of the pyrotechnics is severe and it is clear that components mounted near a pyrotechnic may be severely damaged. One example of a failure due to a shock excitation was the loss of two solid rocket boosters because a water impact switch, used to separate the parachutes from the boosters, functioned prematurely from a shock wave from the frustum separation assembly. Thus an ongoing, thorough effort is needed to evaluate a wide range of pyrotechnics and to assure that they will operate properly with no damage to other components.

The present report summarizes the results of careful tests and analysis of the effects of pyrotechnic bolts, nuts, pin-pullers, and separation joints. The material for pin-pullers and separation joints is being presented for the first time. The devices were operated on appropriate Hopkinson bars which are capable of measuring output strains and accelerations. From the strains, the output forces and moments versus time are calculated, which show in a timewise fashion how the loads are developed by the pyrotechnics and also provide inputs for dynamic stress predictions using computer models of various components which may be damaged. Shock spectra are also presented, by which the frequency components of the excitations are quantified. Acceleration response shock spectra up to 40 kHz are generated from both input accelerations and forces.

The analytical basis of the Hopkinson bar is thoroughly reviewed including both the elementary and more advanced Love theories in the theses by Evans [31] and Parker [12]. They include discussion of both the normal mode, or standing wave, method and the travelling wave method of predicting response of the thin bar, with several examples. Since spherical impactors were used to calibrate the Hopkinson bars, the Hertz theory of impact of two elastic spheres is given. Then the strain and acceleration measurement systems are discussed, with their requirements and frequency limitations.

Typical outputs are shown for pyrotechnic bolts and nuts, which had been discussed in detail in previous, referenced reports. New measured force, moment, and acceleration versus time curves are presented for five candidate pin-pullers for the HALOE satellite. The associated acceleration shock spectra from force and acceleration excitations show which pin-puller will produce the least excitation to nearby components. This is compared, for the first time, with similar results obtained from measurements made when the same pin-pullers were activated on the HALOE structure. Similar

data is given from measurements of Spacecraft separation joints using a Hopkinson bar monitoring system.

Finite element models were made of the Hopkinson bar system in order to attempt to predict the effects of endcaps and adaptors used on the bar during the tests. This analysis had four goals:

(1) to predict the effect of the adaptors on the pulse shape,
(2) to attempt to deduce the true output of the pyrotechnic device,
(3) to determine the frequency content by determining the number of modes needed to represent the response, and
(4) to determine the fineness of the finite element mesh needed to predict the response to these inputs.

2.0 INTRODUCTION

2.1 Background

Many mechanical operations on spacecraft are carried out by remote control using pyrotechnics. The pyrotechnic devices include pin-pullers, explosive bolts, and separation joints. The successful operation of each device is critical to the success of the mission. If the joint between a satellite and the launch vehicle did not completely separate during launching of the satellite, severe damage would result and jeopardize both the launch vehicle and the satellite.

The shock waves from pyrotechnics also have the potential to damage electronic or other low-mass equipment or to activate motion-sensitive equipment. For example, a pyrotechnic caused a space shuttle rocket booster failure. The parachute release system for the booster parachute system was prematurely activated by a pyrotechnic shock wave from a non-separation system, rather than on water impact.

Thus, an ongoing, thorough effort is needed to evaluate a wide range of pyrotechnics and to assure that they will operate properly with no damage to other components. Many proof tests are done on the ground to evaluate the effects of pyrotechnics. Usually accelerations are measured. However, the strains should also be measured at various locations on the structure, since strains are more directly related to material behavior and deformations. In addition, for elastic material, strains can be converted to stresses from which dynamic forces and moments can be deduced. For example, force versus time data show directly the sequence of events from a pyrotechnic pin-puller--first there is a resultant compressive force on the support, followed by a severe tensile force or vice-versa. This information can be used by the pin-puller designer to attempt to design low-shock pin-pullers. It can also be used by structural analysts to

predict the effect of the pyrotechnic shock on adjoining structural and electronic components.

In addition to proof tests, it has been found that Hopkinson Bars can be used to measure the force and acceleration outputs of pyrotechnic devices in a certain direction. The pyrotechnic device is mounted on the end of a long, thin steel bar which is designed to remain elastic during the measurement. Strain gauges are mounted near the input end of the bar and accelerometers are attached at the output end.

Careful Hopkinson Bar tests were made at the Pyrotechnics Laboratory of the Pennsylvania State University in 1971 [Ref. 1] for primaline in a simulated separation joint and for explosive bolts. In 1973, a similar facility was constructed at the NASA Langley Pyrotechnics Laboratory for the evaluation of several candidate explosive nuts and then some low-shock pyrotechnic nuts. Recently, the outputs of several pyrotechnic pin-pullers were compared with the output of a mechanical pin-puller at NASA Langley. These pin-pullers were then mounted on a mock-up of the HALOE structure and strains and accelerations compared with those measured on the Hopkinson Bars. The output of a section of spacecraft separation joint was also measured on the Hopkinson Bar.

In order to better understand the experimental results obtained, theoretical finite element models were made and analyzed for the various experimental arrangements on the Hopkinson Bars. The goals of this analysis were: (1) to predict the effect of the adaptors on the pulse shape, (2) to attempt to deduce the true output of the pyrotechnic device, (3) to determine the frequency content by determining the number of modes needed to represent the response, and (4) to determine the fineness of the finite element mesh needed to predict the response to these inputs.

Also, the Hopkinson Bar Theory and exact solution were used to predict results to be compared to the experimental and finite element model results.

The purpose of this paper is to summarize many of the test results and to indicate the state-of-the-art in measurement, data analysis and prediction of pyrotechnic shock on spacecraft.

2.2 Related Work

The term shock is usually applied to a transient, potentially damaging, external force or ground motion. Earthquakes fall into this category and, even though they produce peaks of only one or two g's, have been of concern since the beginning of man's history. It was recognized early that not only the magnitude but the frequency content and duration

of the excitation was important. The important frequency range is usually between 0.1 and 10 Hz.

The content of repeating signals may be identified by expanding the signal in a Fourier Series [2]. For transient signals, the Fourier Transform provides a bridge between the time and frequency domain in the form of the Fourier Spectrum, which is usually presented in terms of amplitude and phase versus frequency. However, it was shown by Biot [3] and White [4] that the shock spectrum could be directly used in the modal analysis of structures under ground motion excitation and that the shock spectrum could be easily measured in the field during earthquakes. The shock spectrum is a plot of the maximum response of a mass-spring-dashpot oscillator versus its natural frequency. The response may be absolute or relative displacement, velocity, or acceleration of the mass. By installing a group of such oscillators, each with a slightly different natural frequency, the shock spectrum can be directly plotted by noting the maximum response which occurred during the event being monitored. Phase information usually was lost during these tests. O'Hara [5] is credited with showing the relationship between the undamped shock spectrum and the Fourier spectrum.

During the 1940's and 50's, the Navy developed design criteria for predicting the response of ship structures to underwater explosions through a comprehensive test and analysis program. At the same time, there were significant advances in the ability to compute the elastic, dynamic response of structures in three dimensions, an early example being that of Neubert and Ezell in 1958 [6]. This capability was complemented by the specification of a design shock spectrum, through Belsheim and O'Hara [7], suitable for three-dimensional analysis of ship structures. It was pointed out that the dips in shock spectra are likely to be caused by feedback between an internal component and the ship's hull, which should be taken into account in specifying spectra based on measured motions. The frequency range involved in this work was usually less than 1000 Hz.

There were also significant related developments by the groups involved in designing hardened missile sites. The ASME proceedings edited by Barton [8] has examples of modal analysis by Young [9] and work by Young, Barton, and Fung [10], who considered applications of shock spectra to nonlinear systems.

For pyrotechnic shock, the frequency range of interest may be zero to 100 kHz and the severity may be as high as 300,000 g's, both of which present difficulties not encountered in the investigations discussed above with regard to measurement and prediction of effects on structures.

Hopkinson pressure bars have been used to measure severe transients for most of this century and some of the history, theory and limitations are discussed in Section 3.1. Neubert [11] used a Hopkinson bar as an impactor against beams having various end conditions, measuring the applied forces with strain gauges attached to the bar. He predicted the response of the beams to this mechanical excitation using Bernoulli-Euler and Timoshenko uniform beam theory as well as lumped-parameter representations. He also presented a comprehensive summary of the literature up to 1958, for both the Hopkinson bar and dynamic response of beams. Parker [12] and Parker and Neubert [13], [14], updated this history and used the Love bar equation and the Timoshenko beam equation to predict response of bars and beams to pyrotechnic excitation.

Recently Smith [15] summarized some of the work being done related to pyrotechnic shock and includes some references. He pointed out the importance of developing high frequency spectra, to 100 kHz, and emphasized the related difficulties in producing dependable acceleration measurements.

Results of a significant, careful effort were reported by Powers [16], who performed a series of design optimization tests on subscale and full-scale vehicle interstage separation systems, finding shock response spectra to 100 kHz, although useful data can only be extracted up to about 80 kHz. He measured strains at locations very close to the high-energy separation joints. Many other investigators have measured response and processed data only up to 10 or 20 kHz, although there is an increasing awareness that such results are insufficient to accurately represent pyrotechnic shock effects on components and structures.

3. INSTRUMENTATION

The purpose of this section is to review pertinent theory and limitations of the instrumentation used. This consisted mainly of Hopkinson pressure bars in various arrangements, along with appropriate strain gauge and accelerometer instrumentation. To calibrate the system, a hardened steel sphere was used on a ballistic pendulum, so the Hertz theory for impact of elastic spheres is briefly outlined herein.

A thorough introduction to the one-dimensional theory of the Hopkinson bar and the approximate two-dimensional theory of Love [17] are summarized in the theses by Evans [31] and Parker [12] and the paper by Parker and Neubert [13].

3.1 Measurement of Forces and Accelerations using the Hopkinson Pressure Bar

The idea of measuring high, transient pressures was presented by Hopkinson [18] in 1914, and consisted of applying the unknown pressure to one end of a long, thin, steel cylindrical bar. The magnitude of the applied pressure was deduced from measurement of momentum of detachable end-pieces at the other end of the bar. In 1946, Davies [19] improved the method by measuring electrically the variation of either the longitudinal displacement at the measuring end of the bar or the radial displacement of the cylindrical surface of the bar. Davies concluded that if the pressure end of a 1/2 inch diameter bar is subjected to a force which changes instantaneously from zero to a finite value, the pressure in the bar requires a finite time of about 2 μ sec to rise to the value.

In the investigations reported herein, strain gauges were used to measure axial strain in the bar and an accelerometer was used at the output end of the bar to measure axial acceleration.

If the diameter d of the bar is much less than the half-wave length λ of the highest frequency component of the excitation, then the bar is called thin and one-dimensional stress wave theory can be used. The border line between thin bars and thick bars occurs approximately at $\lambda/d = 5$ so a small diameter is needed for the bar to be thin. If $\lambda/d < 5$, radial inertia effects can be accounted for using the Love [17] equation, which can be solved easily. The exact differential equations for a thick, cylindrical bar, which were presented by Pochhammer [20] and Chree [21], have not been solved exactly.

If the bar is thin, then plane sections remain plane after deformation and the axial stress is uniform over a cross-section. The material must remain elastic if the simple theory is to apply, so the axial stress σ must be less than the dynamic yield stress of the bar material. Since stress is force F divided by cross-sectional area A, then it is desirable to have the diameter d sufficiently large to keep the stress in the elastic range.

3.2 Hertz Theory of Impact for Two Elastic Spheres

The theory of the elastic impact between two spheres is presented in the book by Timoshenko and Goodier [22]. It is assumed that the spheres have only a translational velocity and the initial velocity vectors lie on the same line, so the impact is central. The distance between the sphere centers during contact is:

$$r_1 + r_2 - \alpha_1 - \alpha_2 = d$$

where r_i is the radius of the ith sphere and α_i is the movement of the center due to the deformation of the surface of the sphere. The relative velocity between the two spheres is defined as

$$v = \dot{\alpha} = \dot{\alpha}_1 + \dot{\alpha}_1 = -\dot{d}$$

or $$v = v_1 + v_2$$

where v_i is the velocity of the ith sphere.

During contact, the contact force P is related to the acceleration of each sphere by

$$m_1 \frac{dv_1}{dt} = -P \qquad m_2 \frac{dv_2}{dt} = -P$$

Here m_i is the mass of the sphere. Using the above relationships to combine these equations, we have

$$\frac{d^2\alpha}{dt^2} = -P \frac{m_1 + m_2}{m_1 m_2}$$

From the Hertz theory for elastic contact, we use

$$P = n \alpha^{1.5}$$

which assumes that there are no elastic vibrations of the sphere during the impact. This is based on the assumption, due to Rayleigh [23], that the time of contact is very long compared to the period of the lowest mode of vibration of spheres. The value of n is determined by the elastic and geometric properties of the spheres.

$$n^2 = \frac{16}{9 \pi^2} \frac{R_1 R_2}{(k_1 + k_2)^2 (R_1 + R_2)}$$

with $$k_i = \frac{1 - \nu_i^2}{\pi E_i}$$

where ν and E are respectively Poisson's ratio and Young's modulus for the material.

Further, defining

$$n_1 = \frac{m_1 + m_2}{m_1 m_2}$$

we can write

$$\frac{d^2\alpha}{dt^2} = -n n_1 \alpha^{1.5}.$$

Integrating the last equation and substituting the initial condition that the relative velocity $v = v_o$ just before impact, we get

$$\dot{\alpha}^2 - v_o^2 = -\frac{4}{5} n n_1 \alpha^{2.5}$$

If we substitute $\dot{\alpha} = 0$ into the equation to find the maximum $\alpha = \alpha_1$ the result is

$$\alpha_1 = \left[\frac{5 v_o^2}{4 n n_1}\right]^{\frac{2}{5}}$$

The maximum force is then

$$P_{max} = n \alpha_1^{1.5}$$

and the duration of impact can be shown to be

$$t = 2.94 \frac{\alpha_1}{v_o}$$

3.3 Strain and acceleration due to impact of sphere on Hopkinson Bar - theory and experiment.

In order to check the instrumentation, a hardened steel sphere was supported on a light wire in a simple pendulum arrangement [Fig. 3.1] and impacted against the end of the Hopkinson bar. The sphere was carefully aligned so that only axial stresses would be excited in the single bar, with no bending.

There is no exact solution for the problem of an elastic sphere impacting a long, thin elastic bar. However, the response may be estimated by using the solution for the impact between two elastic spheres and using an "equivalent sphere" to represent the end of the Hopkinson bar. This is justified to some extent because initially the stress situation is localized at the end of the bar, the stress pulse is short compared to the length of the bar, and it takes some time for the pulse to move down the bar.

First the velocity of the striker sphere is estimated. The sphere is pulled back a horizontal distance b and simultaneously rises a distance h. For the pendulum used for the pin-puller arrangement, the pendulum length ℓ = 60 inches. The sphere diameter was 1.25 inches and the bar was 0.75 inches in diameter. The parameters ℓ, b, and h are related to the pendulum angle θ by

$$b = \ell \sin \theta \qquad \text{and } h = \ell (1 - \cos \theta)$$

Using a pullback b = 15 inches the height h = 1.9052 inches. If all of the potential energy of the sphere, just before release, is converted to kinetic energy just before impact, then the striking velocity v_o is

$$v_o = (2\ g\ h)^{0.5} = 38.4 \text{ in/s}$$

The results of using the Hertz theory for three different, simplified, representations of the bar are given in the first three lines of the table.

R_1(in)	Bar Equiv. R_2(in)	k_1	k_2	n_1	$\alpha_1 \times 10^3$	P_m(lb)	t_1(μs)	σ_m(psi)
0.625	1.125	k	k	1487	1.981	625	152	1416
0.625	Inf	k	0	1322	1.100	1268	84	2875
0.625	Inf	k	k	1322	1.451	961	111	2175
The measured experimental values were						1100	120	2490

In the first row, the bar is represented by an equivalent sphere with radius equal to twice that of the impacting sphere. For the second row, the radius R_2 of the equivalent sphere was made infinite and the Young's modulus E_2 for the bar was made infinite, making $k_2 = 0$ and $n_1 = 1/m_1$. For the third row, R_2 was made infinite, and $k_2 = k_1 = k$. In the fourth row, the experimental values of the maximum force P_m, time of contact t_1, and maximum stress σ_m in the stress pulse in the bar are listed. It is seen that these values are closest to the predicted values in the third row.

3.4 Frequency Range of Interest

The frequency range required for instrumentation to adequately measure and record transients is the same as the range required to accurately predict structural response analytically.

The pulse length on the Hopkinson bar would be $\ell_p = c\ To$, where To is the timewise length of the pulse, in seconds, and c is the velocity of a dilitational wave in the bar. In Table 3.2.1, the timewise, spacewise and spectral properties are compared for half-sine pulses where To = 10μs and 100μs. The 10μs pulse is 2 inches long on the bar; a minimum of 5 intervals would be needed to adequately portray the pulse shape, which would give h = 0.4 inches for the finite element grid spacing. By a separate analytical process, Parker [12],

used a modal summation to predict strain $\varepsilon = \frac{\partial u}{\partial x}$ and acceleration $\ddot{u} = \frac{\partial^2 u}{\partial t^2}$.

He found that, to predict the strain magnitude on a 10μs half-sine pulse, 200 modes were required on the bar with the highest modal natural frequency being 200 KHz. The corresponding half wave length is $\lambda = c/2fn = 0.5$ in. Acceleration is proportional to the derivative of the strain, and 500 modes were required to predict acceleration accurately, the related wave length being 0.2 inches and the highest frequency 500 KHz. For the 100 μs pulse, the wave is ten times as long, and one-tenth as many modes are required.

Table 3.2.1
Wavelength and frequency content of pulses on bar.

Pulse length, time	10μ sec	100μ sec.
Pulse length on bar, inches ℓ_p	2	20
Mesh spacing on bar at $\ell_p/5$	0.4	4
Highest Natural Freq. for ε to (5%)*	200 KHz	20 KHz
(Half wave length)	0.5 in	5 in
Highest Natural Freq. for u*	500 KHz	50 KHz
(Half wave length)	0.2 in	2 in

* From Parker [12]

3.5 Accelerometers and Associated Amplifiers

The accelerometers used for the recent tests at NASA Langley were as follows.

B & K shock accelerometer Type 8309 was used where the frequency content was expected to be highest, with a capacity of 100,000g peak acceleration. It is designed to have a mounted resonance frequency of 180 KHz, which allows half-sine pulses as short as 30 μsec to be accurately measured with amplitude errors due to ringing of less than 10%. "If a type 2626, 2628, or 2635 Conditioning Amplifier is used . . . then shock pulses as short as 6 μs may be measured [24]". The charge sensitivity was 0.044 pC/g.

Six Endevco Model 2225M5 accelerometers were used with an advertised mounted resonant frequency of 80KHz, 0.03 pk pC/g charge sensitivity, and linear up to 100,000g. The manufacturer suggests that half-sine or triangular pulses should exceed 65 μs to avoid high frequency ringing. The frequency response is given as 2 to 15,000 Hz.

The accelerometers were attached using a threaded stud in a hole made by drilling and tapping the structure.

3.6 Strain Gauges and Bridge Amplifiers

The strain gauges during the recent tests at NASA Langley were Vishay with gauge factor of 2.08 on the bars and 2.075 on the HALOE Model. They were 3/16 inches long and their resistance was 350 ohms. Each strain gauge was monitored through a Vishay BAM-1 Bridge Amplifier in a quarter-bridge arrangement. This means there was one active gauge and one dummy gauge. The wiring was a three-lead wire connection. The dummy gauge was wired in series to a long lead, the combination being connected from terminal D of the bridge to one tab of the strain gauge. A separate lead was connected from terminal B to the same strain gauge tab. The third wire was from terminal C to the other strain gauge tab. This is recommended over the two-wire connection, where the dummy gauge is connected directly across terminals B and D, to eliminate drift due to temperature effects in the leads.

The instructions for calibration of strain signals are as follows [25]

Quarter or Half Bridge $$\mu\varepsilon = \frac{400 \times \text{CAL SET}}{GF \times N}$$

Full Bridge $$\mu\varepsilon = \frac{R_g \times \text{CAL SET}}{GF \times N}$$

To read the aggregate strain from all gauges, always use N = 1, no matter how many gauges are used.

To read the average surface strain with several gauges,

N = 1.3 using an axial and transverse gauge in a uniaxial stress field

N = 2 using two gauges both axially aligned with the stress field

N = 2.6 using two axial and two transverse gauges

N = 4 using four axial gauges.

$\mu\varepsilon$ = Simulated (calibration) strain (microinches/inch)

CAL SET = Position of CALIBRATION switch

GF = Exact gauge factor

R_g = Gauge resistance (of arm connected between binding posts A and C)

For the pin-puller tests, the calibration setting was one (1), resulting in a calibration signal of 192.3 microinches/inch. For the separation joint, the calibration setting was five (5) and the signal was 961.5 µin/in.

4.0 PROCESSING PROCEDURES FOR SHOCK DATA

Timewise transient vibration data may be converted to the frequency domain in the form of either a shock spectrum or Fourier spectrum. For several reasons, structural dynamicists prefer to use the shock spectrum.

bar. Then an additional, circular, groove 0.125" deep x 5/8" diameter was made to contain a ring of primaline. So the primaline was sandwiched between the end of the Hopkinson bar and the end of the brass cap, which had a remaining thickness of 0.10" to be torn by the primaline. The primaline was then fed into the groove, the contained length being about (π0.625"-0.125")=1.84", the 0.125" subtracted to account for the diameter of the hole through which the primaline was inserted. Thus the primaline tore a ring of brass, 0.10" thick x 5/8" diameter. It excited primarily axial stress waves in the bar, due to the symmetry of the end cap.

The second configuration tested on the Hopkinson bar was a brass jacket 1" in diameter and 2 1/2" long, as shown in Fig. 5.2, designed to excite primarily bending vibrations in the Hopkinson bar. A lengthwise groove 1/8" diameter was formed in the jacket and the primaline was inserted into this groove. The jacket was slid over the end of the 1" diameter Hopkinson bar so the end of the jacket was flush with the end of the bar. The primaline then acted as a lateral line source of excitation which excited bending stress waves in the bar.

5.1.2 Configuration tested using explosive bolts.

An apparatus to measure the axial and radial output of explosive bolts on the end of the same Hopkinson bar arrangement is shown in Fig. 5.3. Four sizes of bolts were purchased from Holex, Inc., Hollister, California: 3/8", 5/16", 1/4 and size 10. The total charge in each bolt, explosive plus primer, was respectively 450,440, 210 and 60 milligrams. In addition, some half-charge size 10 bolts were purchased. The bolts are designed to fracture circumferentially at a "break line", which was a specified distance from the bolt head, this line being positioned, in the door-opening application, at the surface between the door and the door-frame.

In the test arrangement, the end of the Hopkinson bar simulated the door frame and a special steel chamber, 1" dia. x 23/32" long, simulated the door. The end of the Hopkinson bar was drilled axially and tapped to accomodate the threaded portion of the bolt. A 3/32" thick steel washer was used between the bolt head and the chamber, as shown. The distance 26/32" matched the distance from the bottom of the bolt head to the break line for a 3/8" dia. bolt. A small, internal, circumferential groove was provided at the break line so the bolt would have clearance to expand and fracture.

5.1.3 Data acquisition equipment.

The pick-ups used were Micro-Measurement Corp. foil, resistance-type, 1/8" long, 120 ohm, strain gauges. Each of these was connected to one active arm of an Ellis BAM-1 bridge-amplifier, the second external arm containing a dummy resistance of 120 ohms. Five bridge amplifiers were used, two with DC to 100 KHz frequency range and three with range to only 25KHz. The signals from the bridge-amplifiers were recorded on a Sangamo 3560 tape recorder, which has a frequency range of 0 to 80 KHz, with a rise time of 5 μseconds. Signals were recorded at 120 ips and played back at 3.75 ips, giving a ratio of record speed to playback speed to 32.

The strain gauges were located, in diametrically opposite pairs, at distance of 5", 10", 20", and 50" from the input end of the bar. In addition, for the explosive bolt tests, a strain gauge was mounted circumferentially on the outer surface of the chamber, to monitor the radial output of the explosive bolt.

5.2 Explosive separation nuts, NASA LARC, 1973.

In 1973 there was interest in determining the shock wave effects of pyrotechnic separation nuts, used for remote release applications, such as separating various items from air- or spacecraft or unfastening quick-opening doors. A Hopkinson bar arrangement was built at the Pyrotechnics Laboratory at NASA LARC and V. H. Neubert acted as a consultant during the tests, which were supervised by L. J. Bement. The results were published in reference [26].

5.2.1 Apparatus

The experimental apparatus consisted of the monitoring system and seven separation nuts. There were six flight-type separation nuts and one nonflight type. The nonflight, noncaptive type was historically the first and simplest release concept. The six flight-type nuts were designated standard design 1 and 2 and Low-Shock design 1, 2, 3, and 4. The standard designs had been utilized considerably in aerospace programs. The low-shock designs were specifically designed to produce less mechanical shock upon actuation. Although each nut could contain two cartridges for redundancy, only one cartridge was used for each functioning.

5.2.2 Monitoring system

The main elements of the monitoring system were two 12 foot, one inch diameter Hopkinson steel bars hung in-line, end to end, with an adaptor containing the separation nut connecting the two bars together through

threaded connections. The purpose of the double or split Hopkinson bars was to measure the force and acceleration output at the stud end and housing end separately. The adaptors are described in detail in ref. [26].

The shock waves were monitored by strain gauges and accelerometers at positions indicated in Figure 5.4. The strain gauges were mounted at diametrically opposing positions on the bars and were wired within the Wheatstone Bridge of the amplifier to cancel the signals due to longitudinal bending of the bars. The gauges, Baldwin Model FAB12344S13, and the amplifiers, Ellis Model BAM-1B, have a frequency response flat to at least 100 KHz. The accelerometers, Endevco Model 2225C, have a resonant frequency of 80 KHz and a mounted resonant frequency of approximately 50 KHz, yielding a monitoring capability that is flat to 10 to 16 KHz. The accelerometer amplifers were Endevco Model 2718.

The dynamic pulses were recorded on an FM magnetic tape recorder Minneapolis Honeywell 7600 with a frequency response flat to 40 KHz (capable of measuring rise times to 6 μ sec.) The equivalent paper speed of the permanent records, achieved by reducing playback speeds, was over 2200 in./sec., or 0.48 milliseconds per inch.

5.2.3 Test Procedure

The experimental program was divided into six major divisions: establish monitoring apparatus, function the six flight-type separation nuts, analyze the performance records and compare nut performances, determine the housing performances with only a standard bolt (no stud monitor), determine the effects of bolt torque on shock performance, and consider the possible effects on a typical spacecraft system.

The behavior of the monitoring apparatus was first established by impacting a steel ball supported like a ballistic pendulum, against the bar. This procedure was much the same as that used for the 1985 pin-puller tests, and is discussed in detail in Reference [26].

The six separation nuts were functioned under as nearly identical conditions as possible; each nut was torqued to 11.298 Nm (100 in-lb) on the stud monitoring bar, and the housing flanges (except for Low-Shock 4, because of its design) were bolted to the housing monitoring bar. Several nuts of each type were functioned. An effort was made to associate the mechanisms of the functioning with the force-time history obtained from the stud and housing monitoring bars. The motion of the monitoring bars was observed with a 400-pps framing camera to estimate the impulsive loading on functioning. This motion is related to potential energy gained by the bar by multiplying the displacement height by the weight of the bars. The

potential energy was then used to calculate the initial kinetic energy, assumed to be 1/2 m v^2, where m is the bar mass and v is the initial velocity.

The performance analysis was accomplished by comparing force and acceleration time histories of each nut type on the same time scales. The acceleration time histories were also processed to find the acceleration shock spectra to 40 KHz with a Q of 10, which is equivalent to 5% of critical damping. Only the first 1.34 milliseconds of the record was used, before bar end reflections appeared, and only the initial shock spectrum was calculated.

The stud performance was monitored using only one Hopkinson bar. This was done to simulate the mounting normally used on the separation systems, in which the nut housing is secured to the structure and the stud is allowed to move. Five nuts (all except Standard Design 2) were functioned with a free stud and were monitored only on the housing side. The force-time histories of the housing were compared to the performance utilizing both monitoring bars. Also, the stud ejection velocities produced on actuation of the nuts and were observed with a 44-pps camera. This velocity was related to kinetic energy 1/2 mv^2.

The effect of torque on shock generation was determined by functioning four additional nuts at higher torque levels using both bars. Their force-time histories were compared to those from the corresponding tests at 11.298 Nm (100 in-lb).

The effect on spacecraft was considered based on the force-time histories. Under consideration were relative shock loads, effects of mounting, and relative displacements on actuation.

5.3 Pin-Pullers at NASA LARC, 1985

5.3.1 Apparatus

The experimental apparatus consisted of the monitoring system and six pin-pullers: Viking I (single initiator and opposed dual initiations) or Viking V (dual), Polaris (dual), RCA BI.V (HI Shear dual), and ICI ATLAS pin retractor. A calibrated impact hammer was also used.

5.3.2 Monitoring Systems

The main elements of the monitoring system [Fig. 5.5] were two cold-rolled steel bars 10 feet long and 3/4 in. in diameter. They were oriented at right angles to each other in order to measure the axial and transverse output forces from the pin-pullers, which were mounted on a special, machined adaptor connected to the input ends of the bars. This

adaptor was about 2-3/4" x 3-11/32" x 1-1/4" overall and was drilled and tapped with 0.750" diameter -16 UNF threads.

The output end of each bar was fitted with a machined steel end cap 1-1/4" dia x 1-1/2" long which was centrally drilled and tapped to accommodate the accelerometers. The longitudinal strain gauges were located 17.82 in. from the input ends of the bars, and were numbered 1, 2, 3, 4, on the transverse bar and 5, 6, 7, 8 on the axial bar. The gauges were located successively 90° apart around the circumference of the bar, with gauges 2, 4, 6 and 8 lying in the horizontal plane. Since a longitudinal stress wave travels about 200,000 in/s in the bar, a pulse about 0.001 s long could be observed at the strain gauge location before there was any interference from a reflected wave.

The signals were recorded on an FM tape recorder with frequency range to 80 Khz. The characteristics of the strain gauges accelerometers and amplifiers are given in sections 3.5 and 3.6.

5.3.3 Test Procedure

The apparatus was calibrated using a steel spherical impactor before the pin-pullers were tested. The steps were:

1. The axial bar was tested first by itself, with end caps at each end. The impact end was then impacted with the steel sphere of 1.25 inches diameter on a 60 inch pendulum. Strain gauges 5, 6, 7, and 8 were monitored separately and the B & K accelerometer was located on the output end of the bar. The horizontal pull-back of the sphere was 15 inches.
2. A blasting cap was detonated at the input end of the single bar set-up described in 1.
3. The double Hopkinson bar arrangement was assembled and impacted in the direction of the axis of the axial bar with the steel sphere on the same pendulum. The eight strain gauges were monitored. The B & K accelerometer was on the output end of the axial bar and an Endevco accelerometer on the transverse bar.
4. The pin-pullers were attached to the adaptor and activated.

5.4 Pin-pullers on HALOE Mock-up

5.4.1 Apparatus

The apparatus was a full-scale model of the HALOE structure [Fig. 5.6]. The five pin-puller devices used were: Mechanical Viking I (dual), Viking V (with one & two actuators), RCA BI. V (Hi- Shear) and the ICI ATLAS pin retractor. A calibrated impact hammer was also used.

5.4.2 Monitoring System

There were eight strain gauges on the model. Gauges 1, 2, 3, and 4, were located parallel to the axis of a hollow aluminum cylindrical section between the main frames and the outboard elevation gimbal was 2.875 " long with 3.25" diameter. The gauges were located in order of the numbers around the circumference, as on the Hopkinson bar, so 1 and 3 were diametrically opposite, as were 2 and 4.

Strain gauges 5 and 6 were orthogonal and located on the heavy ring on the outboard gimbal at a point about 3/4 inch from the pin-puller attachment. Gauges 7 and 8 were orthogonal and at a point on the hollow, rectangular cross-section between the two gimbals.

Five accelerometers were monitored. The B & K accelerometer was located on the ring of the outboard gimbal adaptor, close to the pin-puller. The main frame is seen at the top of Fig. 5.6. Accelerometers 3 and 4 were orthogonal and near the tip of the tapered end, on the left. Endevco accelerometers 5 and 6 were orthogonal and located at the upper right-hand corner of the frame. There were no accelerometers numbered 1 and 2. The accelerometers were attached with threaded studs to mounting blocks. The axes of the accelerometers 3, 4, 5 and 6 were parallel to the plane of the main frame. No accelerations were measured perpendicular to the main frame, which would have been the most flexible direction in the low frequency range.

5.4.3 Test Procedure

The pin-pullers were mounted and activated, one-by-one, at the location shown in Fig. 5.6. The instrumentation was the same as that used for the tests described in Section 5.3.

5.5 Spacecraft Separation Joint at NASA LARC, 1985

5.5.1 Apparatus

The apparatus consisted of a 12 inch long section of the separation joint [Fig. 5.7] and a monitoring system, which was made up of an aluminum tapered plate adaptor and a single Hopkinson bar [Fig. 5.8].

5.5.2 Monitoring System

The Hopkinson bar used in the test was the same axial bar used in the pin-puller tests [Sect. 5.3] with the strain gauges 5, 6, 7 and 8 and the B & K accelerometer in the same locations. During the calibrations using the steel sphere on the ballistic pendulum, an Endevco accelerometer was used in place of the B & K accelerometer, for comparison purposes.

The tapered plate was 12 inches wide x 0.29 inches thick at the outboard end, where the separation joint was attached, and 1 in. x 1 in. at the other end, into which the Hopkinson bar was screwed. The plate was screwed tight to the bar and it happened that the plane of the plate was at a 30 degree angle to the horizontal. The steel end cap 1-1/4" dia x 1-1/2" long was on the output end of the bar, for attaching the accelerometer.

5.5.3 Test Procedure

The steps in testing were as follows:

1. The bar itself was first impacted at the input end with the 1-1/4" sphere on a 78" long ballistic pendulum. Since the pendulum length was different from that of the pin-puller tests, the pull-back was increased to 17-1/8", calculated to give the same rise to the sphere as in the pin-puller tests. There was neither an adaptor nor an end cap on the input end of the bar, but the usual end cap for the accelerometer mounting was screwed onto the output end.
2. The tapered plate adaptor was screwed onto the input end of the Hopkinson bar and impacted with the steel sphere. The presence of the adaptor attenuated the signals received by strain gauges and the accelerometer, so tests were done with both 17-1/8" and 30" pull-back of the impacting sphere, the 30" pull-back used to increase the magnitude of the signals.
3. Seven separate tests were done with various charges and notched separation plates, as summarized in Table 6.5.1. The tests were numbered 11 through 17.

5.6 Spacecraft Separation Joint at NASA LARC, 1986

5.6.1 Apparatus

In late 1986, several spacecraft separation joints were tested using the same apparatus as described in section 5.5, except that a smaller aluminum tapered plate adaptor was used between the separation joint and the Hopkinson bar. The adaptor was 0.28 inches thick and only 3 inches wide. At the separation joint end, a three inch long section of separation joint was tested. The overall length of the adaptor was 3.50 inches. A sketch is shown in the inset in Figure 6.55.

5.6.2 Monitoring Systems

The monitoring system was the Hopkinson bar as described in section 5.5.2.

5.6.3 Test Procedure

The steps in testing were as follows

1. The bar with the small 3" wide, tpaered plate adaptor was first impacted with the 1-1/4" diameter steel sphere or a five foot pendulum. A 15" pull-back was used.
2. Three tests were done with separation joints
   a) 7 grains per foot off-center, constant thickness, no separation.
   b) 11 grains per foot on-center, constant thickness, no separation.
   c) 11 grains per foot on-center, varying thickness, separation.

5.7 Analytical Predictions Using Finite Element Models

In order to better understand the experimental results obtained, theoretical finite element models were made and analyzed for the various experimental arrangements on the Hopkinson bars. In this approach, the bar and adaptors, which have distributed mass and stiffness and an infinite number of degrees of freedom, are replaced by a system with lumped mass and stiffness and a finite number of degrees of freedom. A mesh is laid over the system, and response calculated only at the mesh points. In this process, the first problem is to devise a finite element model which will adequately represent the behavior of the system being modelled. Some of the considerations are as follows:

1. The elements interconnecting the mesh points must adequately represent the behavior of the system being modelled. This means that the different types of distortion must be accounted for, such as stretching, twisting, bending, shearing and the Poisson effect. In addition, the resulting acceleration, velocities, or deflections must be accurately predicted.
2. The mesh spacing on the structure must be fine enough to be able to represent the propagation of the highest frequency, shortest, stress wave expected.
3. If a modal solution is used involving a series solution of the sum of modal contributions, then sufficient modes must be used to represent the true solution.

The first consideration is satisfied by the choice of element itself, such as beam element, plane stress or plane strain plate element, plate

bending element, cylindrical shell element, or solid element--to name a few examples.

A standard way to check the size of the mesh is to make the mesh smaller and smaller, keeping everything else constant. If the elements are chosen properly, a finer mesh results in a more accurate solution. A finer mesh also results in a more expensive solution, so the goal is to choose the mesh that is just fine enough to do the job. A second way to determine mesh size is by doing a related problem for shock for which an exact solution is available. Of course, if the exact solution were available for the problem of interest, then the finite element approximation would not be needed.

The third consideration has to do with the frequency domain. By knowing the frequency content of the excitation, usually from a shock or Fourier Spectrum of the excitation, we can anticipate the range of frequencies of the structure that will be responding. The modal solutions converge most rapidly for displacement. Quantities that involve the first derivative of displacement, such as velocity or strain, are more difficult to predict because the modal series converges more slowly. Acceleration, being the second derivative of displacement, is the most expensive to predict by the modal approach because of very slow convergence of the modal series involved. This means that the frequency content of an acceleration pulse extends to a higher range than that of the associated displacement pulse.

The computer program used was SAPIV [27] coded in FORTRAN IV. The program has eight finite elements which may be employed, singly or in combinations. Two elements were used in the present analysis: the three-dimensional beam element and the plane stress/plane strain element. The beam element is one-dimensional, with a nodal point at each end, but at each node, three displacements and three rotations are calculated, accounting for axial dilatation, torsion, lateral shear and bending deflection and rotation. The plane stress element has four nodal points with two translational degrees of freedom at each node. Two nodal points may be given identical locations, thus forming a triangular element. The element is used to represent thin plates, where the loading and deformations are in the plane of the plate. It could, therefore, be used to represent a beam in bending if a gridwork is placed over the depth of the beam as well as the length.

Five configurations were analyzed using finite elements:

1. Hopkinson bar with plain ends and no end adaptors.
2. A bi-metal Hopkinson bar with plain ends and no adaptors.

3. Hopkinson bar with end caps on each end.
4. Hopkinson bar with HALOE pin-puller adaptor on input end and cap on output end.
5. Hopkinson bar with aluminum and steel separation joint adaptors on input end and endcap on output end.

The theoretical bar was 78 inches long and three/fourths inch in diameter. Since SAPIV does not account for rigid-body modes readily, the bar was anchored at the output end, rather than free as in the experiments. This is acceptable if the solution is used only up to the time when reflections from the output end would appear at the monitored point. The monitored point was 14 inches from the input end for theoretical comparisons and 17 inches from the end for comparisons with experimental data. Four force input pulses were used as inputs: one was from experimental measurement of the pulse produced using the steel sphere impactor, the other three were half-sine pulses of 10, 100, and 500 microsecond duration. The 10 μs pulse is in the range of length of the output from the spacecraft separation joint while the 100 μs pulse is about the same length as some of the pin-puller pulses. The first two pulses were used, in part, to compare with the work of Parker related to explosive bolt outputs [12].

5.7.1 Single Hopkinson Bar with No Adaptors or Endcaps

The solution was varied in three ways in order to check convergence of the finite element representation. The four variables were:

1. the duration of the pulse input
2. the element grid size, or the number of elements used to represent the bar.
3. the time increment, Δt.
4. the number of modes used in the solution. The SAPIV program has two options for timewise solutions. One is a direct integration of the n simultaneous degrees of freedom, which is equivalent to using all n modes. The other choice involves modal summation, where a specified number of modes are used. Table 5.7.1 summarizes the variations in the solutions.

Table 5.7.1 Number of Modes used for Bar with No Endcaps

Grid size (inches)	Number of modes used		
	10 μs pulse	100 μs pulse	500 μs pulse
1/8		n	n
1/4	n	n	n
1/2	n,5,10,20	n,5,10	
1	n	n,3,5,10,30	
2	n	n	n

5.7.2 Bi-metal Hopkinson Bar with no Endcaps.

Some of the adaptors used on the steel Hopkinson bars were made of aluminum. Therefore, at the early stages of the analysis, the adequacy of the finite element program to predict the effect of wave propagation through an interface between the two materials was checked. In this case the exact solution for the transmitted and reflected wave is known. The pulse was applied to an aluminum bar 78 inches long, which was solidly connected to a steel bar of the same length. The forces were calculated in the aluminum bar 39 inches from the input end.

Two cases were solved. The force was found for a half-sine force pulse of 10,000 pounds magnitude, 100 μs long, and the grid spacings were 1/2 and 1 inches.

5.7.3 Single Hopkinson Bar with Endcaps.

The check-out of the experimental set-up was made using a steel sphere impactor with endcaps on each end of the Hopkinson bar. The measured force input was used on a theoretical, finite element model in order to predict the effect of the endcaps on the force transmission. In addition, this model was analyzed using a theoretical half-sine 100 μs pulse with 1100 and 1250 pounds magnitude, to compare with the input from the spherical impactor. The experimental force-time curve for the spherical impactor, which was about 130 μs long, was also digitized and the forces predicted in the bar 17 inches from the input end, at the location of the strain gauges on the bar.

5.7.4 Hopkinson Bar with Pin-Puller Adaptor

A Hopkinson bar with a pin-puller adaptor on the struck end and an endcap on the output end was modelled. Experimental results for a similar arrangement were obtained through the use of a spherical impactor. Forces were calculated 14 inches for the struck end and only the one inch grid spacing was used, since the pin-puller pulse is relatively long. The convergence of the solution was determined by varying the length of the input pulse and the number of modes summed, as indicated in Table 5.7.2

Table 5.7.2 Theoretical inputs to bar with pin-puller adaptor

Magnitude (lbs)	Pulse Duration (μs)	Number of Modes
10,000	10	n,30,50
10,000	100	n,20,30,50
1,100	100	n,20,30,50
1,250	100	n
1,065	130 (experimental pulse)	

5.7.5 Hopkinson Bar with Separation Joint Tapered Plate Adaptor

The last configuration modelled theoretically was a Hopkinson bar with a large aluminum tapered plate adaptor on the input end [Fig. 5.8]. Analysis was also completed for a steel adaptor of the same dimensions, because both the adaptor shape and material have an effect on the wave transmission to the bar. In this case, the plane stress elements and beam elements were both used, the former for the tapered plate and the latter for the beam. A problem arises at the interconnection of the plane stress element and the beam element because the plane stress element does not have a rotational degree of freedom at the nodes, only displacement in two directions. Thus, to handle the compatibility condition that the slope of the beam and plate must be the same at the interconnection, the beam was extended into the plate to the next node, so the beam and the plate overlapped at two nodes. The physical properties of both were adjusted locally to account for the actual configuration at the interface. Convergence was verified by varying the grid size and the length of the input pulse, as summarized in Table 5.7.3.

Table 5.7.3 Solutions for Hopkinson Bar with Tapered Plater Adaptor

Adaptor material	Grid size (in)	Input pulse length (μs)
Aluminum	1/2	10,100
	1	10,100,130
	2	10,100,130
Steel	1/2	
	1	10,100
	2	10,100

6.0 RESULTS

6.1 Primaline and Explosive Bolts at PSU, 1971

The first test for which data was recorded was for the 5/8" diameter ring of primaline in a brass end cap n the end of the Hopkinson bar. The record of the force output on the bar 5" from the primaline showed a compressive pulse about 10 μs long followed by a tensile pulse of about the same length and magnitude. The primary frequency associated with such a wave is 50,000 Hz. The stress wave was dispersed, with a resultant change in shape, as it travelled down the bar. The primaline was in contact with the end of the bar and the output force was initially a compression as the pressure built up to tear the 0.10" thickness of brass. The tension pulse which followed was apparently due to the end cap pulling on the end of the bar. Further down the bar, the first pulse was primarily compressive, meaning that the stress wave was still changing shape when it was 5" from the struck end.

In reference [1], strain records are shown from the detonation of a 1/4" explosive bolt on the end of the bar. The strain gauges were on diametrically opposite sides of the bar 20" from the input end. If the strains are in phase, the stress wave is dilatational; if they are the same shape and magnitude but opposite in sign, the stress is due to pure bending. Initially there is a compressive pulse and the strains are in phase. The pulse length is about 20 μs, the peak strain is 1165 μin/in, the peak stress is 34,950 psi, and the peak force is 27,450 pounds.

At the 5" station, stresses as high a 55,000 psi were recorded, but the strain gauges on the mild steel bar showed no permanent set. This is assumed to be due to the increased yield stress of the material associated with the high rate of loading.

These results are summarized from the report to NASA by Neubert and Parker dated Nov. 24, 1971 [1]. The report also includes predictions of

strain and accelerations using the elementary bar theory, which predicts no dispersion, and the more exact Love theory, reproduced in Fig. 6.1 - 6.3. The theoretical force input was a half-sine wave 10 μs long and of 30,000 pounds peak force. The modal series solution for strain at 20" and 50" from the input end of the bar is shown in Fig. 6.1. The solutions are plotted for 50, 100, 200, and 500 terms of the series. It is seen that 100 modes is sufficient to predict the maximum strain with 10% error. The natural frequency of the 200th mode is 200 KHz for the elementary bar theory. The predicted pulse shapes at the two stations are practically identical, as expected for elementary bar theory.

In Fig. 6.2, the convergence of the modal series for acceleration is depicted and it is seen that 500 modes are required, confirming that many more modes are required to predict acceleration than strain. The peak acceleration was predicted as 430,000g at the output end of the bar, which was too high to measure with the accelerometers on hand at the time.

The stress predicted using Love theory is shown in Fig. 6.3 for x = 5", 10", and 50". It is seen that the pulse is primarily compressive at the 5" station, and the magnitude of the compressive stress decreases and the tensile tail develops as the wave travels down the bar. I was also demonstrated that the dispersion of a 25 μs pulse is much less than that of the 10 μs pulse.

Parker [12] and Parker and Neubert [13] also predicted the response of Bernoulli-Euler and Timoshenko beams to the same input pulse.

6.2 Explosive Nuts at NASA LARC, 1973

The results summarized here are from the final contract report by Neubert [28] and the related published paper by Bement and Neubert [26]. The results from the six parts of the experimental program outlined in Section 5.2 are discussed here in the same order.

The monitoring apparatus was checked using the steel sphere impactor. These results are discussed in detail in Section 6.6, since they are similar to those in the pin-puller and separation joint tests. With regard to adaptor effects, no appreciable losses were produced by the straight cylindrical adaptor or the 45° expansion conical adaptor. The noncaptive nut was functioned during this step.

Only a limited comparison of nut performance is made here, but there is considerable detail in the Ref. [26]. The behavior of Standard Design 2 and Low-Shock Design 4 may be compared from Figs. 6.4 and 6.5, which show force-time and acceleration-time records for stud force and housing force, as sensed on the separate Hopkinson bars between which the nut was

connected. For Standard Design 2 the peak compressive force on the stud was 32,600 pounds with a duration of about 100 μs and the maximum acceleration was 43,000g. For Low-Shock Design 4, the housing force was larger than the stud force, the maximum housing force being 910 lb. compression and the maximum acceleration 3,880g.

The frequency content of the acceleration signals was found by plotting the absolute acceleration shock spectra from 4 to 40,000 Hz [Figs. 6.6 and 6.7] for the stud and housing. Note that there is some crossing of the curves so that Low-Shock 1 has the highest spectral values below 1000 Hz and the lowest values above 10,000 Hz. Thus, if we were concerned with low frequency output, we might choose Standard Design 1 or Low-Shock 4. In the high frequency range Low-Shock Designs 1 and 4 appear best.

Examples of force performance using free studs are shown in the paper for Low-Shock Designs 2 and 4, compared to the blocked force obtained using the two-bar monitoring system. The initial tensile loads, produced by pressurization of the nut body and the forces necessary to overcome friction in the retaining cylinder withdrawal were considerably increased for all nuts, with increases of two to six times greater using the free studs compared to the blocked studs. The shape of the curves stayed about the same, even though the maximum value increased. The secondary loads were appreciably increased for Standard Design 1 and Low-Shocks 1 and 4. However, for Low-Shock Designs 2 and 3, the magnitude of the forces during the secondary phase remained about the same, even though the shape of the curves changed somewhat. The velocities at the studs achieved on functioning varied from zero to 2.80 m/sec (9.2 ft/sec) and are given in Table II of Ref. [26].

The effect of torque on force-performance histories is shown presented in Ref. [26]. The performances of the noncaptive nut, Standard Design 1, and Low-Shock Design 1 were essentially the same within normal functional variations, but the loads produced by Low-Shock Design 4 were considerably increased. Since the only force required to achieve separation in Low-Shock Design 4 is that of moving the small-mass retaining cylinders, an increase in friction caused by an increase in torque level would significantly affect the force to initiate and stop this motion.

The shock effects on spacecraft with regard to forces and accelerations produced by the separation nuts can be decreased using the low-shock designs. Some penalties must be considered in the form of increased weight, volume, and complexity of the release mechanism over the existing commonly used pyrotechnic separation nuts. Other practical

suggestions are presented for attaching items with the nuts and for functioning nuts that have two gas-generating cartridges. Also the questions remain as to which parts of the spacecraft are susceptible to pyrotechnic shock and which frequency ranges are the most important.

6.3 Pin-Pullers at NASA LARC, 1985

The results for calibration of the Hopkinson bar monitoring system using the spherical impactor are presented in Section 6.6. The data for the pin-pullers on the orthogonal Hopkinson bar system is given here, while that for the pin-pullers on the HALOE mock-up is presented in Section 6.4.

The purpose of the two orthogonal bars, with the pin-puller fastened to an adaptor at the intersection of the two bars, was to measure axial and transverse force and moment output. The distance from the strain gauges to the output end of each bar was 103 inches, so that the time before a reflection could appear at the strain gauge from the free end was 2 x 103 in/(200,000 in/s) or 1.03 milliseconds. Since the gauges were only 17 inches from the input end, the second reflection, which came from the input end, occurred 0.17 milliseconds later at the strain gauges, or 1.20 milliseconds from time zero. Because the output end acted practically as an ideal free end, the force-time data was extended by subtracting the first reflection of the force pulse by shifting the initial pulse to t = 1.03 ms, changing its sign, and adding to the initial record. Thus for $0 \leq t \leq 1.03$ ms, the force-time plots represent experimental data; for $t \geq 1.03$ ms the force-time data has been modified to attempt to eliminate the first reflection in the range $1.03 \text{ ms} \leq t \leq 1.20$ ms, but it includes reflections for $t \geq 1.20$ ms. Since the accelerometer was at the output end, the initial wave and the first reflection added in the bar to double the acceleration. Thus, the accelerometer records were valid until the second reflection arrived at the output end, or valid for the time it took the stress wave to travel three bar-lengths, or 1.80 milliseconds. Actually, the accelerometer signal was zero until the stress wave travelled one bar-length, or for $0 \leq t \leq 0.60$ ms. No attempt was made to correct the acceleration records for end reflections, except to divide the signal by 2 when the acceleration shock spectra were calculated.

In Fig. 6.8, the axial and transverse force-time plots are shown for the Viking I pin-puller with two initiators fired simultaneously. Here, the compressive force is negative and tensile force is positive. The solid line represents the axial force and the dashed line, the transverse force, which is seen to be relatively small. The axial force shows compression for the first 0.53 ms, with -500 pounds maximum force; this is followed by

a tensile region for 0.41 ms with 1075 maximum force. The tensile region for $t \geq 1.15$ ms is mainly due to reflections.

In Figures 6.9 through 6.12, the axial force-time output of the Viking I (two initiators fired) is compared with that for the Hi-Shear, Mechanical, Viking V, and Viking I (one initiator fired) pin-pullers. It is seen that all the pin-pullers, except the mechanical, show a compressive force region followed by a region of tensile force. For the mechanical, the order is reversed: the first force region is tensile, followed by a compressive region. The approximate maximum force values and durations of the first two regions for each pin-puller are summarized in Table 6.3.1.

Table 6.3.1 Maximum Axial Force and Duration for Pin-Pullers on Bar

Pin-Puller	First Region		Second Region	
	Max. (lb)	Duration (ms)	Max (lb)	Duration (ms)
Mechanical	575	0.36	- 615	0.18
Viking I (One Init)	- 175	0.53	1075	0.57
Viking I (Two Init)	- 500	0.53	1075	0.41
Viking V	- 800	0.42	1350	0.28
Hi-Shear	- 375	0.42	1240	0.20

Based on this summary, it appears that the Mechanical pin-puller generates the least output force, with the Viking I (one initiator) the second least. The area under the force-time curve is equal to the impulse delivered. The area is equal to some factor x maximum force x duration, where the factor depends on the details of the curve shape. From this point of view, the Hi-Shear and Mechanical have the shortest overall duration for the first two regions, as seen in the Table above. Table 6.3.1 gives no information about the frequency content which is discussed below.

Bending moment versus time plots are shown for the Viking I (two init) in Fig. 6.13. Before there are end reflections, the bending moment is due directly to the eccentricity of the applied forces at the end of the bar, so knowing the maximum force and the corresponding moment, we could estimate the eccentricity. Bending pulses disperse rapidly, however, and may attenuate considerably by the time they have travelled 17 inches down the bar. Nevertheless, comparison of the bending moments at that station gives an idea which pin-pullers are most likely to produce bending in an

actual structure. It was found that the largest bending moments were produced by the Viking V pin-puller.

The initial and residual acceleration shock spectra for the axial and transverse force from the Viking I Pin-Puller, are shown in Figures 6.14 and 6.15. Note that the magnitudes of the residual spectra are less than the initial spectra over most of the frequency range. The early troughs in the residual spectra are due to the finite length of the force-time record. The initial spectra for the axial force for the other four pin-pullers are compared with those of the Viking I (two initiators) in Figure 6.16. To aid in the comparison, numerical values from each spectrum are tabulated at 10, 1000, and 30,000 Hz in Table 6.3.2 for both the axial and transverse forces.

Table 6.3.2 Shock Spectra values at selected frequencies for axial and transverse force for the pin-pullers.

Pin-Puller	Shock Spectra Values (g)					
	Axial Force			Transverse Force		
	10 Hz	1000 Hz	30,000 Hz	10 Hz	1000 Hz	30,000 Hz
Mechanical	1.6	2.7	0.3	0.3	0.2	0.2
Viking I (One Init)	2.7	1.8	1.0	0.5	0.6	0.9
Viking I (Two Init)	2.8	5.1	1.1	1.1	1.3	0.9
Viking V	4.4	5.2	1.5	0.8	0.9	1.4
Hi-shear	3.3	5.1	0.9	1.8	4.4	0.6

The table above shows that the mechanical pin-puller spectral values are the lowest and the Viking I (One Init) next lowest. The HI-Shear has much higher transverse values in the low frequency range than the others.

6.4 Pin-Pullers on HALOE Structure

The experimental results from the pin-pullers on the HALOE structure are unique in several respects. First, it is the first time that both strain and acceleration measurements were made on an actual structure and processed up to 50 KHz. Second, it is the first time strain data was processed to deduce forces and moments on a beam-like structure from a pyrotechnic event. Third, it is the first thorough study in which the

pyrotechnics were activated on both the Hopkinson bar arrangement and a space structure, for comparison.

6.4.1 Experimental Stresses Versus Time

Strains were converted to stresses by multiplying the measured strains by Young's modulus for the aluminum material. Since the Viking V pin-puller appeared to generate the largest outputs, examples of the timewise stresses are shown in Fig. 6.17 and 6.18.

The stress from SG1 is compared with that from SG2 in Fig. 6.17.These gauges were on the circumference of the cylindrical section. It is interesting to note that these records have some similarity in shape, especially for the first part of the signal. Except for SG3, they tend to show an initial compressive region followed by a tensile region, much like the same pin-puller on the Hopkinson bar. For this reason, even though the cylindrical section does not qualify to be a long thin beam or bar because of its small length to diameter ratio, the data was also processed in pairs for these gauges to determine forces and moments, which are presented below in section 6.4.2.

Stress comparisons between strain gauges 5, 6, 7, and 8 are especially interesting because gauges 5 and 6 were very close to the pin-puller. The stress computed from SG5 is compared with stress from SG6 in Fig. 6.18. The peak stresses from strain gauges 5 and 6 are in the range of 1350 to 2100 psi while the early peaks from gauges 7 and 8 are 250 to 500 psi. The early peaks on gauges 1 through 4 are in the 250 to 4450 psi range. Recall also that gauges 5 and 6 were on the heavy ring, while the other six were on thin members. Gauges 1 through 4 were outboard from the shock, between the pin-puller and the support frame, while gauges 7 and 8 were between the pyrotechnic and the anchored base. Thus, there appears to be some attenuation of stress with distance from the pin-puller, expecially in the higher frequency stress components.

6.4.2 Experimental Forces and Moments Versus Time and Shock Spectra of Forces.

The forces and moments versus time for the Viking V pin-puller obtained from strain gauges 1 and 3 and 2 and 4 are shown in Fig. 6.19 and 6.20. The forces deduced from the two pairs of gauges are amazingly the same, indicating that the short cylinder appears to be acting like a bar with a plane stress wave. Even more amazing is the similarity of the force-time pulse to that measured on the Hopkinson bar, in both shape and

magnitude (See Fig. 6.11). The moments calculated from the two sets of gauges are also quite similar.

Force versus time data is given in Figures 6.21 - 6.23 for the other three pin-pullers. For each pin-puller, there is an early region, about 100 μs long, in which the shape of the force-time curve is similar to the axial force measured on the Hopkinson bar. That is, there is first a compressive region followed by a tensile region, except for the mechanical, where the tension comes first.

The initial and residual acceleration shock spectra calculated from the force-time histories in Fig. 6.19 for SG1 & 3 and SG 2 & 4 are shown in Figures 6.24 and 6.25. As expected from the similarity of the time-wise signals, the spectra are almose identical from the two pairs of gauges. The sharp notch at about 40 KHz is apparently a breakdown in numerical accuracy due to the time interval used in digitizing the data.

The initial shock spectra for the forces calculated from strain gauges 2 and 4 are presented in Figures 6.26 - 6.28, where the spectrum for the Viking I is compared with that for the Mechanical, Viking V, and Hi-Shear pin-pullers. The levels from the mechanical and Viking I pin-pullers are about the same, over the entire frequency range, while the Viking V and Hi-shear levels are about double those of the Mechanical and Viking I.

6.4.3 Experimental Accelerations Versus Time and Their Shock Spectra

Acceleration-time histories for the Viking V pin-puller as sensed on the B & K accelerometer, mounted very near the pin-puller, and Endevco accelerometer 3, which was further away, may be compared by inspecting Figures 6.29 and 6.30. The richness and severity of the high frequency content of the B & K compared to the others is immediately obvious. The peak acceleration on the B & K is about 1100g while that on the other accelerometers is about 1/5 that level. Comparison of the initial and residual shock spectra calculated from these accelerometer signals is made by comparing Figures 6.31 and 6.32. Below 1000 Hz, the spectrum from the B & K is about twice that from accelerometer 3. However, there is a surprising cross-over at about 1000 Hz, and accelerometer 3 shows levels up to 6 times higher than the B & K between 1000 and 10,000 Hz. Between 10 KHz and 40 KHz accelerometer 3 again drops below the B & K, which rises to a level of about 5000g. Accelerometers 4 through 6 also show the highest g levels in the 1 to 10 KHz range, but not as high as accelerometer 3. Thus, the spectra show that the high frequency accelerations, above 10 KHz, appear to be attenuated with distance by about a factor of six. There is only slight attenuation in the low frequency range, but amplification

occurs with distance in the 1 KHz to 10 KHz range. This is not understood, but may be due to a resonance condition in the support frame. Note that none of these details with regard to frequency content could be appreciated simply by looking at the acceleration-time curves.

The initial shock spectra for the signals from the B & K accelerometer are shown in Figures 6.33 - 6.35, where the spectrum for Viking I (Two Init.) is compared with the spectrum for Viking V, HI-shear, and mechanical pin-pullers. Here there is surprisingly little difference in the spectral levels of the pyrotechnic pin-puller. However, the level for the mechanical pin-puller is about four times that of Viking I below 50 Hz and about one-fourth that of Viking I above 10,000 Hz.

6.5 Spacecraft Separation Joint at NASA LARC, 1985

The results from the calibration tests using the steel sphere impactor are presented in Section 6.7, where they are compared with finite element predictions.

The seven separation joint tests were arbitrarily numbered 11 through 17. A single string of explosive was used in each test, but the charge and position varied as summarized in Table 6.5.1. The charges were either 8.7 or 11 grains per foot and the position was either center of off-center. In addition, the thickness of the material torn in the pre-grooved joint varied, from one end of the joint section to the other end, during the first three tests but was constant for the last four tests. The varying thicknesses had been used previously to determine, on a single test, how thickness of joint material torn was related to charge strength. In the table, "Var." means varying thickness, and "Cnst." means constant thickness material in the separation joint itself.

Table 6.5.1 Separation Joint Tests with Maximum Forces and Accelerations

No.	Plate Thkns	Charge (gr/ft)	Location	Max. Force Tens	Max. Force Comp.	Max. Moment (in lb)		Force Sh Sp at 100 Hz	Acc. Sh Sp at 100 Hz
11	Var.	8.7	Off-ctr	2500	-3500	+225	-175	8.8	---
12	Var.	8.7	Center	4000	-1500	+200	-110	10.2	20
13	Var.	8.7	Off-ctr	1750	-1750	+275	-275	6.5	52
14	Cnst.	8.7	Center	4000	-1000	+300	-275	10.2	30
15	Cnst.	8.7	Center	2150	-1500	+115	-100	5.5	9
16	Cnst.	11.0	Center	3000	-1150	+200	-200	7.5	---
17	Cnst.	11.0	Center	4500	-1250	+325	-350	11.8	---

6.5.1 Force Versus Time and Associated Shock Spectra.

The strain gauges operated satisfactorily throughout the tests, with no indication of any permanent set. The maximum stress at the strain gauge occurred on Test 17 with a peak of 10,200 psi, which is well below the static yield point of the steel bar. The tapered aluminum plate adaptor had a larger cross-sectional area than the steel Hopkinson bar, and showed no visual evidence of permanent deformation.

Initially there was a strong electrical noise signal which appeared with the strain signal. The magnitude and shape were quite similar to that of a dispersing compression pulse, but the time of appearance was much earlier than the fastest stress wave could have arrived at the strain gauge. The fact that it was electrical noise was confirmed by hanging another steel bar, instrumented with strain gauges, near the bar on which the separation joint was mounted. The same type of noise signal apeared on the stress-free bar. The conclusion was that it was electrical noise generated during the detonation of the separation joint. This was then further confirmed by grounding the test bar, which eliminated most of the noise signal.

The force-time curves for Tests 11, 13 and 17 are given in Figures 6.36 - 6.38. The force-time curve for Test 17, which produced the largest forces, is shown in Figure 6.38. There is an initial compressive region having a maximum of -625 pounds and a duration of 130 μs, followed by severe tension having a maximum of 2250 pounds. Since it is thought that the separation joint separates within 10 μs after detonation, it is expected that the duration of the excitation should be of that order-of-magnitude. This is seen in the high frequencies superimposed on the force-time signal. The lengthening of the pulse is apparently due to dispersion and reflection of the stress wave as it travels through the separation joint itself, and then through the tapered plate adaptor, and the adaptor-bar interface.

The force-time curve for test 11, in Figure 6.36, has an initial compressive region, but the tension region which follows is much shorter than that on Test 17.

The force-time curves sometimes showed practically no initial compression, an example of which is given from Test 14 in Figure 6.37. The reasons for the highly varying shapes of force-time outputs from different joints is not completely understood, but the regions are long enough that they are believed to be true happenings. One main difference is thought to be the pre-test tightness of contact between the oval metal tube (which expands, but contains the explosion) and the spacer plates to which the

doublers are riveted. An initially tight contact could readily transmit compression, for example, but a loose fit would not. It is thought that there is a brief initial expansion of the containing tube in all directions, but then the major axis of the oval shortens as the tube expands in the direction of the minor axis. Finally this containment tube has a nearly circular cross-section.

The force shock spectra for Tests 14 and 17 are compared in Figures 6.39.

6.5.2 Acceleration-time and Acceleration Spectra Results.

The acceleration records were obtained with the B & K accelerometer only for tests 12, 13, 14 and 15. For Test 11, the signal was too small because of the gain setting. After Test 17, the accelerometer connection to the bar was noted to be loose and that the looseness also apeared to affect measurements during Test 16.

Acceleration-time records are shown in Figures 6.40 - 6.41 for tests 12 and 14. In Figures 6.42 - 6.43, the acceleration shock spectra from Tests 12 and 13 are compared with the spectrum from Test 14. Below 1000 Hz, Test 13 levels were the most severe, being about six times the level for Test 14. Above 1000 Hz, the spectra show relatively little difference, on the average.

6.6 Spacecraft Separation Joint at NASA LARC, 1986

The force-time output from the steel sphere impactor on the small 3" wide, tapered plate adaptor is shown in Figure 6.54. The peak force was about 580 pounds and the initial tensile pulse duration was 215 μs.

The force-time output from the 3" long section of the separation joint is shown in Figure 6.55. The charge was 7 grains per foot off-center. The maximum tensile force is 3500 pounds and the maximum compressive force was -2700 pounds. This might be compared with the force-time curve in Figure 6.37 for separation joint test 14 in Figure 6.37 which was 8.7 grains per foot, on-center with constant thickness joint. The shape of the curve is similar for the first 400 μs, but the peak forces for test 14 were 4000 and -1000 pounds for a 12 inch long section of separation joint. We expect that, since using the smaller adaptor puts the charge closer to the end of the Hopkinson bar, the pulse measured will be more severe-which is what has been demonstrated.

The maximum forces from the three tests are given in Table 6.5.2

Table 6.5.2 3" Separation Joint Forces

Plate Thickness	Separation	Charge (gr/ft)	Location	Max. Force (lb) Tension	Compression
cnst.	no	7	off-ctr	3500	-2700
cnst.	yes	11	center	3100	-3900
varying	no	11	center	1300	-2000

6.7 Analytical Results for Hopkinson Bar

The results summarized in this section were obtained through execution of the five finite element models outlined in section 5.6.

6.7.1 Single Hopkinson Bar with No Adaptors or Endcaps

Convergence to an adequate finite element model was obtained by four variations:

1. the duration of the pulse input.
2. the element grid size, or the number of elements used to represent the bar.
3. the number of modes used in the solution.
4. the size Δt of the time increment.

Table 5.6.1 summarizes the variations in the solutions used for convergence.

The magnitude of the half-sine pulse input used was 10,000 pounds. By lengthening the duration of the pulse input, the peak force response of an element at 14" from the input end of the bar approached the magnitude of the input pulse. Since the finite element uses thin bar theory, the exact solution indicated that force in the first stress wave should be exactly the same as the input force. The peak values obtained for a 1/4" element grid size, for 10 μsec, 100 μsec, and 500 μsec input pulses were 5551, 8844, 9762 pounds respectively.

The element grid sizes used were 1/20, 1/8, 1/4, 1/2, 1 and 2 inches. Figure 6.44 shows the force versus time output for spacings of 1, 1/4, and 1/20 inches, for a 10 μsecond pulse input. Figure 6.45 shows a similar comparison for a 100 μsecond pulse input for 2, 1, and 0.50 inch grids. Both plots display the fact that as the element spacing is reduced, the solution becomes closer to the input function. There is also an oscillating force "tail", after the first force peak, that eventually dies out. Reducing the element grid size causes this oscillation to diminish. A point is reached where reducing the grid size further affects the solution only minimally. Figure 6.44 shows that for a 100 μsecond pulse,

reducing the grid spacing from 1" to 1/2" yields nearly the same result. A 1/4" and 1/8" grid was also solved and the gain in force magnitude between a 1" and a 1/8" element size was only 99 pounds while the cost of executing the program tripled. Then, economically, the 1 inch grid size represents an adequate finite element model of the solution for the force response to a 100 μsecond pulse.

The modal solution used involves a series solution of the sum of modal contributions. The number of modes needed to sufficiently represent the true solution was found for a 1" grid, 100 μsecond pulse. Figure 6.46 shows that the magnitude of the peak force response increases with increasing number of modes used. Direct integration of the n simultaneous differential equations with n degrees of freedom, which is equivalent to using all n modes, was also carried out and compared to a modal solution where 30 modes were used. With a 1 inch grid, the direct integration uses 77 modes, yet using only 30 modes yields little difference in peak force magnitude. Only the time for the element to experience the force differed slightly.

6.7.2 Bi-Metal Hopkinson Bar with no Endcaps

The effect of wave propagation through an interface between two materials was studied since some of the adaptors used on the steel Hopkinson bars were constructed of aluminum. The results are presented in the thesis by Evans [31]. In one situation, an aluminum bar was solidly connected in series to a steel bar. In this situation, if an initial wave travels from the aluminum bar through the interface, part of the wave is reflected and part is transmitted through to the steel bar. It was found that force in the transmitted wave was about 1.40 times that in the initial wave, while the acceleration was about 0.55 that of the initial wave.

6.7.3 Single Hopkinson Bar with Endcaps

The experimental set-up used in the steel sphere impactor tests had endcaps on both ends of the Hopkinson bar. Various theoretical pulse magnitudes were used as input to the finite element model, but the closest to the experimental was the impulse with 1100 pound maximum force. The response calculated from the finite element model for a bar with endcaps is shown compared to that with a pin-puller adaptor on the input end (Fig. 6.47). It is evident that using a pin-puller adaptor decreases the maximum force transmitted to the bar and lengthens the pulse, so that the area under the force-time curve remains approximately the same.

6.7.4 Hopkinson Bar with Pin-Puller Adaptor

A Hopkinson bar with a pin-puller adaptor on the input end and an endcap on the output end was modelled using finite elements. The convergence of the solution was determined by varying the length of the input pulse and the number of modes summed, as tabulated in Table 5.6.2. The results are presented in the thesis by Evans [30].

6.7.5 Hopkinson Bar with Separation Joint Tapered Plate Adaptor

The last configuration modelled theoretically was a Hopkinson bar with a large, tapered plate adaptor, both aluminum and steel, on the input end. Table 5.6.3 summarizes the variations used to obtain convergence.

As the grid size decreased from 2" to 1/2", very little variation in the peak force magnitude was found. Only the reflected waves, or the force "tail", varied. The best solution for a 10,000 pound pulse of 100 μsecond duration, for a 1/2 inch grid, with an aluminum tapered plate adaptor is shown in Figure 6.48. It is seen that the magnitude of the force response, due to the effect of the large, tapered plate, is much less than the 10,000 pound input pulse.

The experimental forces obtained using the spherical impactor with and without the separation joint tapered plate adaptor are shown in figure 6.49. The dash line is the theoretical force for the bar with the adaptor from the finite element solution.

To check the finite element analysis within itself, a double length bar was analyzed as shown in the inset in Fig. 6.50. The coordinate x was measured from the center of the bar, where the force F(t) was applied. The bar was clamped at $x = -L$ and had an endcap at $x = +L$. The force F(t) was taken as that of the spherical impactor but with twice the magnitude, the reason being that the pulse immediately splits into two, with half going to the right as compression and half to the left as tension. Thus, before any reflections arrive from the clamped end, the loading situation at the free end should be the same as in the experiment. With this finite element model, the effect of the endcap on the acceleration at the free end was predicted in reference [31]. This predicted acceleration is compared to the measured acceleration in Figure 6.50.

The measured peak acceleration is 30 per cent higher than that predicted from the finite element solution using the measured force as input. Possible reasons for the difference are: (a) the endcap did not behave as a solid, elastic cylinder as modelled in the finite element solution, (b) the finite element mesh was not fine enough.

In order to see the effect of pulse length on magnitude on the force spectrum, three spectra are compared in Figures 6.51, 52, and 53. In Fig. 6.51, the acceleration response spectrum for the force in the bar with no adaptor using the spherical impactor with 17-1/8 inch pullback is shown. In Figure 6.52, the spectrum for the same situation but with the large separation joint tapered plate adaptor installed is shown. The magnitude is reduced by a factor of about 0.4 in the range below 1000 Hz but there is an increase due to the adaptor at 30 kHz. The spectra for the force input in separation joint Test 17 is shown in Figure 6.53. There is a factor of eleven increase in magnitude in the low frequency range and a factor of 20 increase at 30 kHz. Thus, as expected, the high frequency content of the separation joint excitation is much greater than that of the spherical impactor.

7.0 Summary and Conclusions

Detailed results are presented in Section 6, for the various tests and analyses. Some of the more significant results and accomplishments are as follows:

1. Output forces, as well as accelerations, versus time were measured on Hopkinson bars for explosive bolts, explosive nuts, pin-pullers and separation joints. This represents a wide range of excitations, with regard to magnitude and length of pulse. Considering the frequency limitations of the Hopkinson bar, the strain gauges, the amplifiers, and the recording system it is felt that these results are reliable. The shortest pulse measured was about 12 μs long, from the explosive bolt. The fracture of the separation joint appears to happen in less than 10 μs, but the force signal received from the adaptor was much longer, because of the filtering effect of the adaptor.

2. The shock spectra were processed to 40 kHz. The levels of the acceleration shock spectra were highest in the 10 kHz to 40 kHz range. There is of course the question as to whether these high frequency signals can damage spacecraft components. In steel or aluminum, a frequency of 40 kHz corresponds to a half-wave length of 5 inches, so it would seem that items of that order of magnitude of dimension would be especially vulnerable to damage.

3. Force shock spectra were computed, apparently for the first time for pyrotechnic shock, where the input to the mass-spring-dashpot system was force per unit mass.

4. Unique Hopkinson bar arrangements were used. In addition to the usual single bar, a split bar was used for the explosive nut tests. Two orthogonal bar were used successfully for the first time to measure the output forces, moments, and accelerations of the pin-pullers.

5. Force-time and acceleration-time outputs and their associated shock spectra were compared for four different pin-pullers. Overall, the mechanical pin-puller produced the least severe output. These results have not been previously available anywhere.

6. The same types of pin-pullers that were tested on the Hopkinson bars were also tested on an actual structure. The timewise force outputs compared favorably with those measured on the Hopkinson bar, giving credance to the use of the bar to compare devices. A Hopkinson bar set-up is much less expensive than a spacecraft mock-up.

7. The attenuation of acceleration with distance from the pyrotechnic as measured on the HALOE structure is especially interesting. Usually one expects the acceleration signal to be attenuated with distance, which appeared to be the case in the higher frequency range. However, in the lower frequency range there was actually amplification, the acceleration on the HALOE support frame being higher than immediately adjacent to the pyrotechnic.

8. Force-time and acceleration time outputs from seven different variations of separation joints.

9. The behavior of the thin Hopkinson bar was represented analytically using finite elements. The fineness of the element gridwork and the number of modes needed to trace pulses of four different lengths was determined, the lengths being 500, 120, 100, and 10 μs. The prediction of the acceleration response to the shortest pulse, 10 μs, requires a mesh spacing of 0.025 inches, which is one-tenth that required for the 100 μs pulse.

REFERENCES

1. Neubert, V. H. and Parker, R. P., "High Frequency Shock of Spacecraft Systems," Final Report, NASA Contract NGR 39-009-146, Nov. 24, 1971. (See also Reference 13).

2. Fourier, Analytical Theory of Heat, 1822.

3. Biot, Maurice A., "Transient Oscillations of Elastic Systems," Thesis No. 259, Aeronautics Department, California Institute of Technology, 1912.

4. White, Merit P., "Formulation of Shock Problems," in Neubert, V. H. (Ed.), Shock Analysis of Lumped Parameter Systems, Proceedings for Short Course, The Pennsylvania State University, 1964.

5. O'Hara, G. J., "A Numerical Procedure for Shock and Fourier Analysis", NRL Report 5772, June 5, 1962.

6. Neubert, V. H. and Ezell, W., "Dynamic Behavior of a Foundation-Like Structure," in Plunkett, R. (Ed.) Mechanical Impedance Methods for Mechanical Vibration," ASME Colloquium, New York, NY, 1958, pp. 77-86.

7. Belsheim, R. O. and O'Hara, G. J., "Shock Design of Shipboard Equipment-Dynamic Analysis Method," NRL Report 5548. Also NAVSHIPS 250-423-30, 1960.

8. Barton, M. V. (Editor), Colloquium on Shock and Structural Responses, ASME, New York, NY, 1960.

9. Young, Dana, "Response of Structural Systems to Ground Shock," in M. V. Barton (Ed.), "Shock and Structural Response," ASME, New York, NY, 1960.

10. Young, Dana, Barton, M. V., and Fung, Y. C, "Shock Spectra for Nonlinear Spring-Mass Systems and Their Applications to Design," AIAA Journal, Vol. 1, No. 7, July 1963, pp. 1597-1602.

11. Neubert, Vernon H., Response of a Beam to Transverse Impact, Doctoral Dissertation, Yale University, 1957.

12. Parker, Robert Paul, "High Frequency Response of Bars and Beams," Doctoral Dissertation, The Pennsylvania State University, 1973.

13. Neubert, V. H. and Parker, R. P., "Timewise Output of Pyrotechnic Bolts," Proc. of the 44th Shock and Vibration Symposium, Shock and Vibration Information Center, Washington, DC 20375.

14. Parker, R. P. and Neubert, V. H., "High Frequency Response of Beams," Journal of Applied Mechanics, Vol. 42, pp. 805-808, December 1975.

15. Smith, James Lee, "Effects of Variables Upon Pyrotechnically Induced Shock Response Spectra," NASA Technical Paper 2603, Marshall Space Flight Center, May 1986.

16. Powers, D. R., "Strain Histories Associated with Stage Separation Systems Using Linear Shaped Charge," The Shock and Vibration Bulletin No. 53, Part I, pp. 89-96, May 1983.

17. Love, A. E. H., The Mathematical Theory of Elasticity, Cambridge, 1927.

18. Hopkinson, B., Philosophical Transactions of the Royal Society of London, Series A, Vol. 213, 1914, p. 437.

19. Davies, R. M., "A Critical Study of the Hopkinson Pressure Bar," Phil. Trans. Royal Society, Series A, Vol. 240, 1948.

20. Pochhammer, L. "Uber Fortplanzungsgeschwindigkeiten Kleiner Schwingungen in einem unbegrenzten isotropan Kreiszylinder," J. f. reine u. angew. Math. (Crelle), Vol. 81, 1876.

21. Chree, G., "The Equations of an Isotropic Elastic Solid in Polar and Cylindrical Coordinates, Their Solution and Application," Trans. Camb. Phil. Soc., Vol. 14, 1889.

22. Timoshenko, S. and Goodier, J. H. Theory of Elasticity, McGraw-Hill, New York, 1951, pp. 383-384.

23. Lord Rayleigh, Philosophical Magazine, Series 6, Vol. 11, p. 283, 1906.

24. B & K Instruction Manuals for the Shock Accelerometer Type 8309 and Amplifier 2635.

25. Vishay Instruction Manual for BAM-1 Bridge Amplifier.

26. Bement, Laurence J. and Neubert, V. H. "Performance of Low-Shock Pyrotechnic Separation Nuts," 8th Aerospace and Mechanisms Conference, NASA Langley, Oct. 18, 1973.

27. Bathe, K., Wilson, E. L., and Peterson, F. E. SAP IV, Report No. EERC 73-11, University of California, Berkeley, California. June 1973, Revised April 1974.

28. Neubert, Vernon H., "Measurement and Analysis of Force-time Outputs of Pyrotechnic Nuts," Final Report, NASA Contract No. NAS 1-12045, November, 1973.

29. Neubert, V. H., Evans, Maria J. and Bement, L. J., "Measurements, Data Analysis, and Prediction of Pyrotechnic Shock," Final Report, NASA Grant NAG 1-543 #4, August, 1986.

30. Evans, Maria J., Neubert, V. H., and Bement, L. J., "Measurement, Data Analysis, and Prediction of Pyrotechnic Shock from Pin-Pullers and Separation Joints," DOD 57th Shock & Vibration Symposium, New Orleans, Oct. 1986.

31. Evans, Maria J., "Analysis and Prediction of Pyrotechnic Shock Using a Hopkinson Bar," M.S. Thesis, The Pennsylvania State University, in Process.

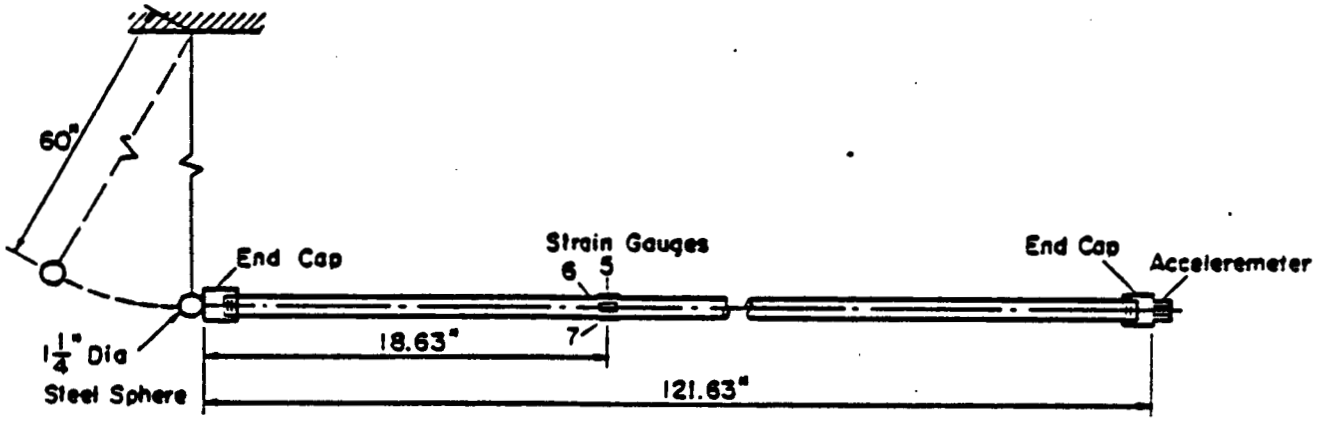

Elevation

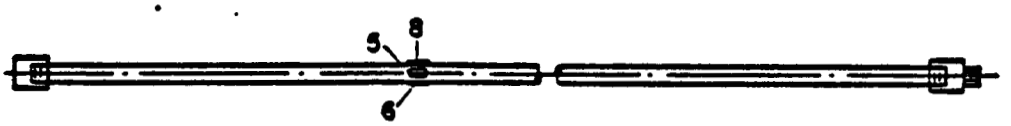

Plan View

Figure 3.1 Single Hopkinson bar with ballistic pendulum.

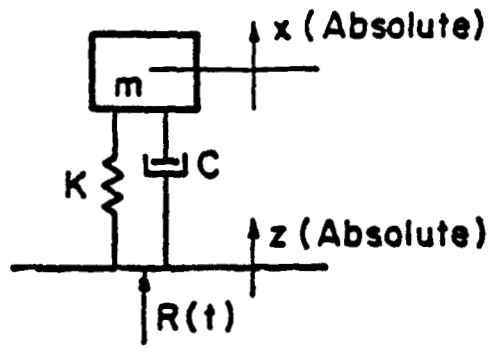

Figure 4.1 Base-driven mass-spring-dashpot filter.

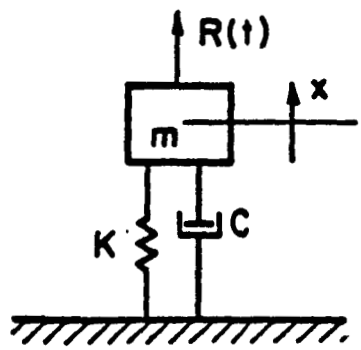

Figure 4.2 Force-driven mass-spring-dashpot filter.

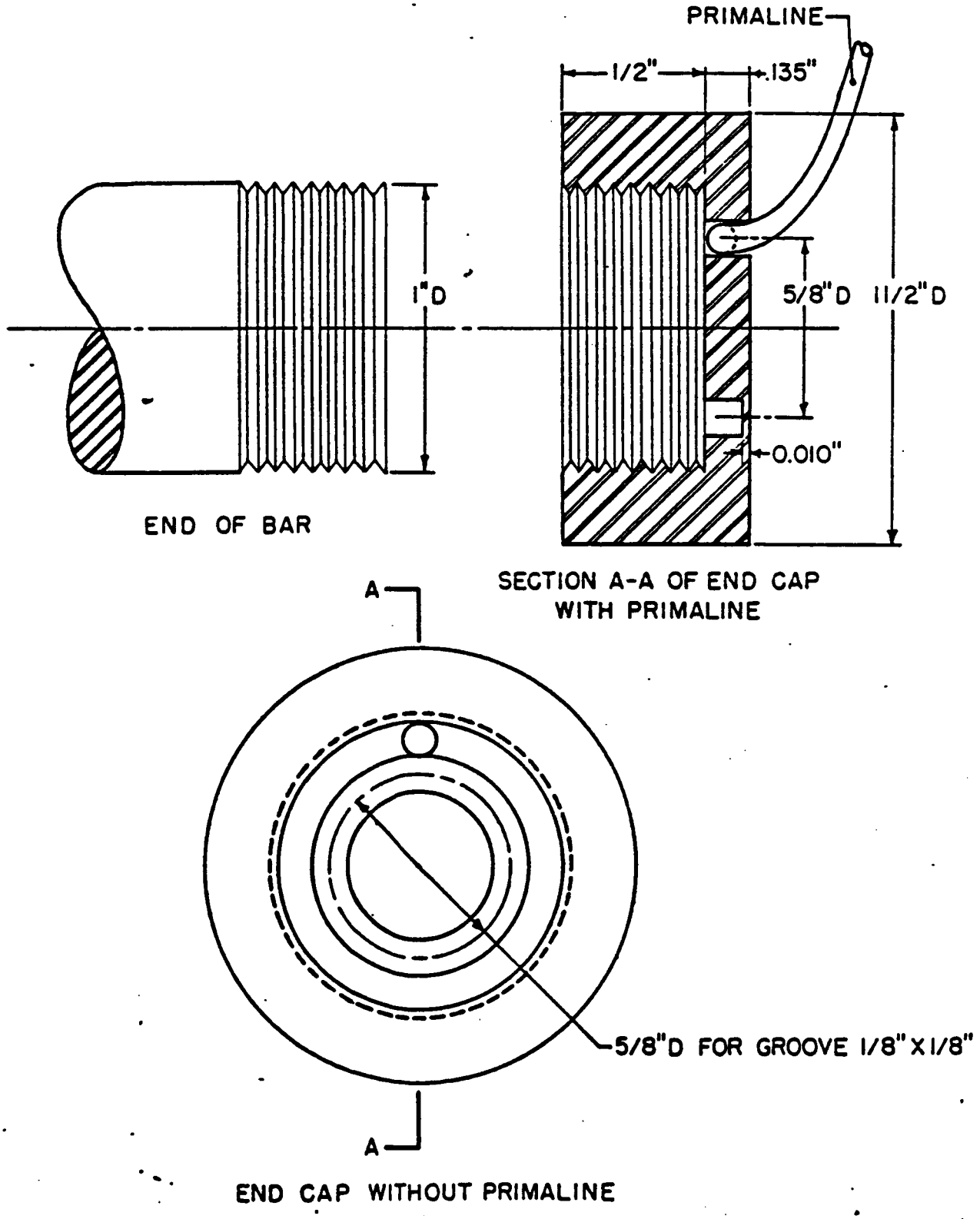

Figure 5.1 Brass cap on end of Hopkinson bar.

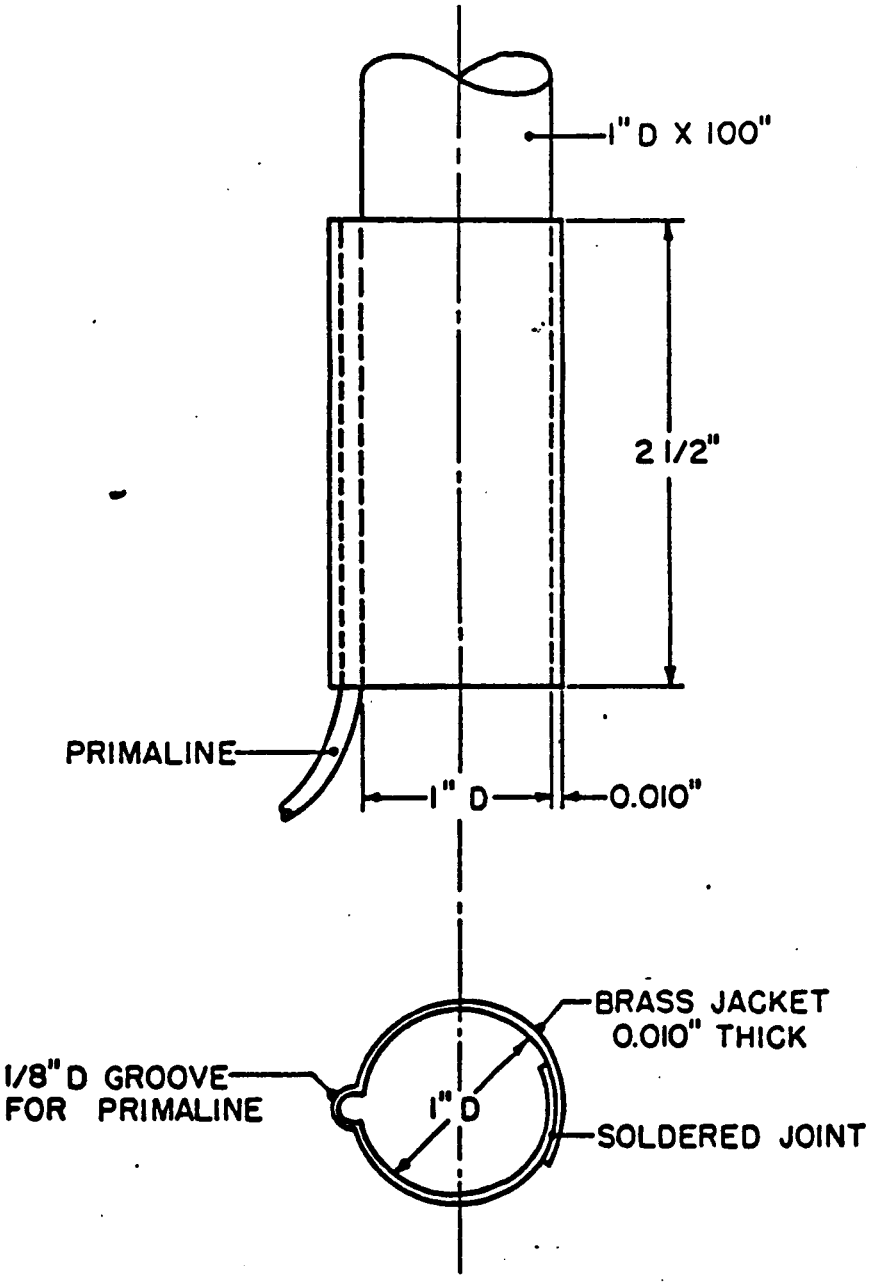

Figure 5.2 Brass jacket on side of Hopkinson bar.

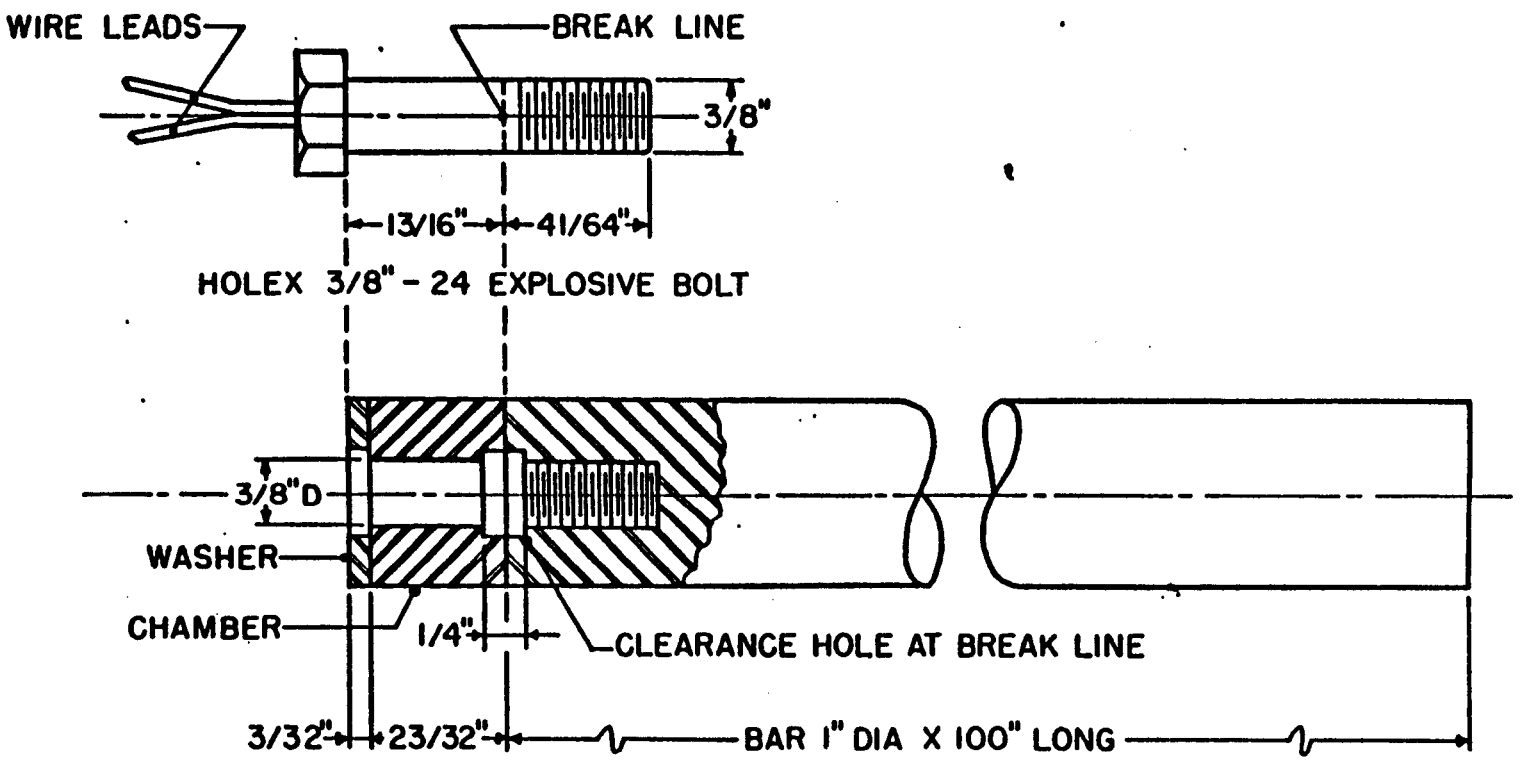

Figure 5.3 Explosive bolt in chamber on end of Hopkinson bar.

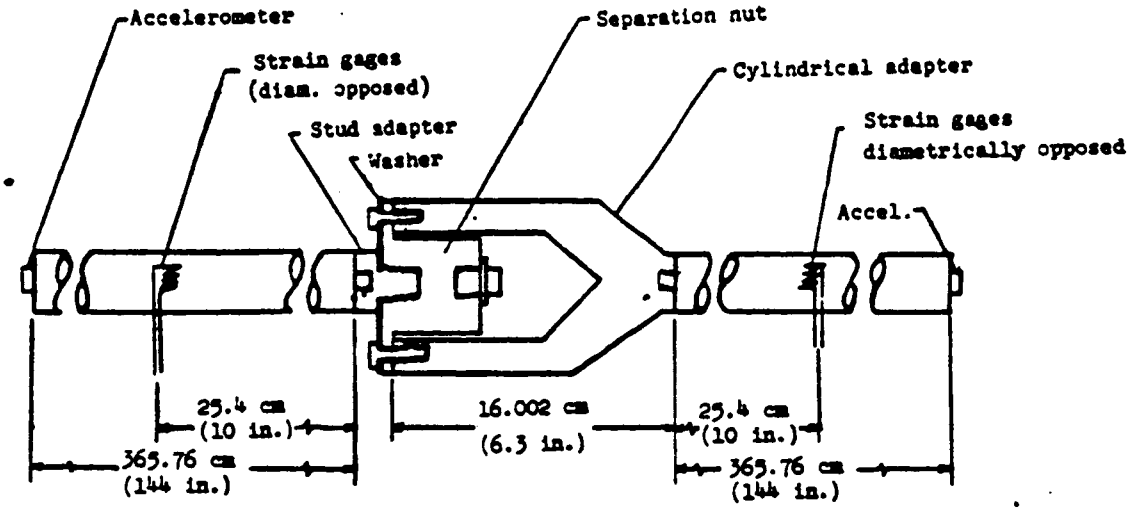

Cross section of shock monitoring apparatus.

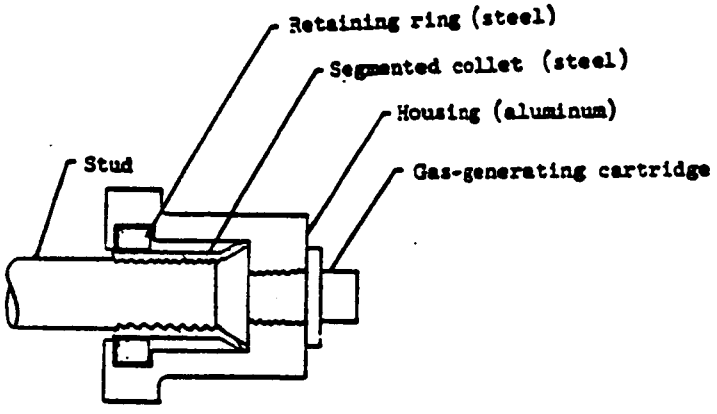

Cross section of noncaptive separation nut.

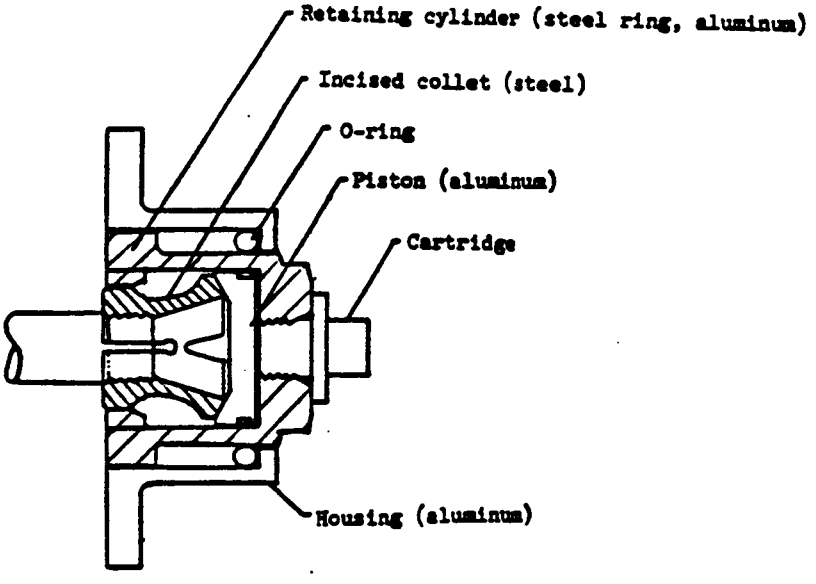

Cross section of Standard Design 1.

Figure 5.4 Monitoring system for explosive nuts at NASA LARC, 1973.

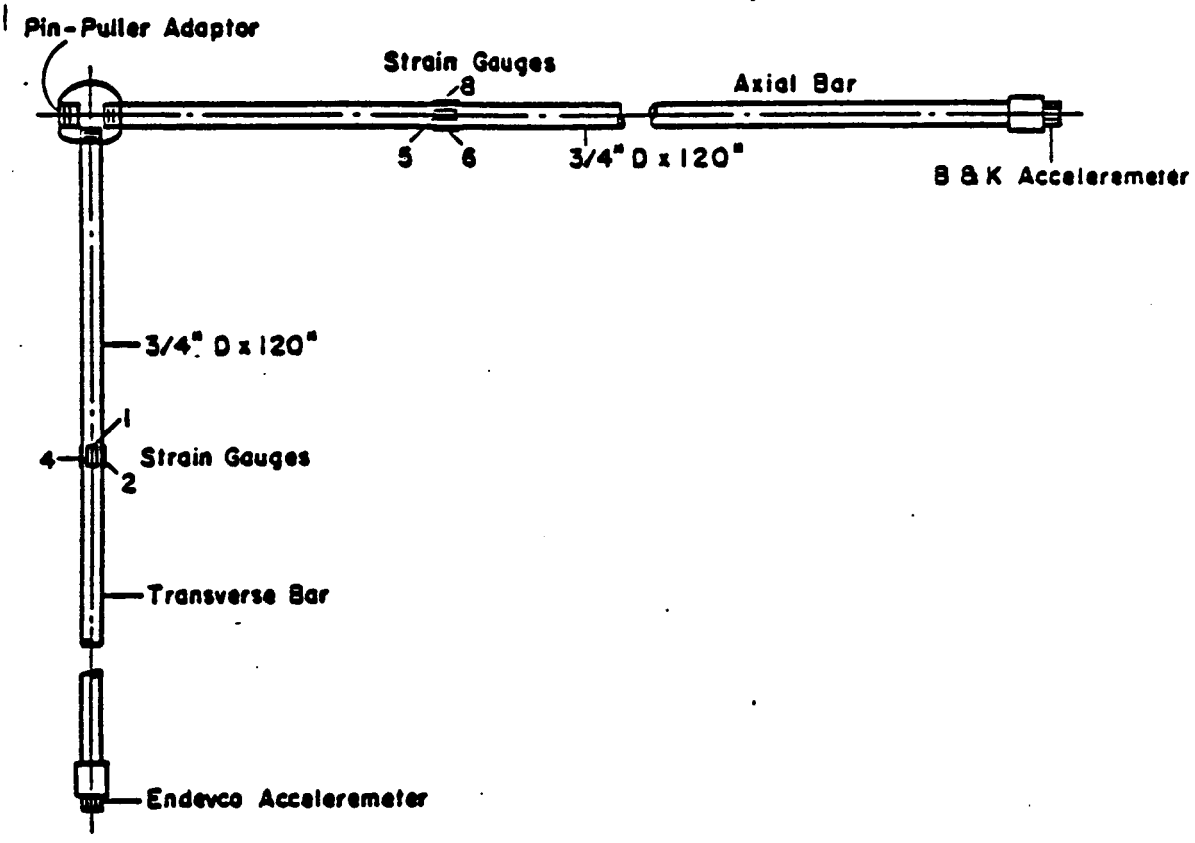

Figure 5.5 Plan View of Orthogonal Hopkinson bars for pin-puller tests.

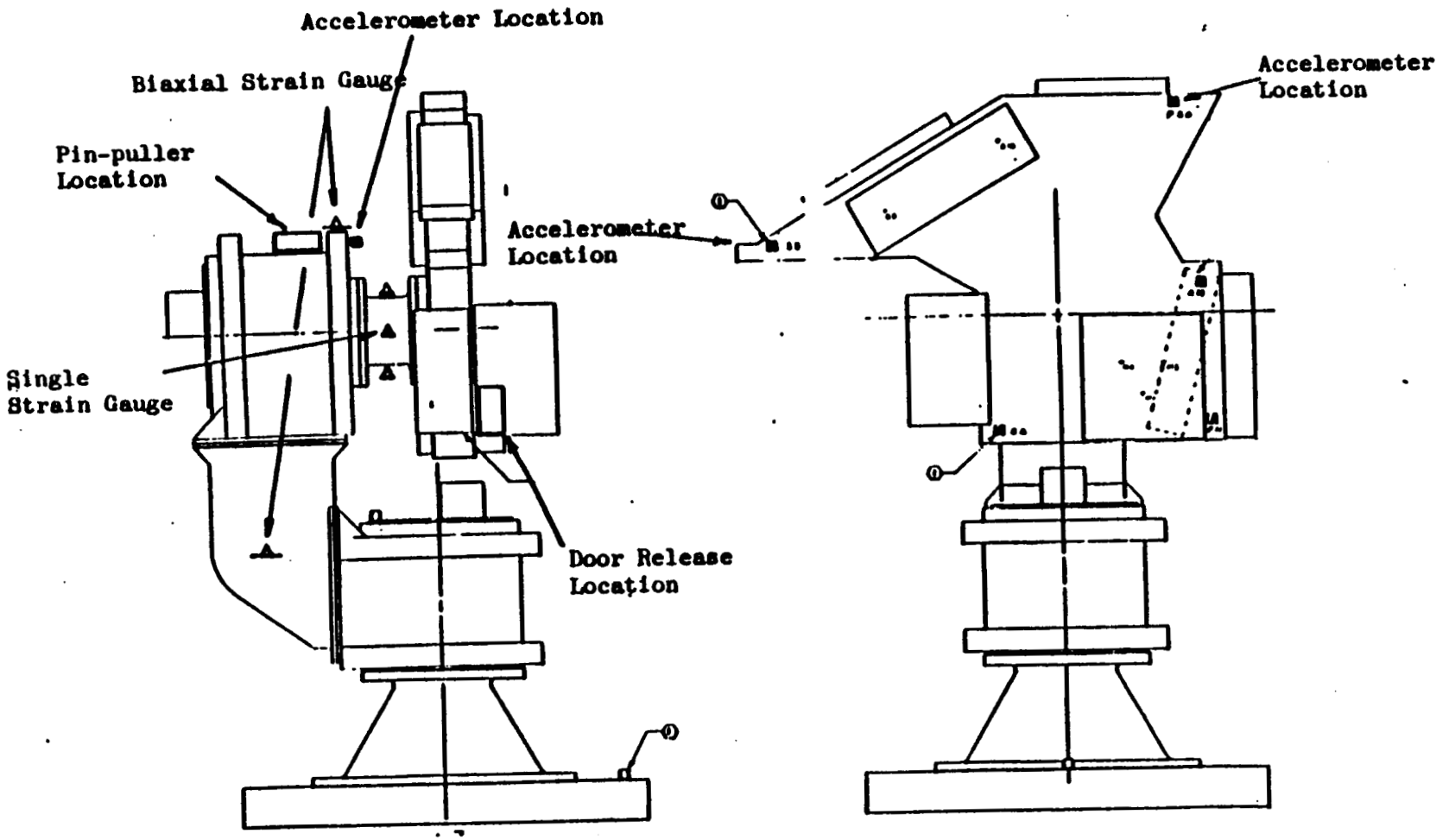

Figure 5.6 Location of strain gauges and accelerometers on HALOE structure.

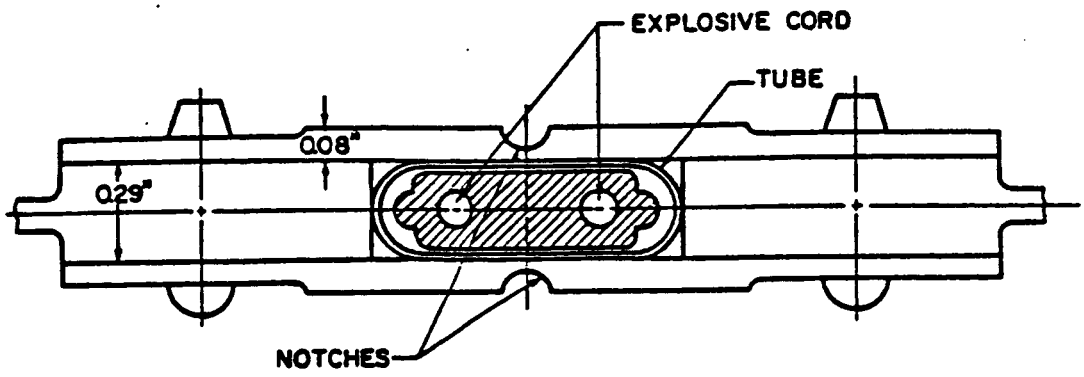

Figure 5.7 Cross-section of spacecraft separation joint.

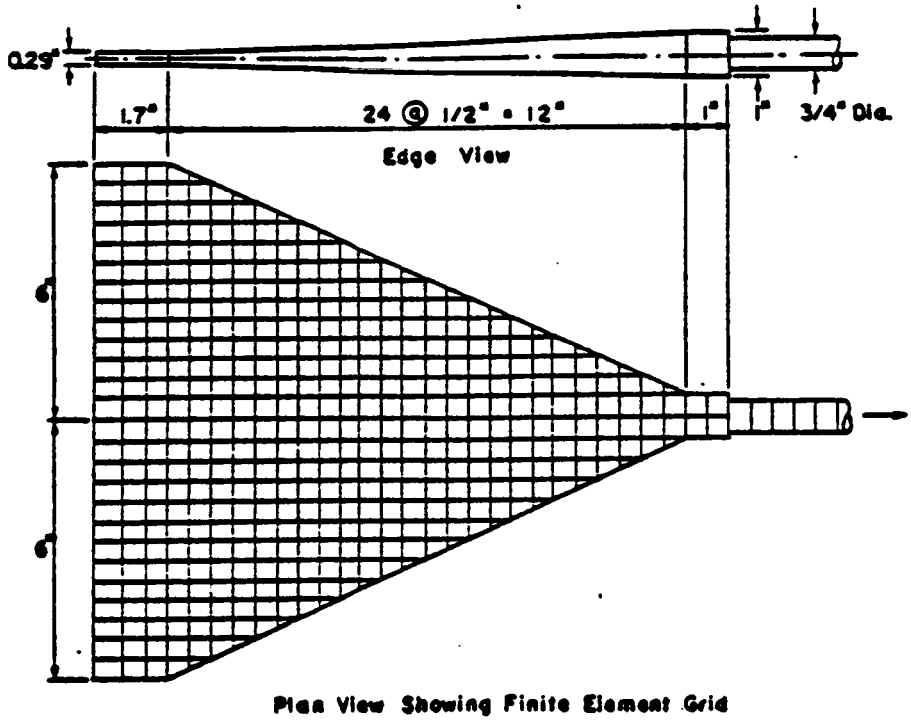

Figure 5.8 Separation joint tapered plate adaptor with 1/2" finite element mesh.

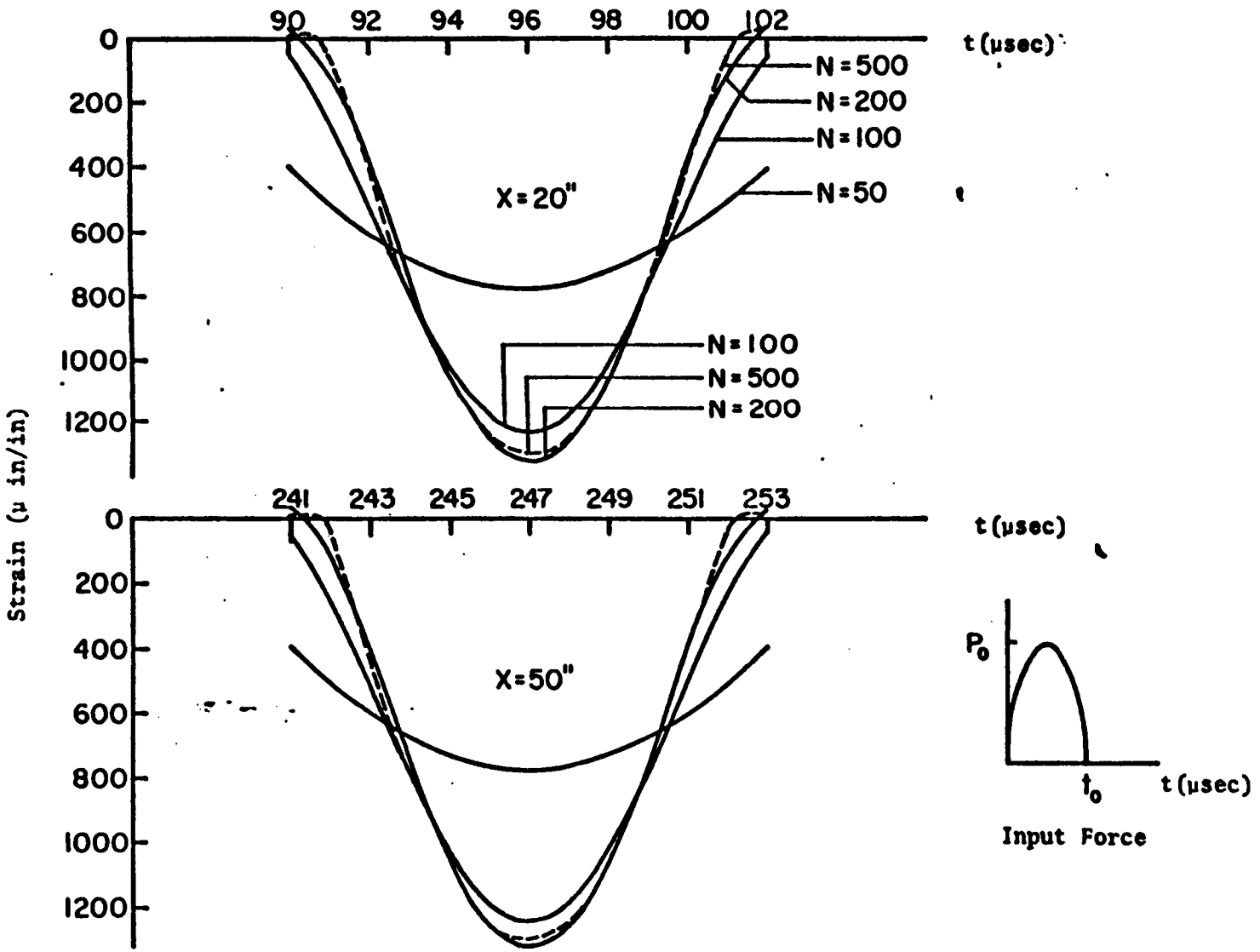

Figure 6.1 Strain versus Time, Elementary Bar Analysis, t_o = 10 μsec, P_o = 30,000 lb.

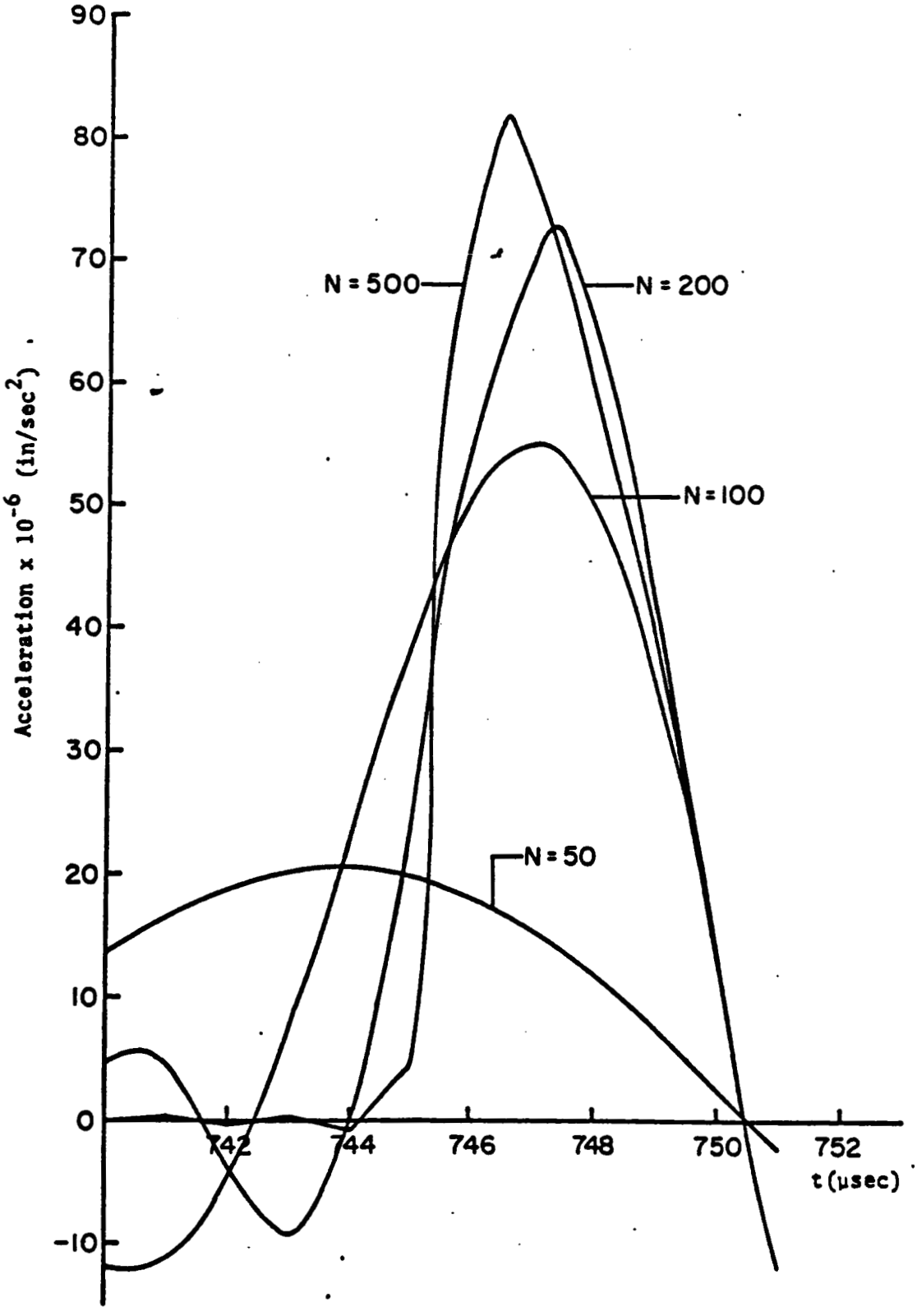

Figure 6.2 Acceleration Versus Time, x = 50", Elementary Bar Analysis, t_o = 10 μsec, P_o = 30,000 lb.

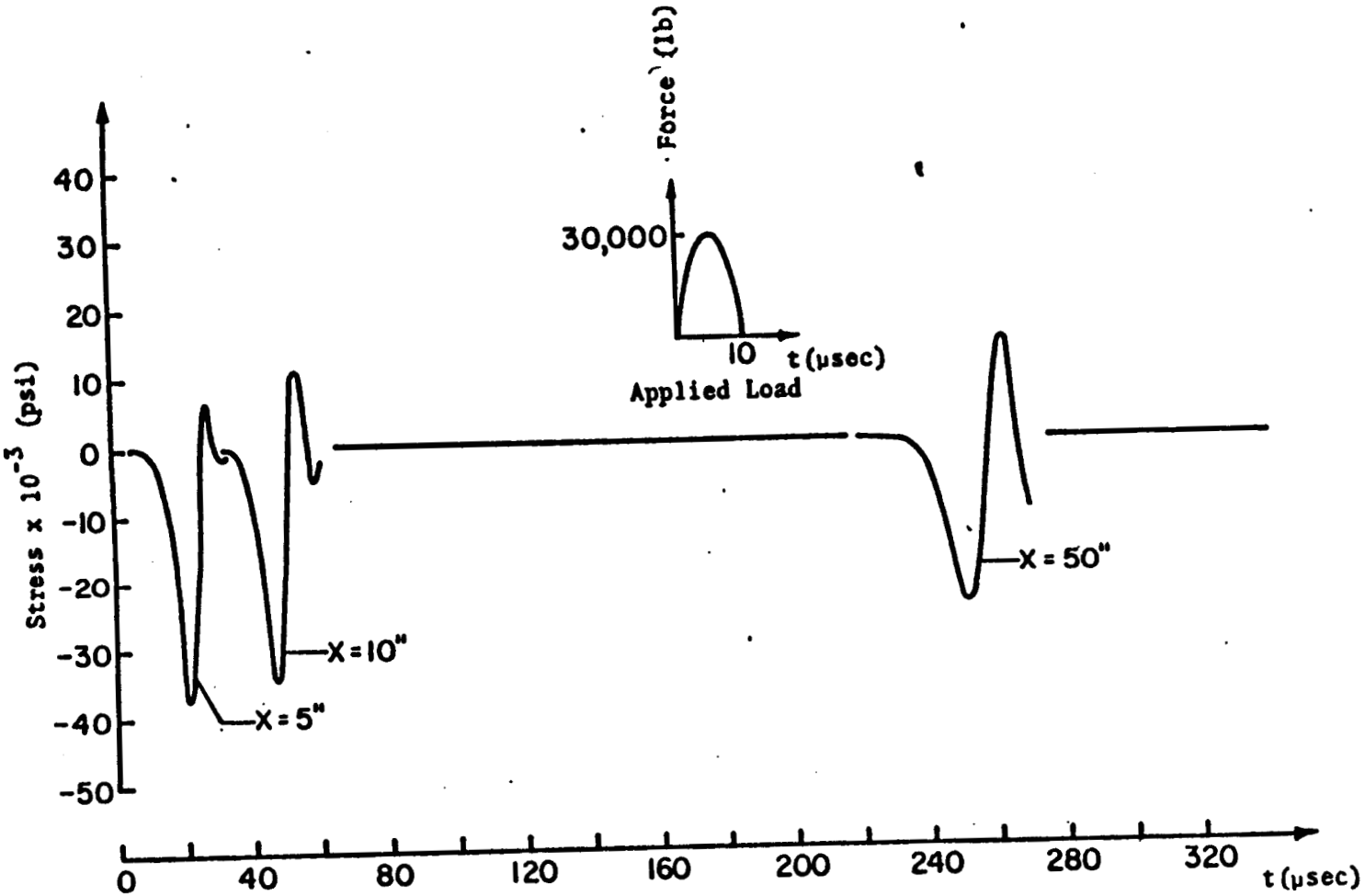

Figure 6.3 Stress Versus Time, Love Theory, t_o = 10 μsec, P_o = 30,000 lb.

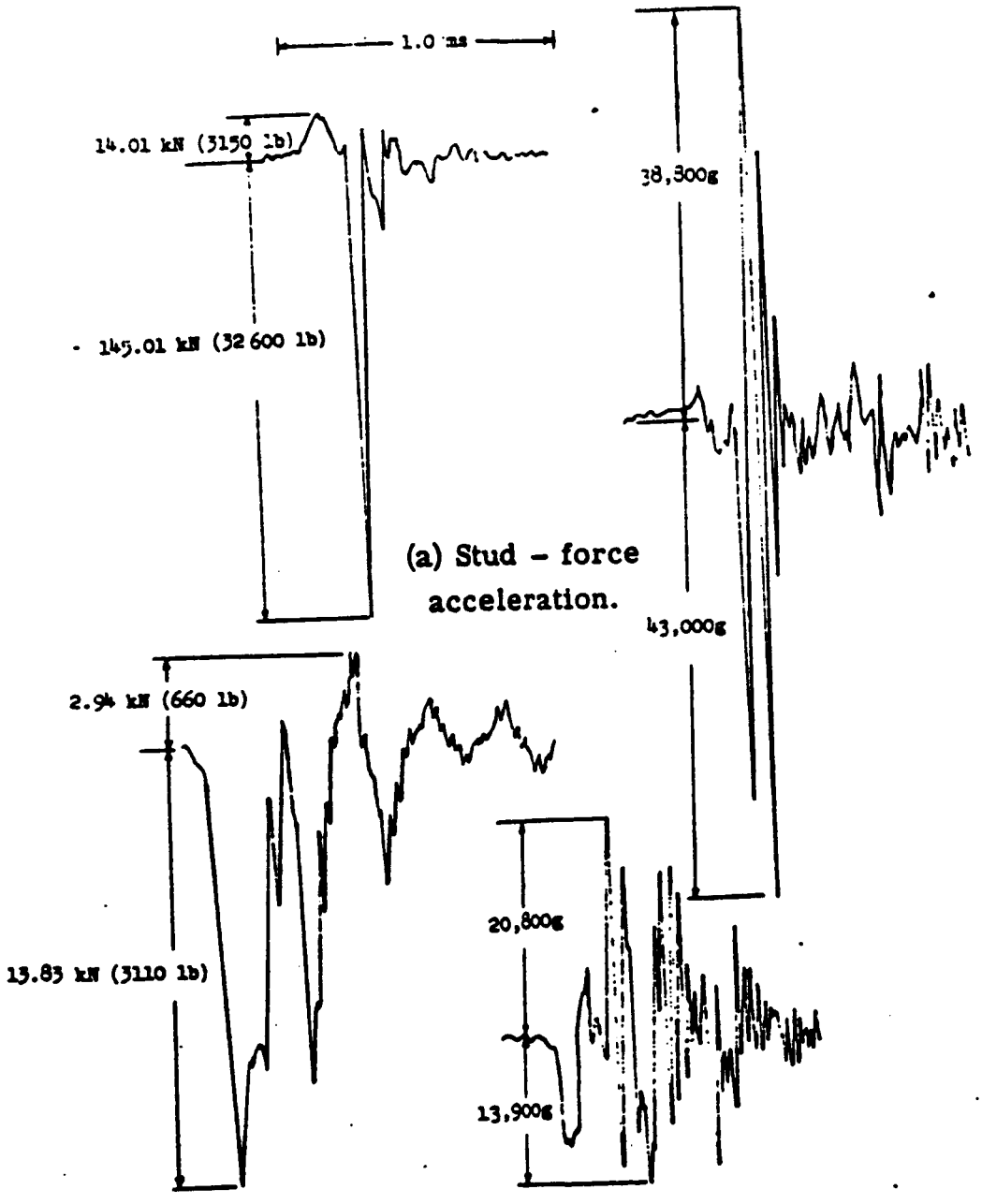

(a) Stud – force acceleration.

(b) Housing – force, acceleration.

Figure 6.4 Force and acceleration performance of Standard Design 2, explosive nut.

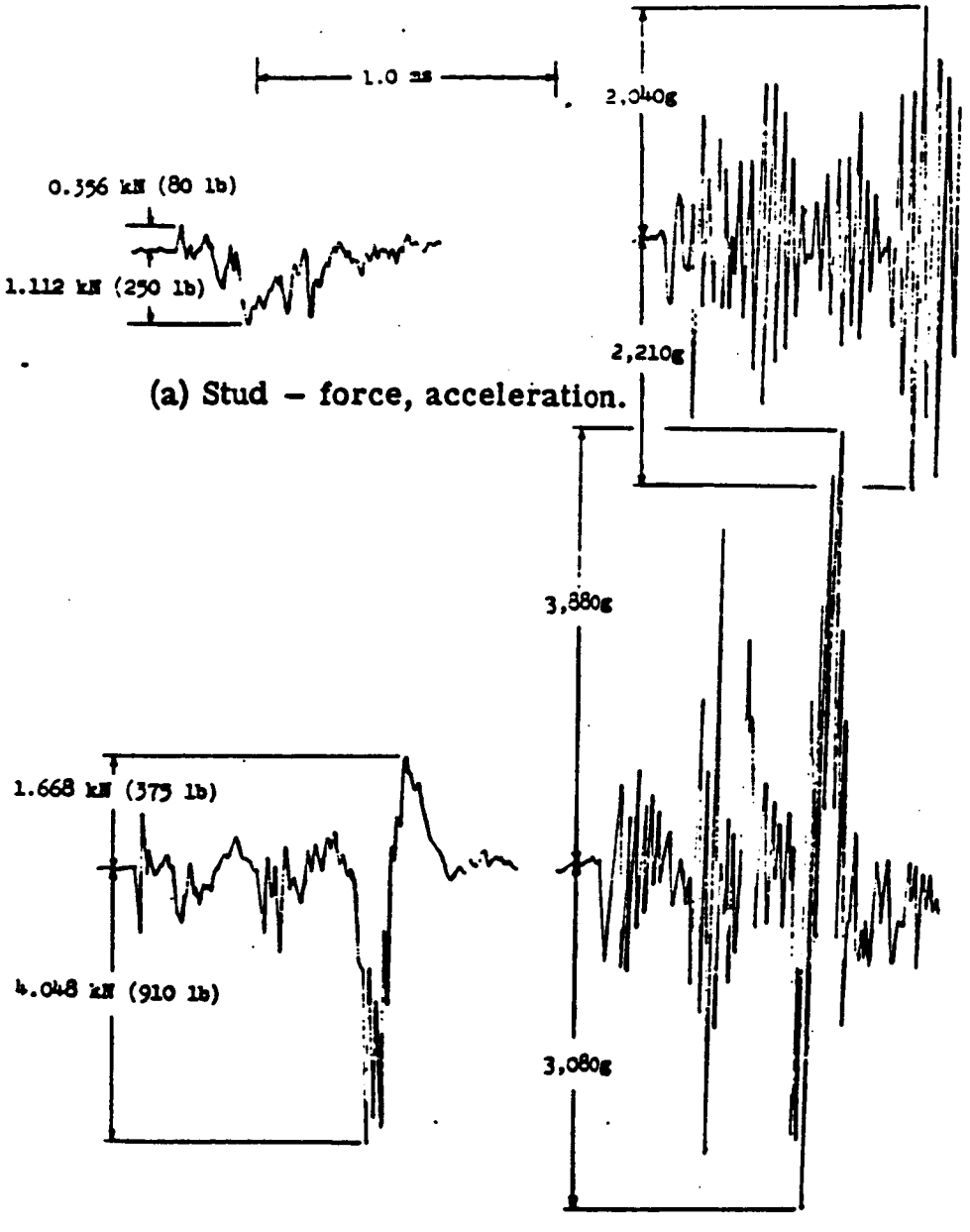

(a) Stud – force, acceleration.

(b) Housing – force, acceleration.

Figure 6.5 Force and acceleration performance of Low-Shock Design 4.

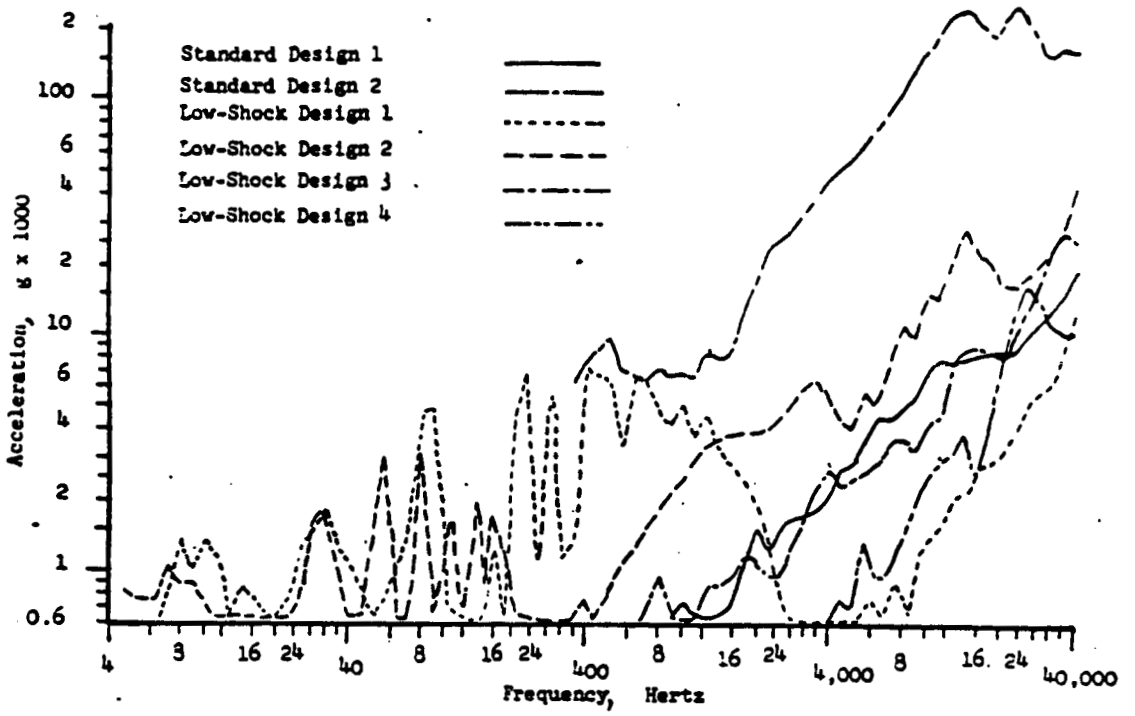

Figure 6.6 Stud performance spectra comparison.

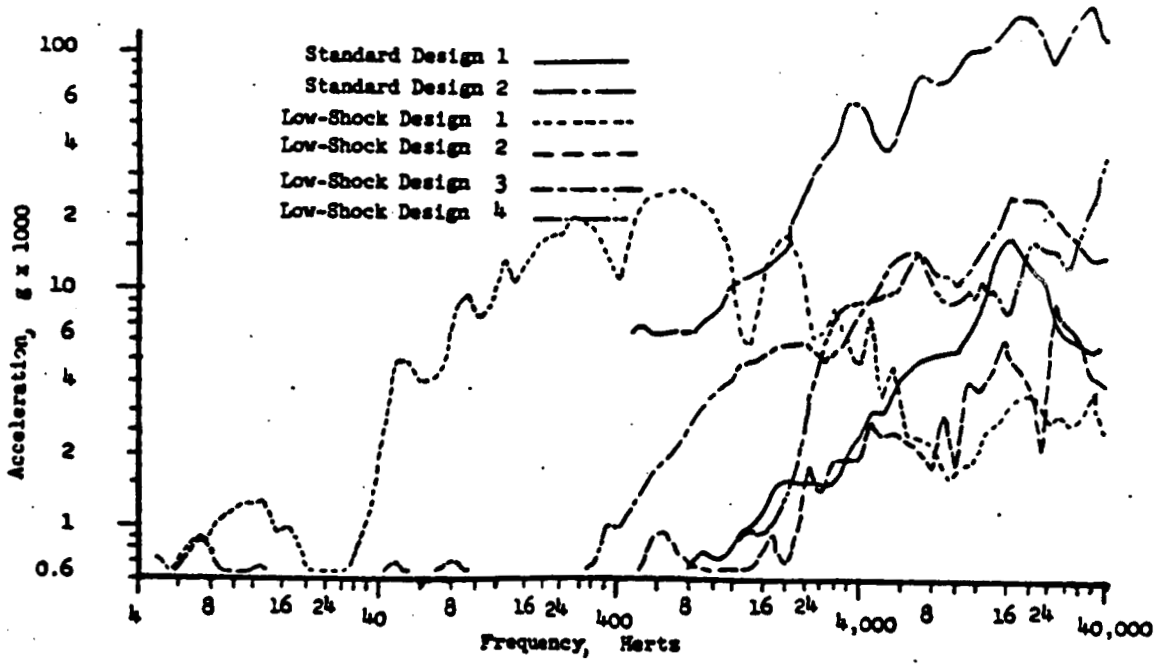

Figure 6.7 Housing performance spectra.

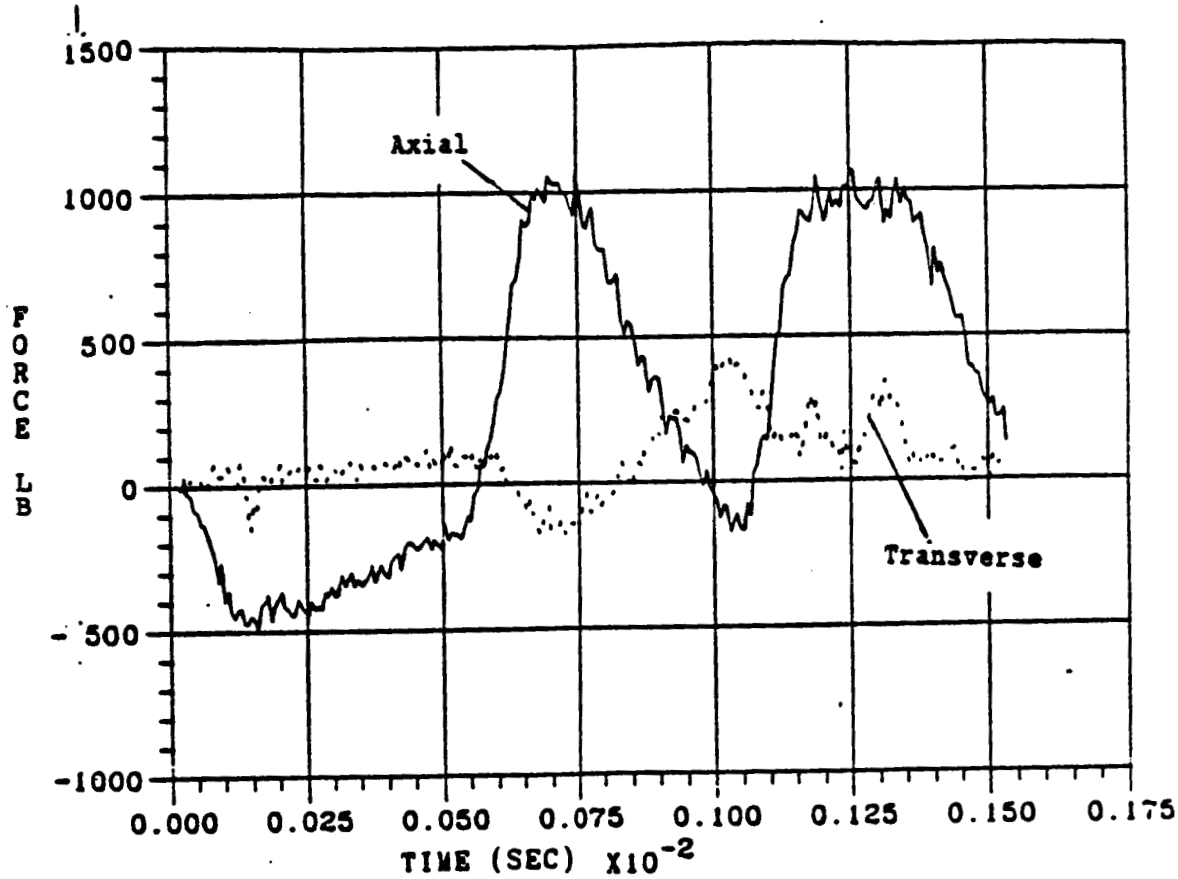

Figure 6.8 Axial and transverse force, Viking I pin-puller (Two Init.)

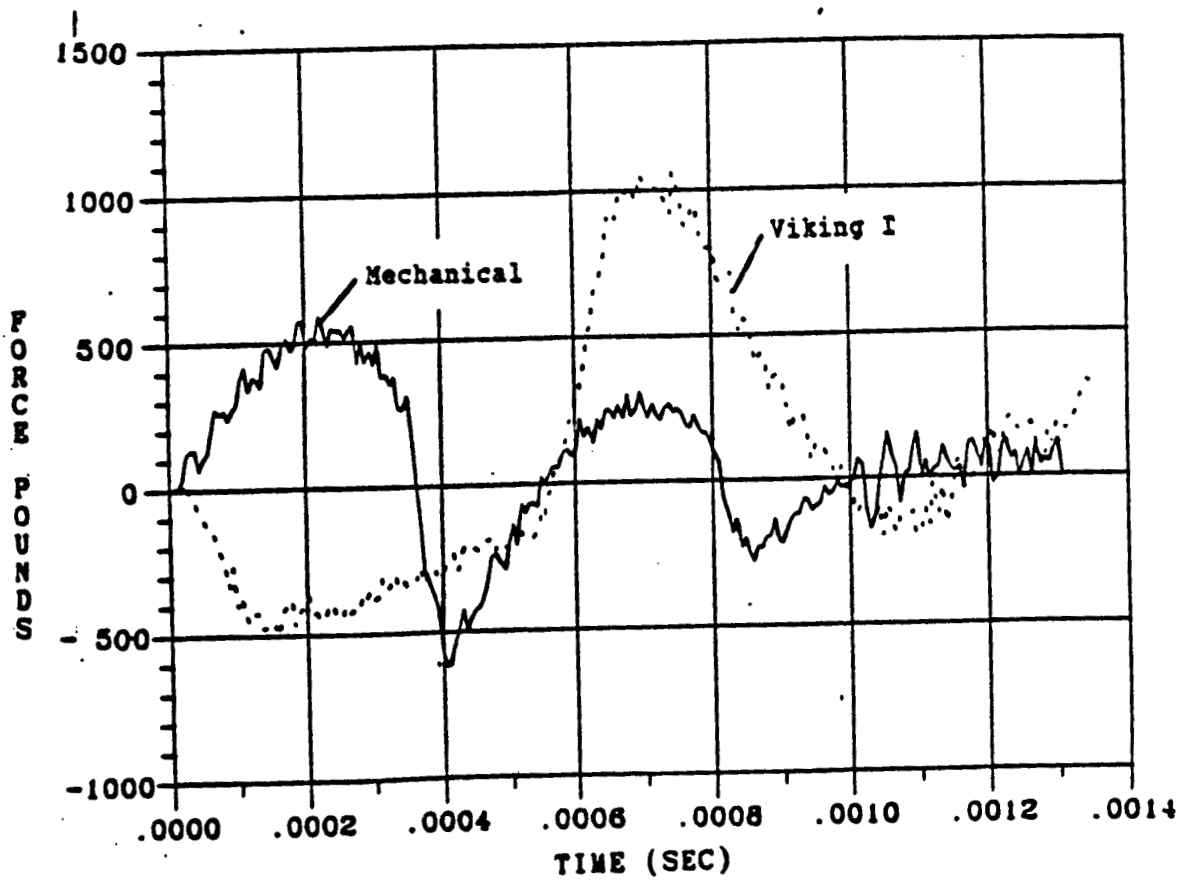

Figure 6.9 Axial force vs. time, Viking I (Two Init.) and Mechanical.

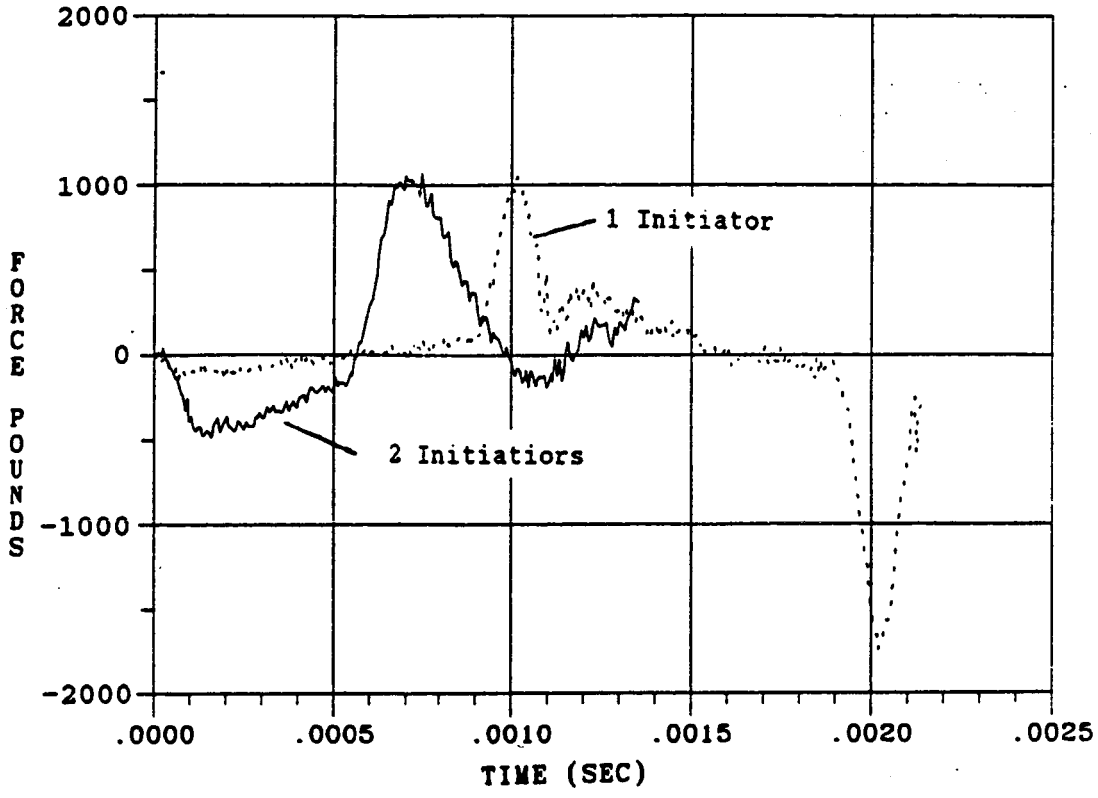

Figure 6.10 Axial force vs. time , Viking I (Two Init.) and (One Init.).

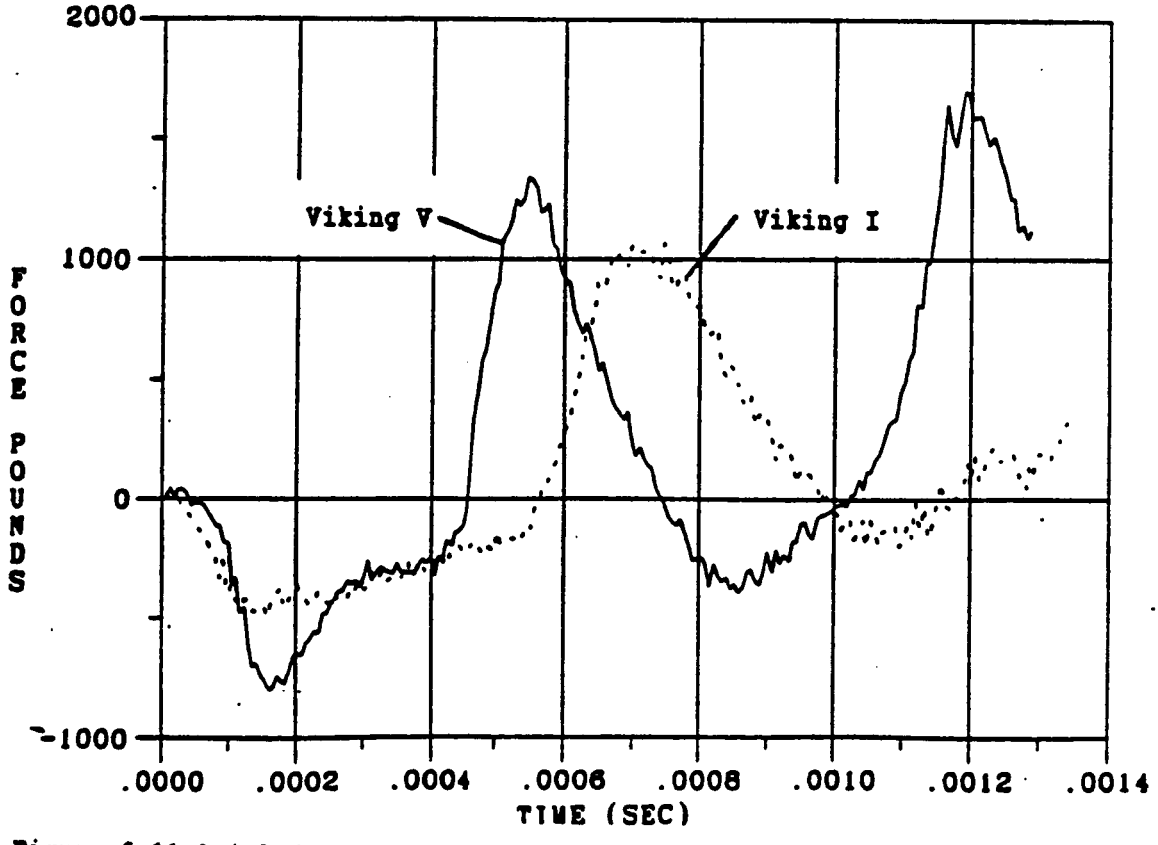

Figure 6.11 Axial force vs. time, Viking I (Two Init.) and Viking V.

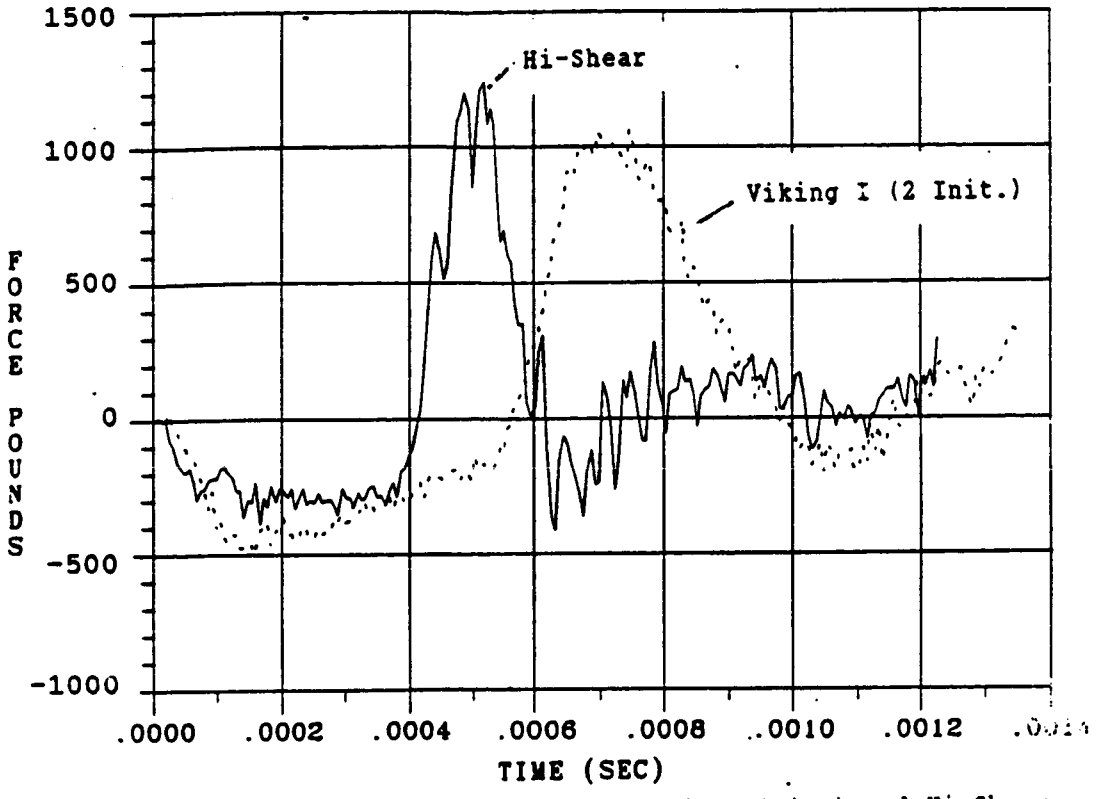

Figure 6.12 Axial force vs. time , Viking I (Two Init.) and Hi-Shear.

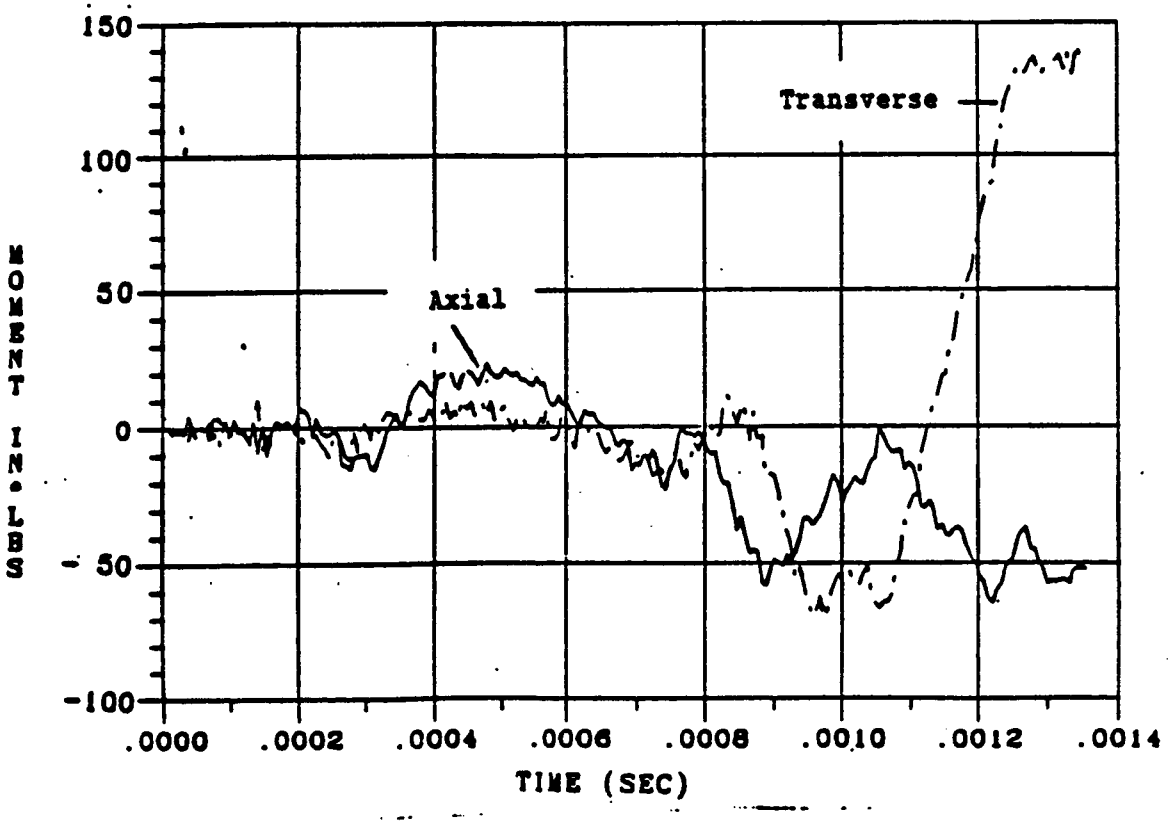

Figure 6.13 Axial and transverse moment, Viking I (Two Init.).

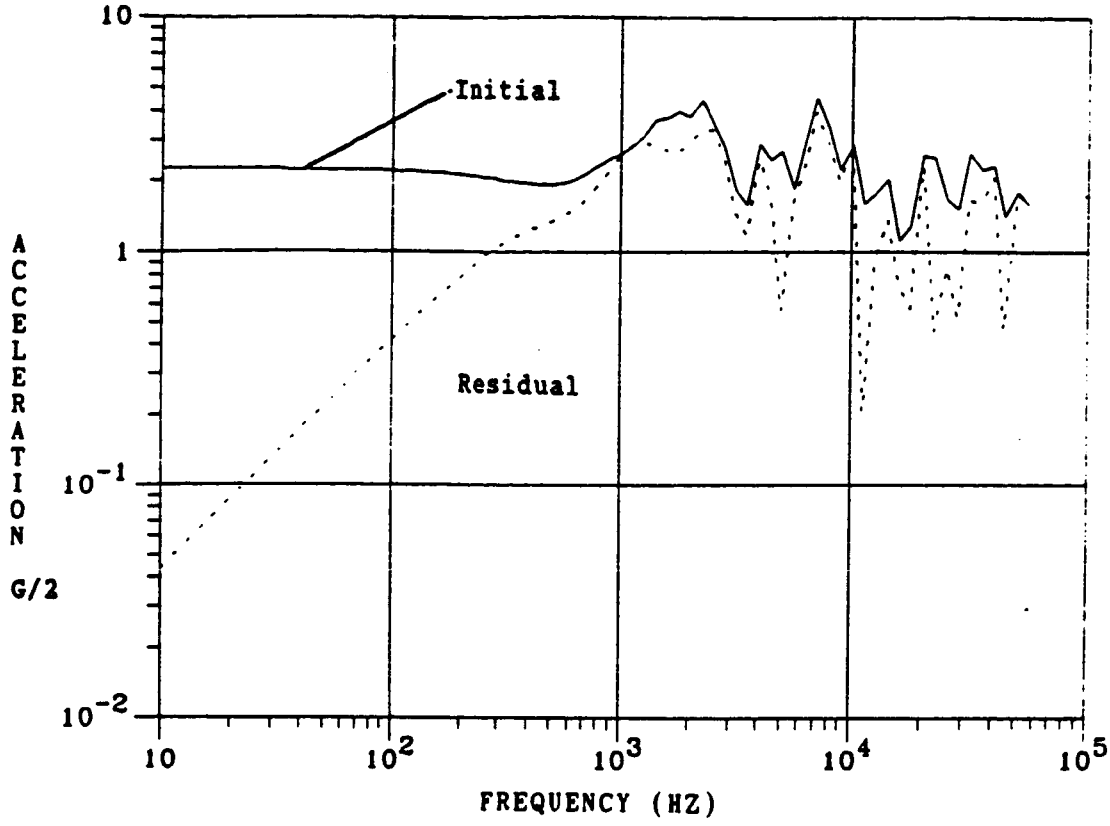

Figure 6.14 Initial and residual shock spectra, axial force, Viking I.

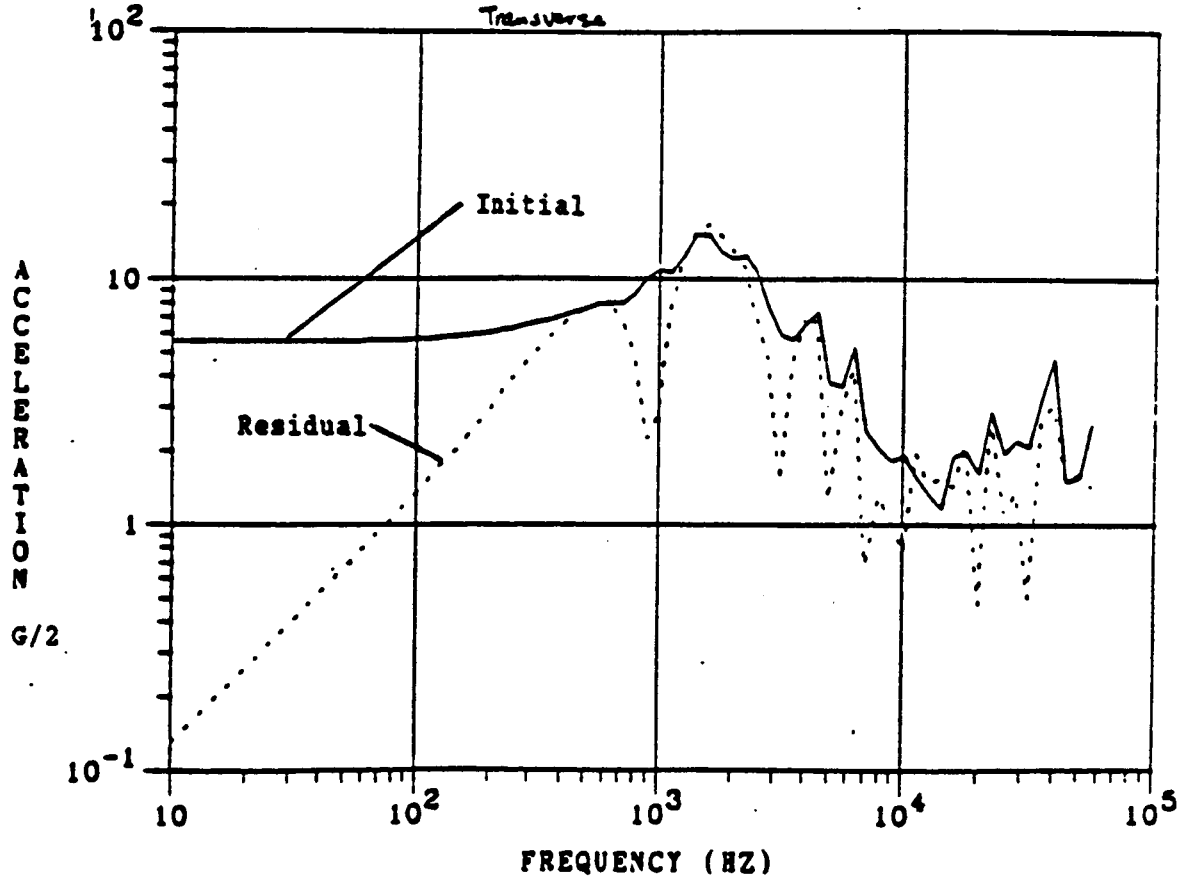

Figure 6.15 Initial and residual shock spectra, transverse force, Viking I.

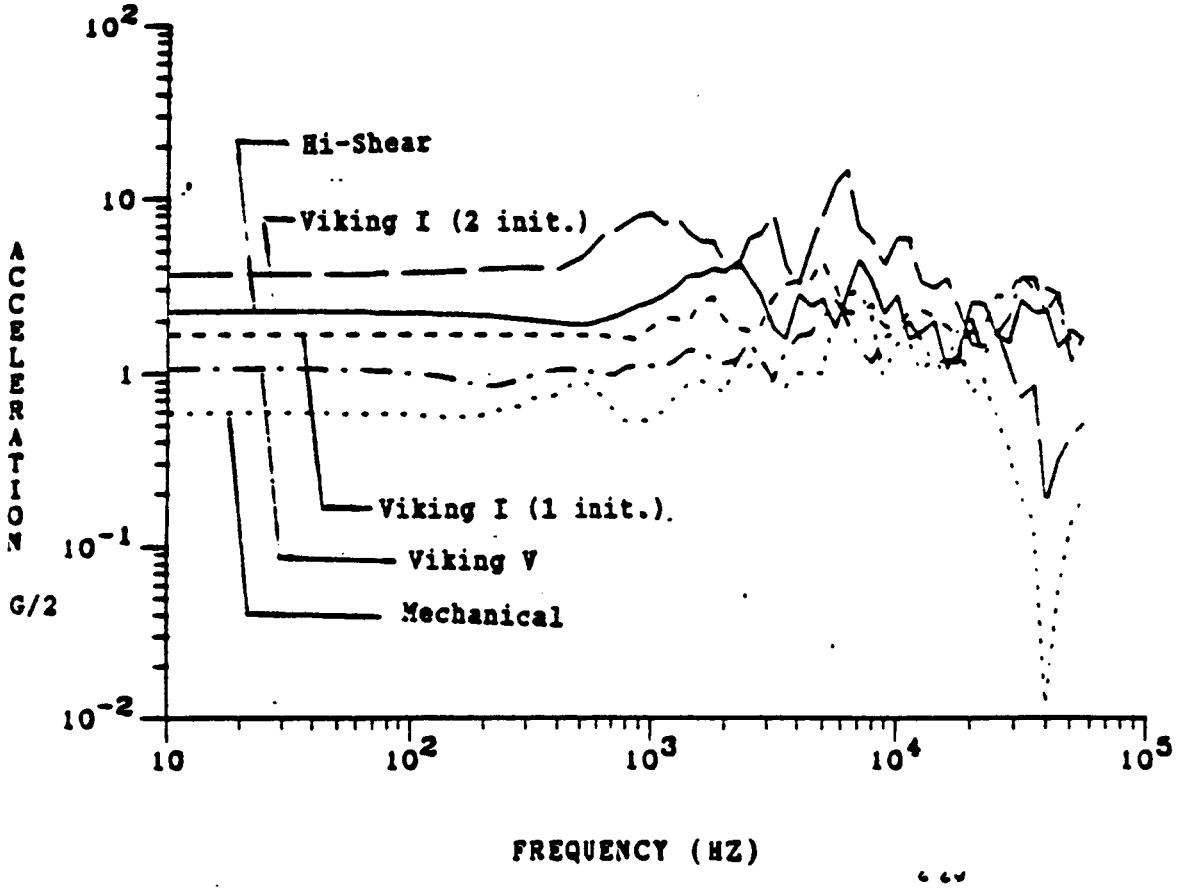

Figure 6.16 Initial shock spectra for forces from five pin-pullers.

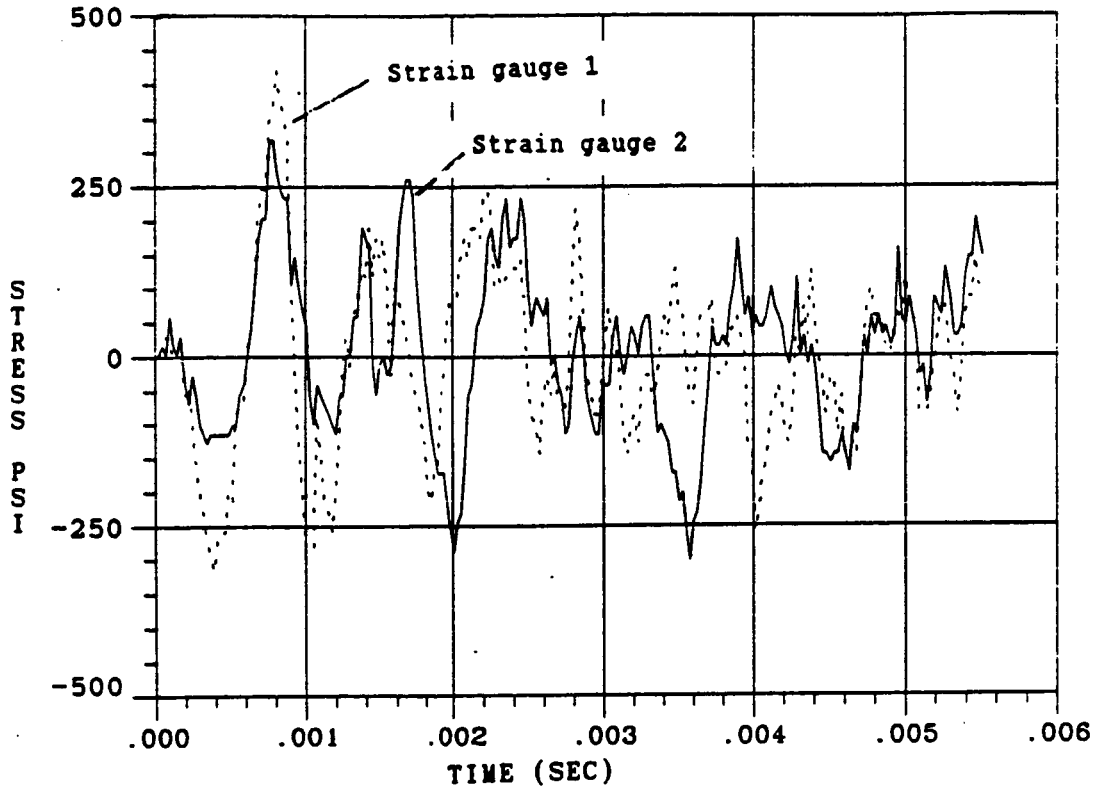

Figure 6.17 Stress vs. time, HALOE Viking V, SG1 and SG2.

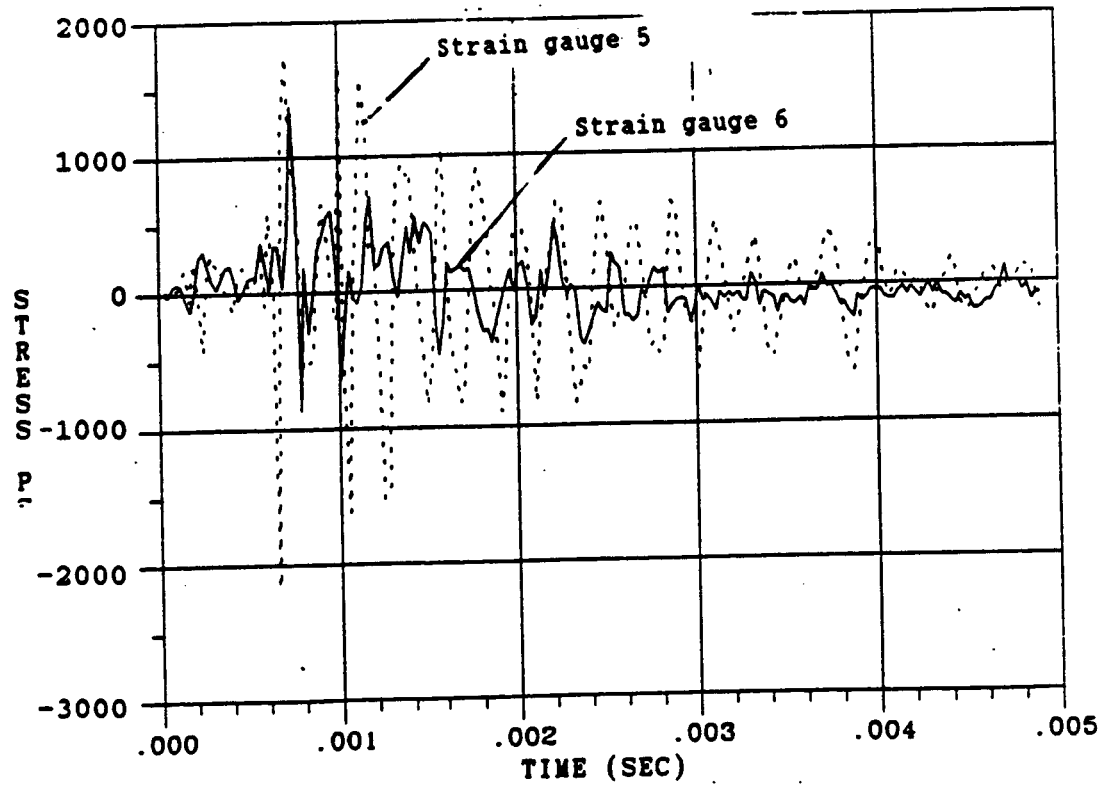

Figure 6.18 Stress vs. time, HALOE Viking V, SG5 and SG6.

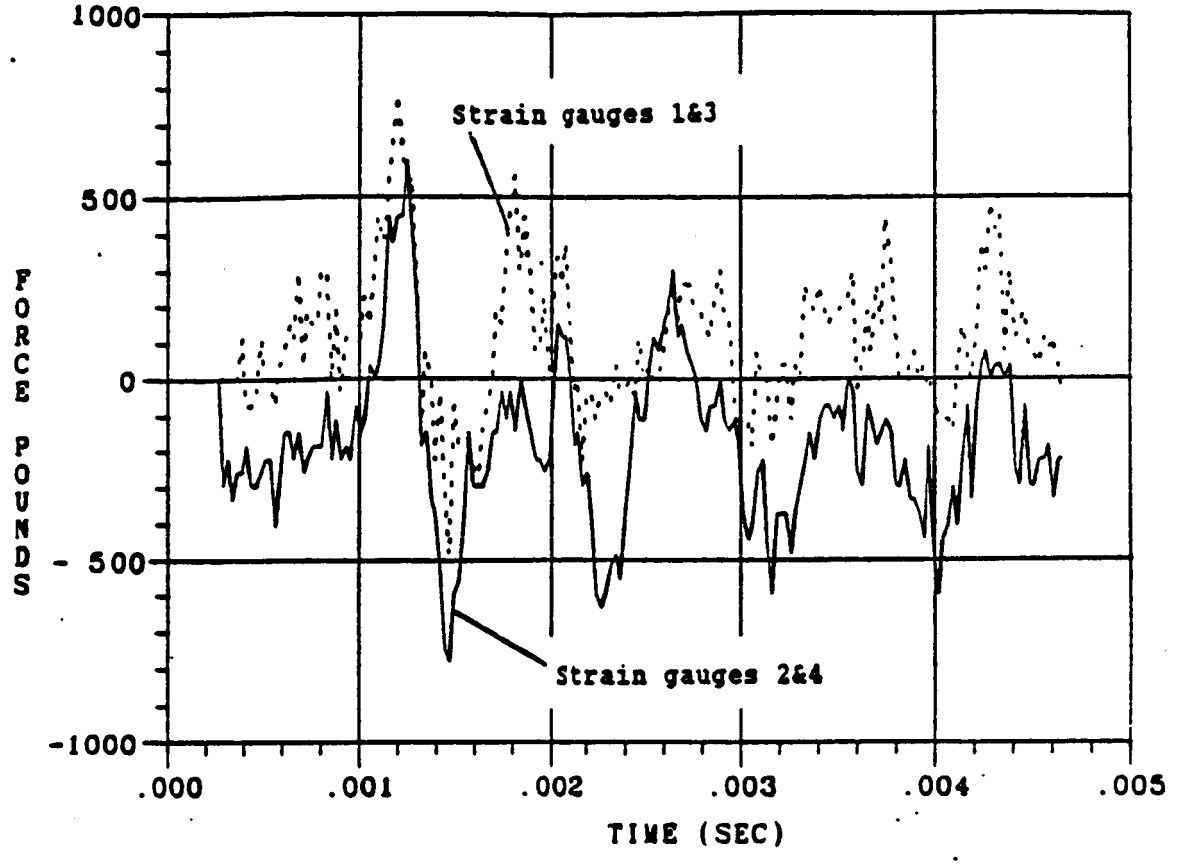

Figure 6.19 Force vs. time, HALOE Viking V, SG 1&3 and 2&4.

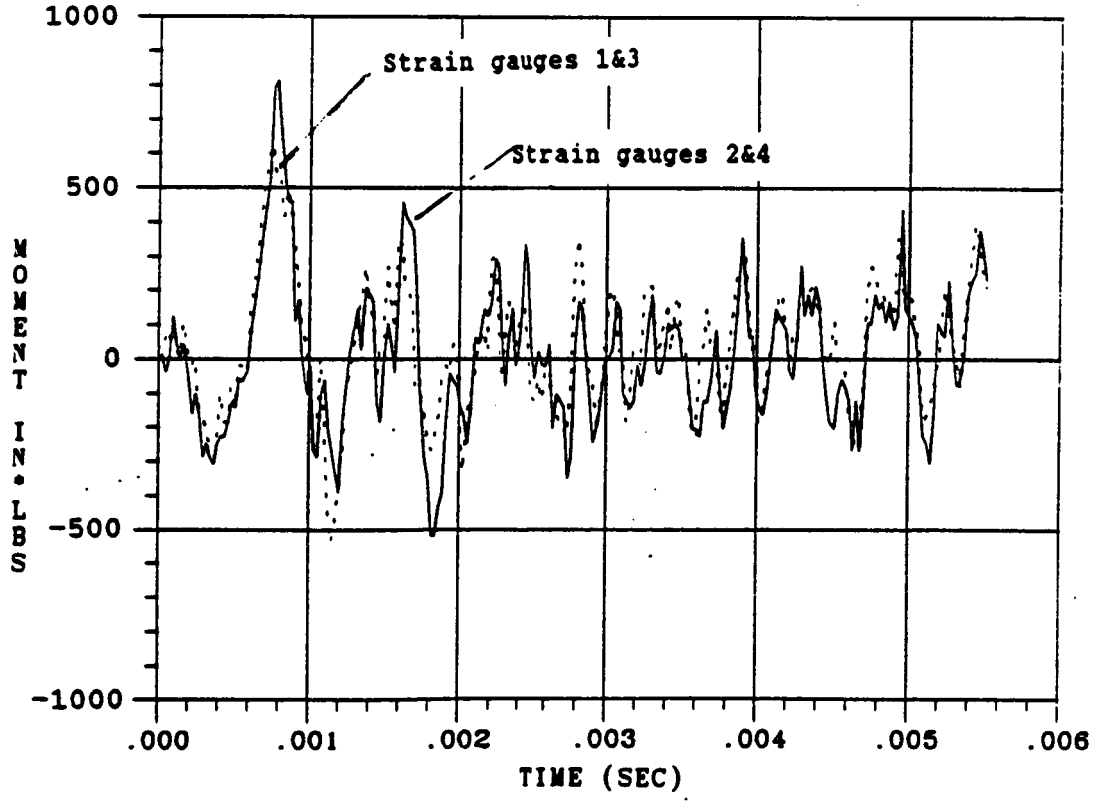

Figure 6.20 Moment vs. time, HALOE Viking V, SG 1&3 and 2&4.

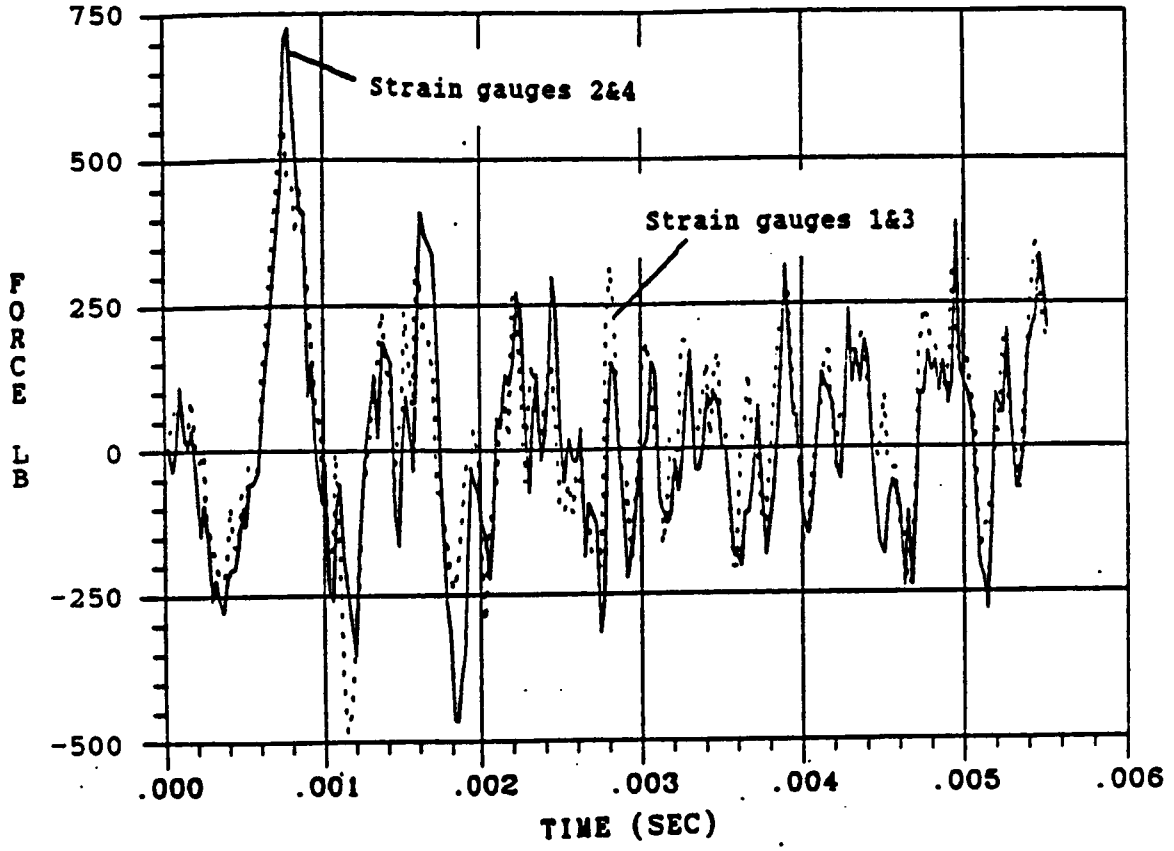

Figure 6.21 Force vs. time, HALOE Viking I (Two Init.), SG 1&3 and 2&4.

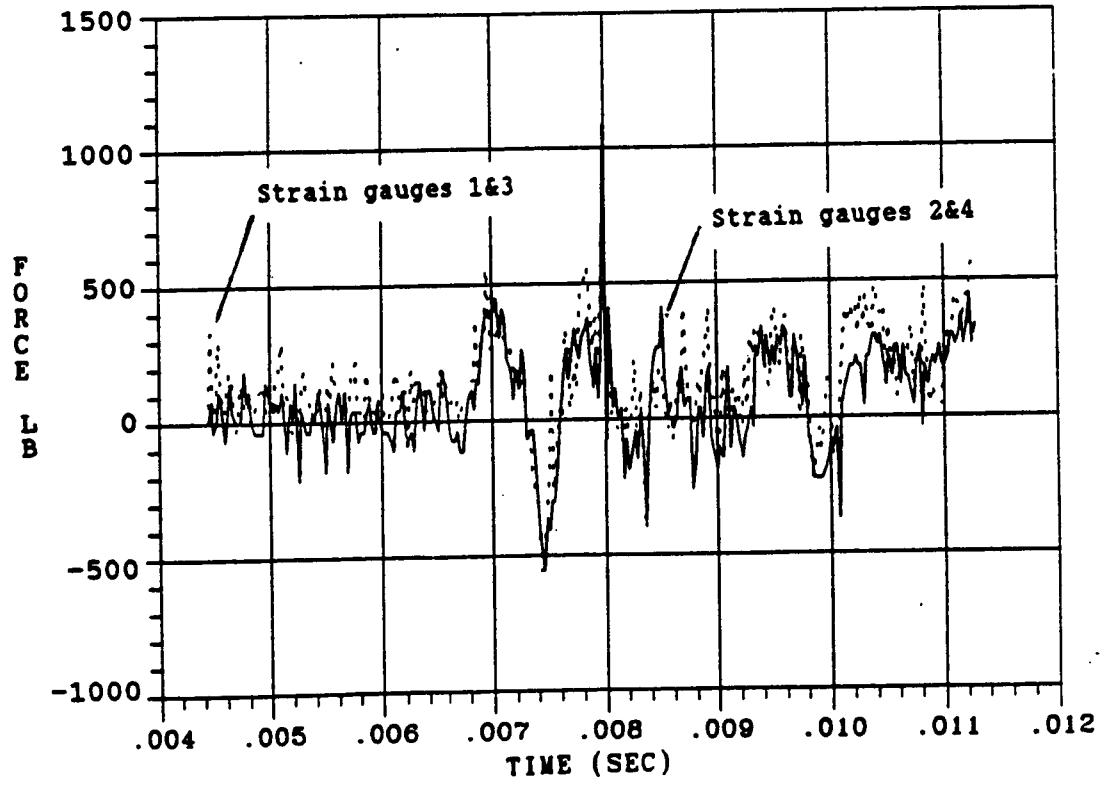

Figure 6.22 Force vs. time, HALOE Mechanical, SG 1&3 and 2&4.

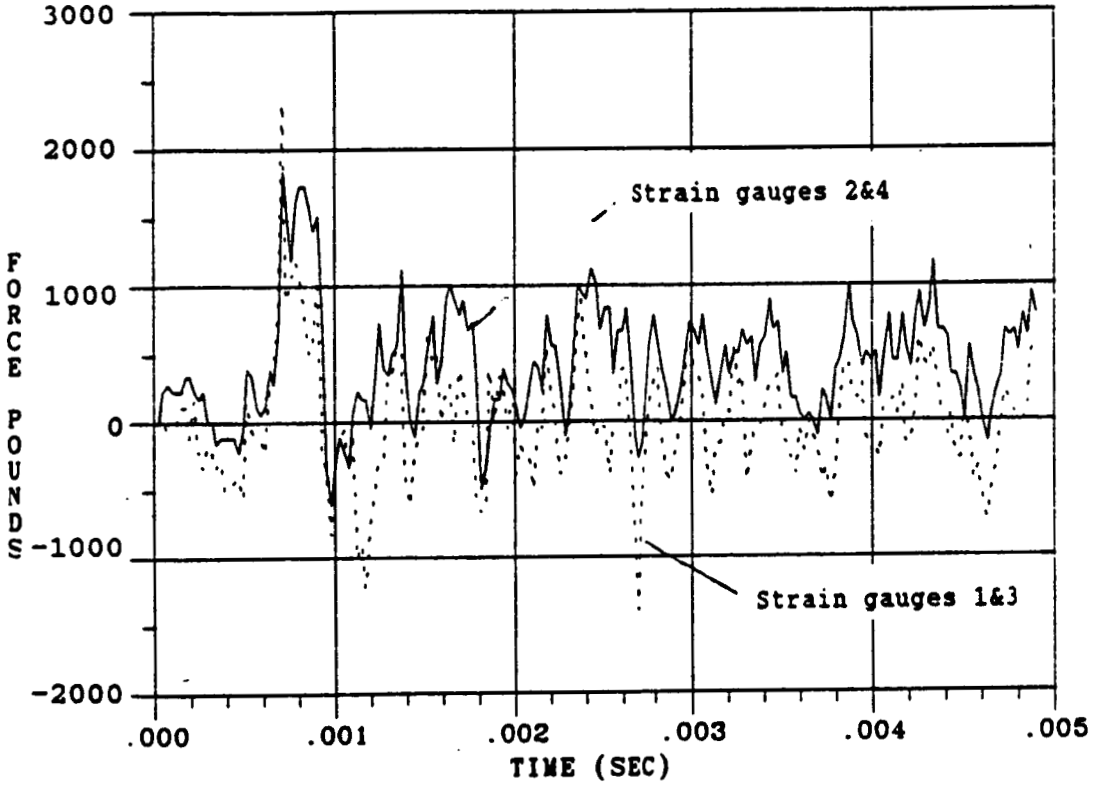

Figure 6.23 Force vs. time, HALOE Hi-Shear, SG 1&3 and 2&4.

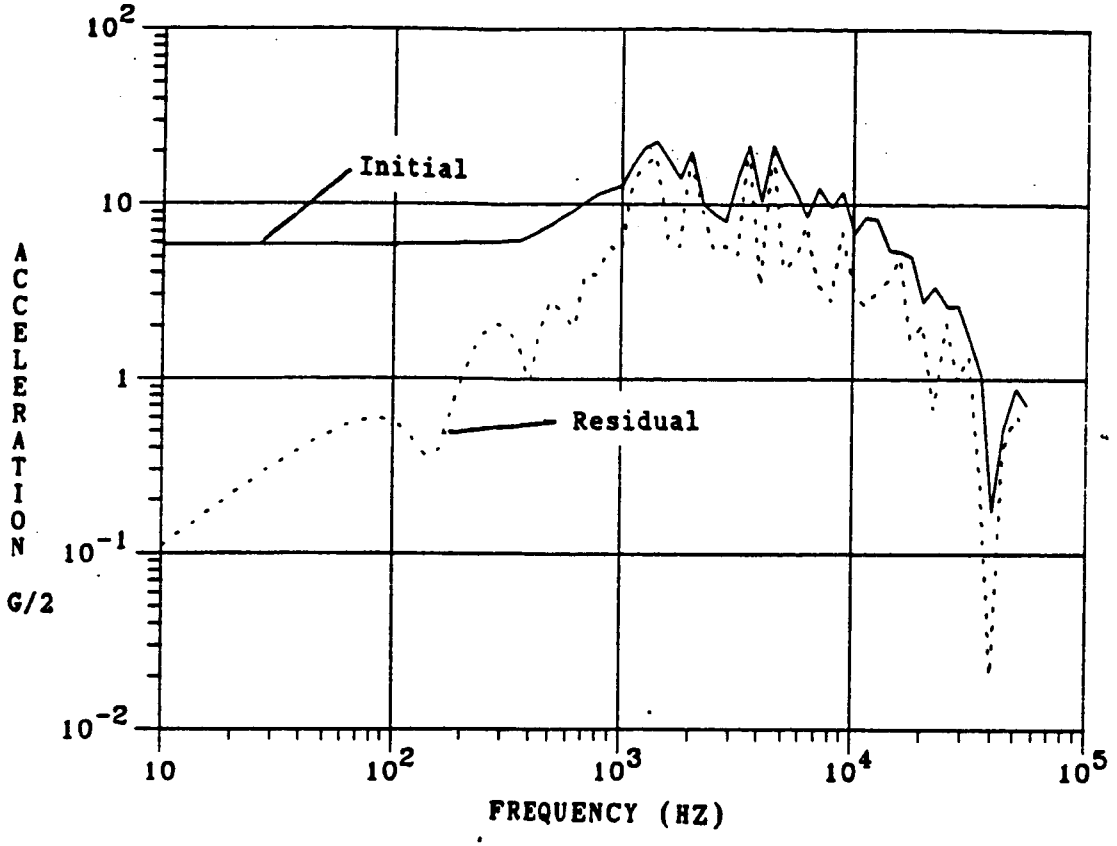

Figure 6.24 Initial and residual shock spectra, force from SG 1&3, Viking V on HALOE structure.

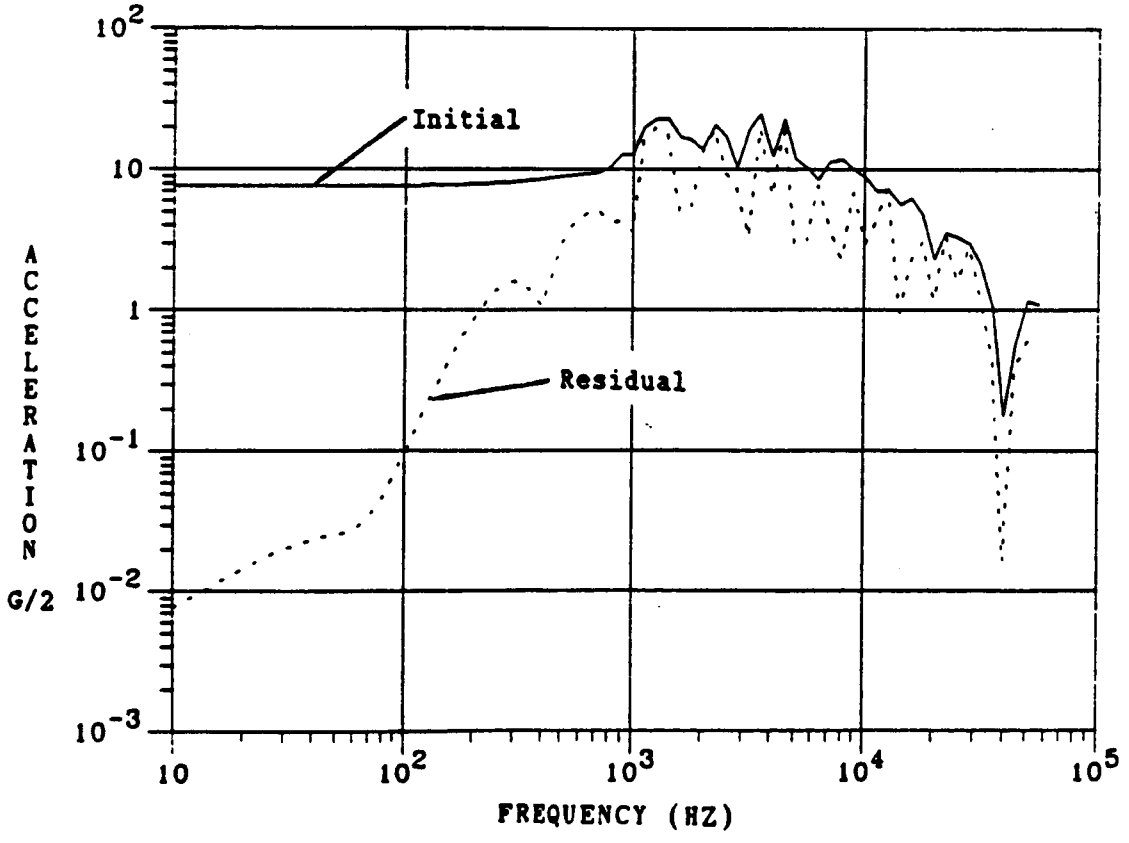

Figure 6.25 Initial and residual shock spectra, force from SG 2&4, Viking V on HALOE structure.

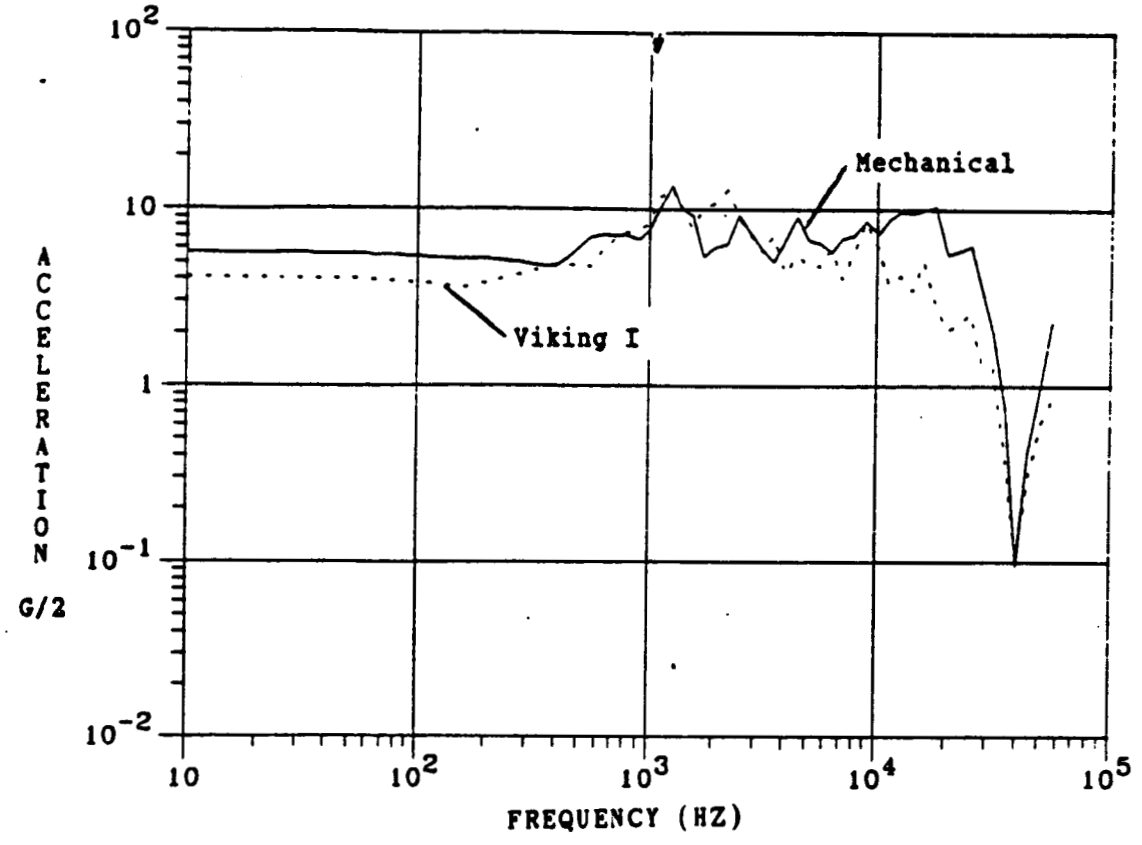

Figure 6.26 Initial shock spectra from forces, HALOE Viking I and Mechanical

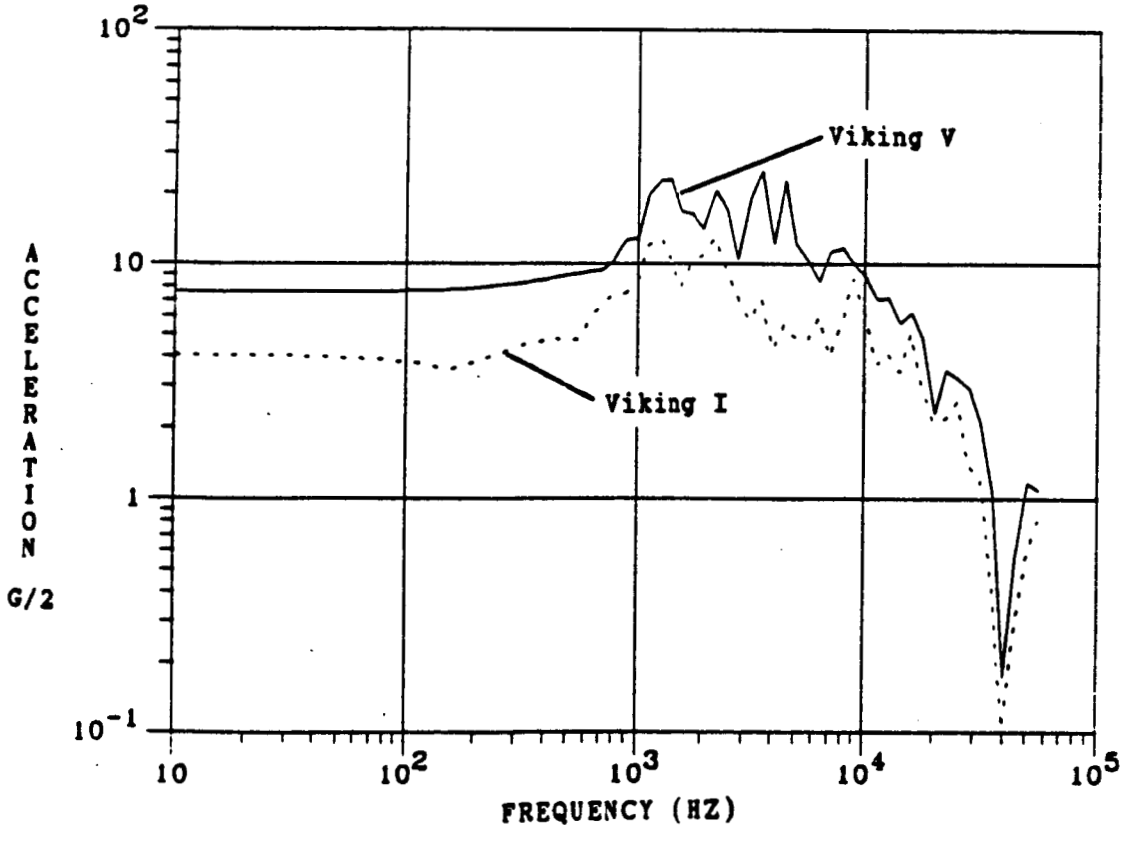

Figure 6.27 Initial shock spectra from forces, HALOE Viking I and Viking V.

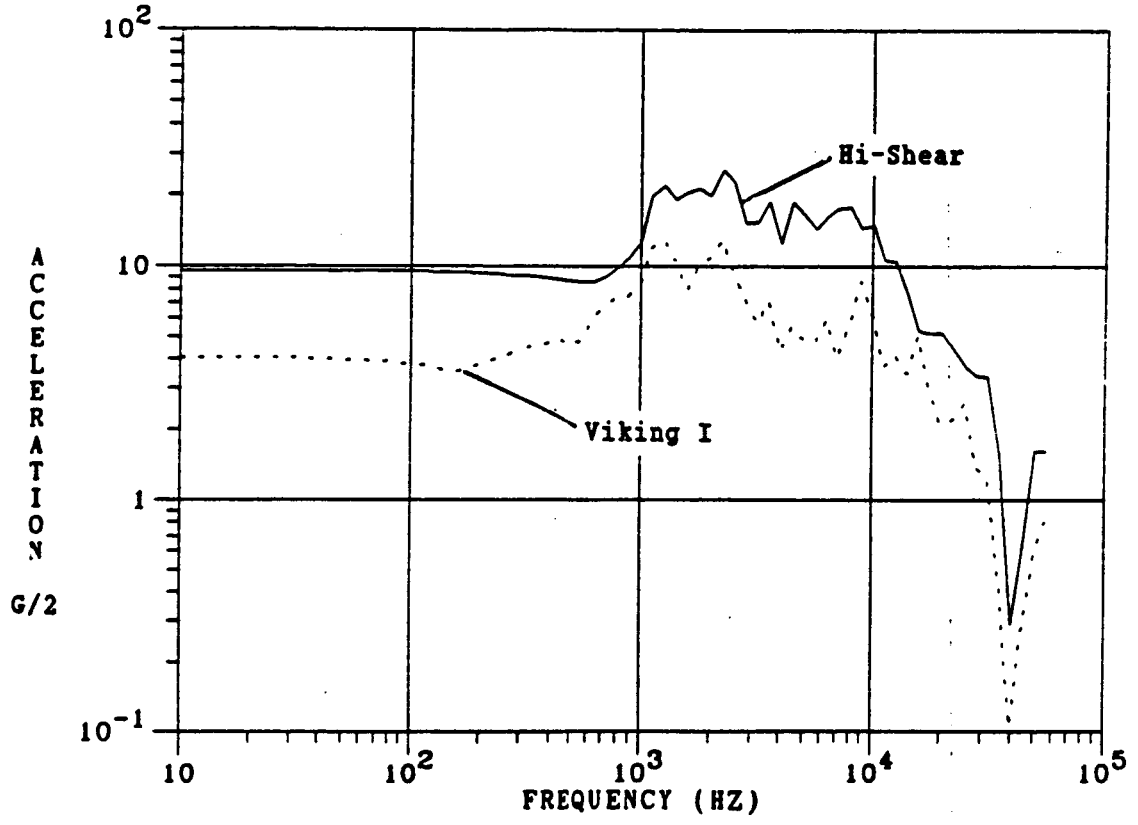

Figure 6.28 Initial shock spectra from forces, HALOE Viking I and Hi-Shear.

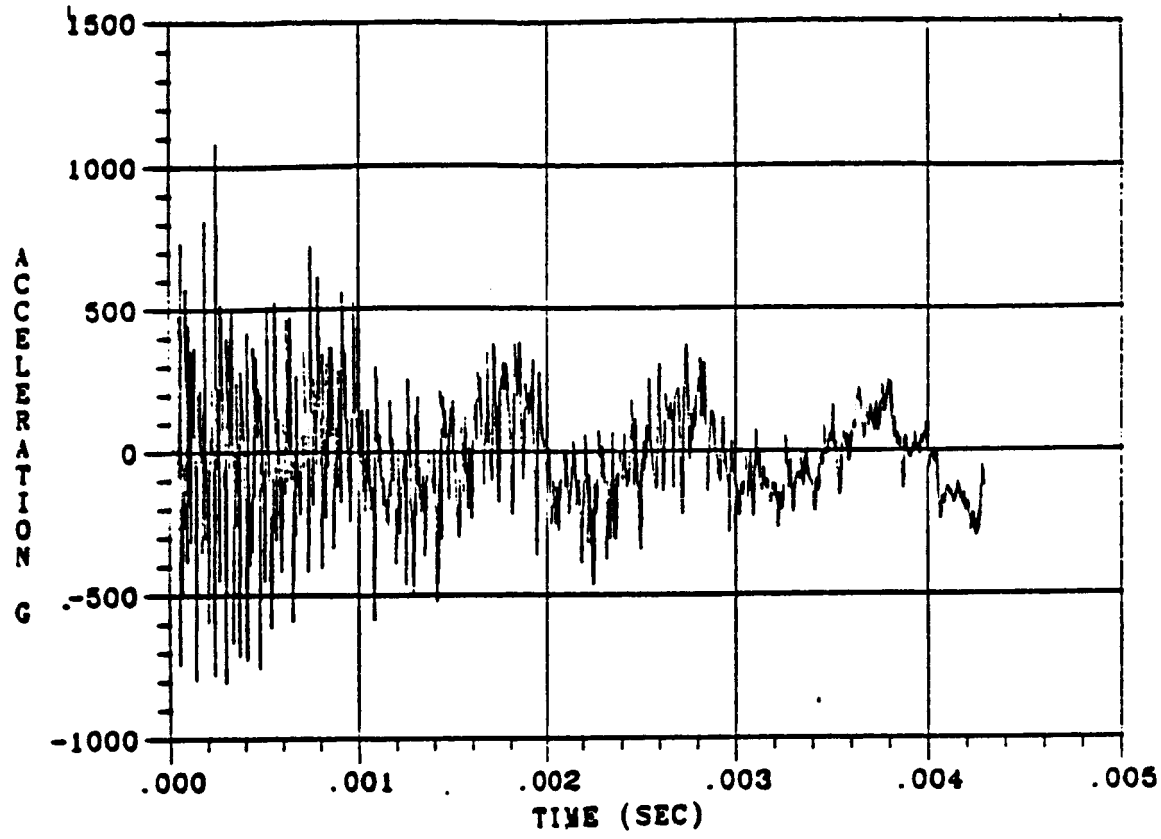

Figure 6.29 Acceleration vs. time, HALOE Viking V, B&K accelerometer.

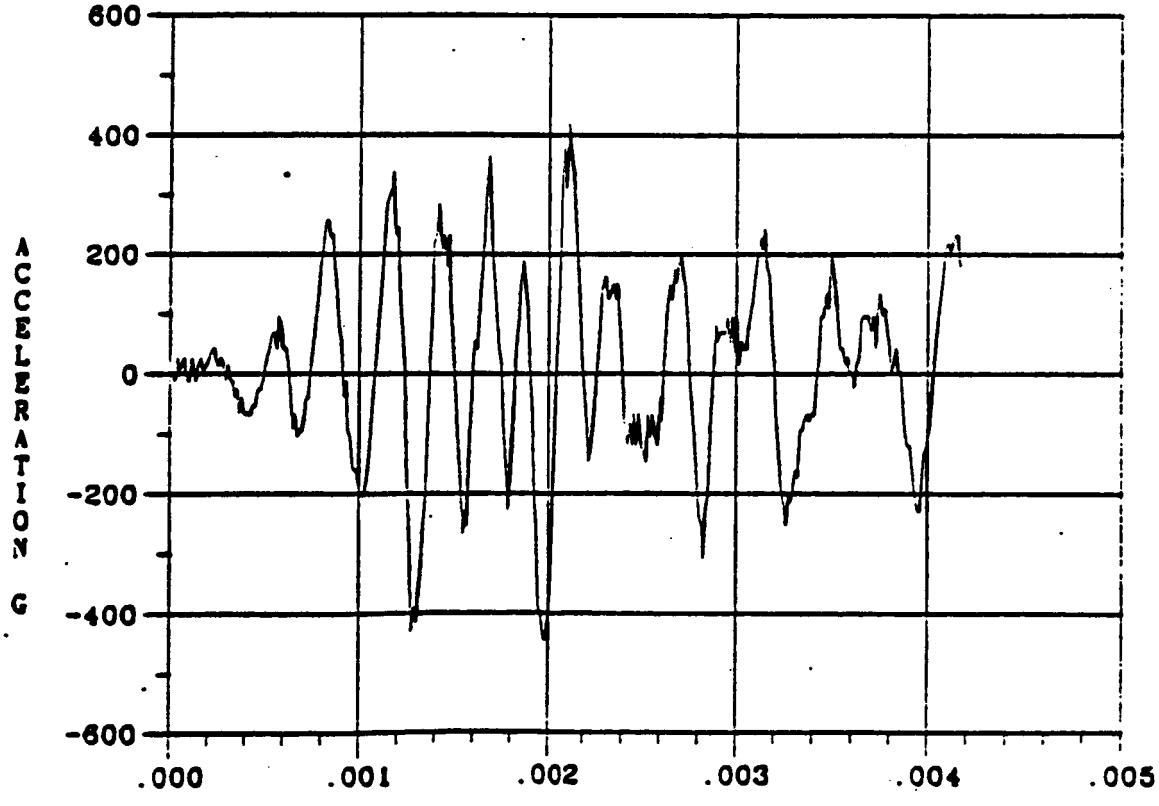

Figure 6.30 Acceleration vs. time, HALOE Viking V, accelerometer 3.

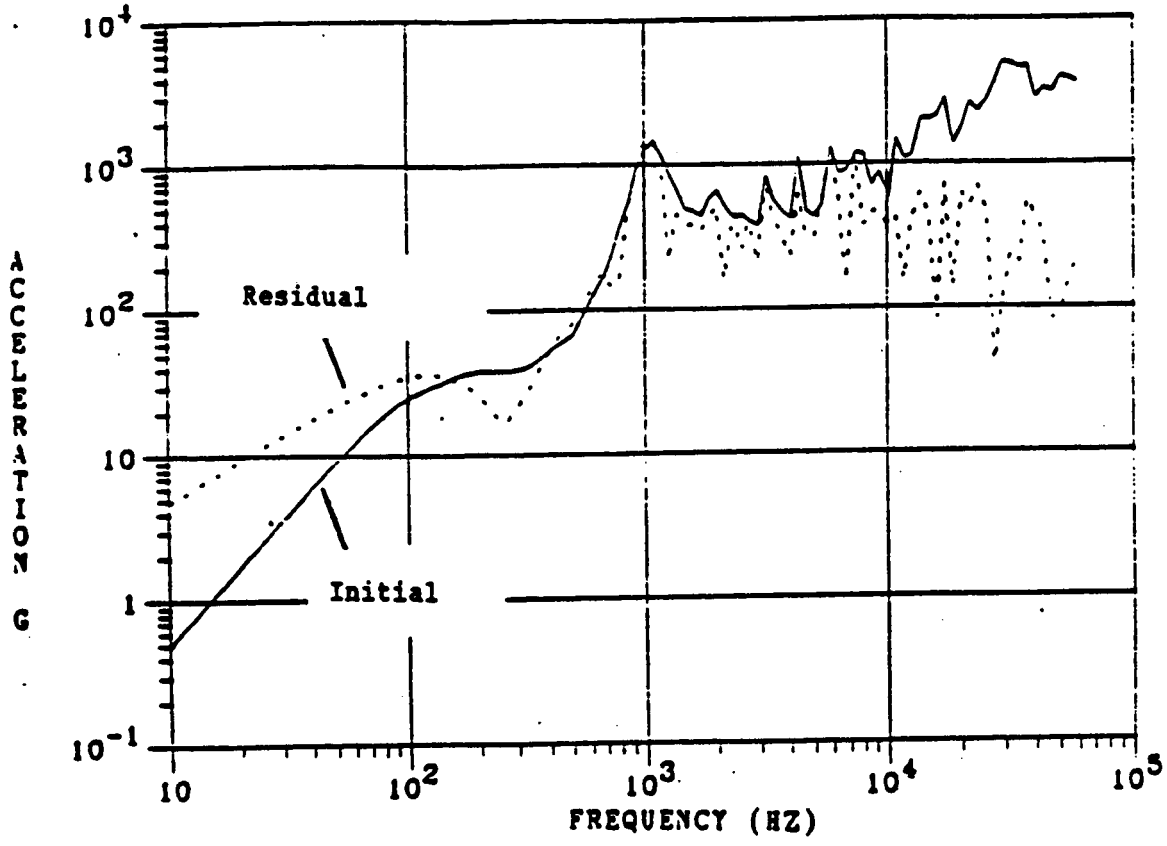

Figure 6.31 Initial and residual shock spectra, HALOE Viking V, B&K accel.

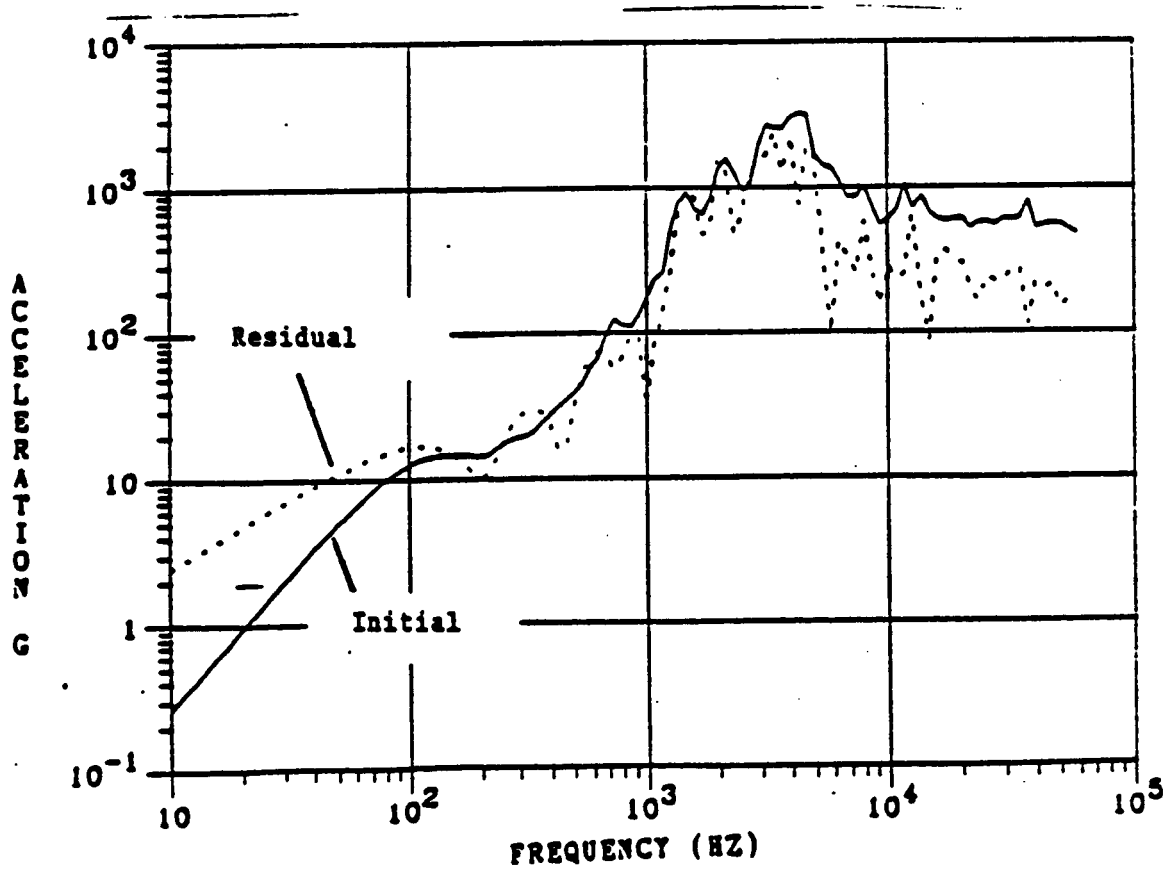

Figure 6.32 Initial and residual shock spectra, HALOE Viking V, accel. 3.

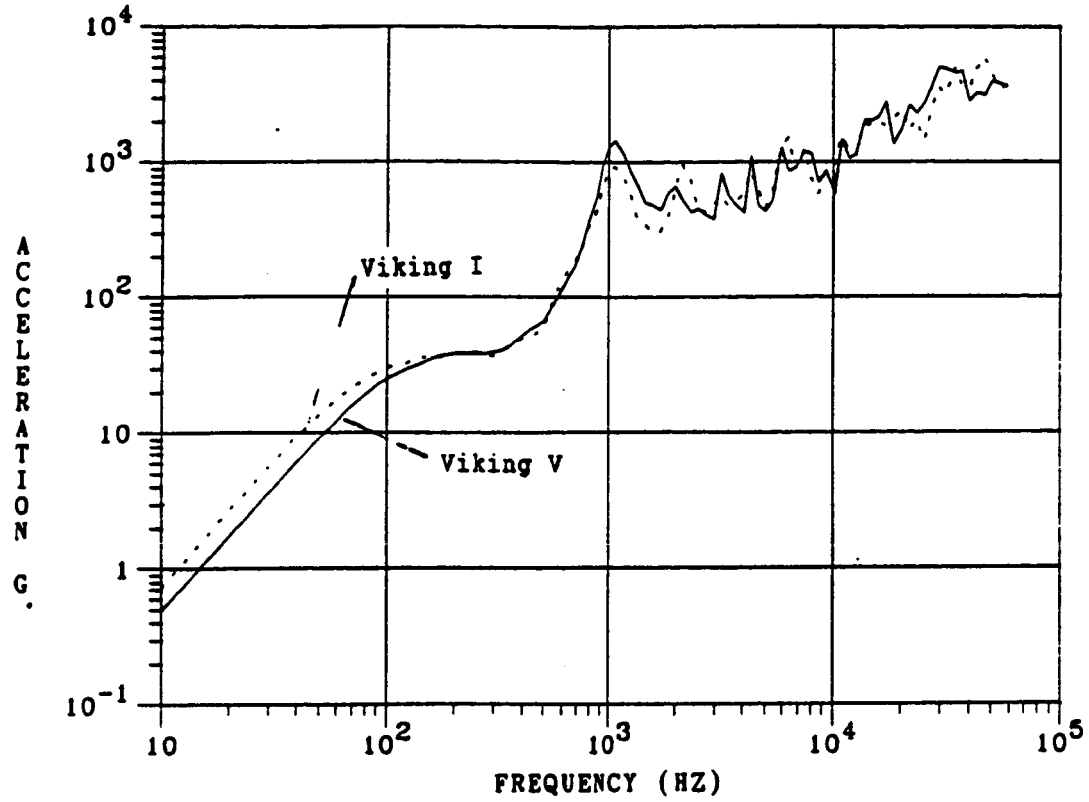

Figure 6.33 Initial shock spectra, HALOE Viking I and Viking V, B&K accel.

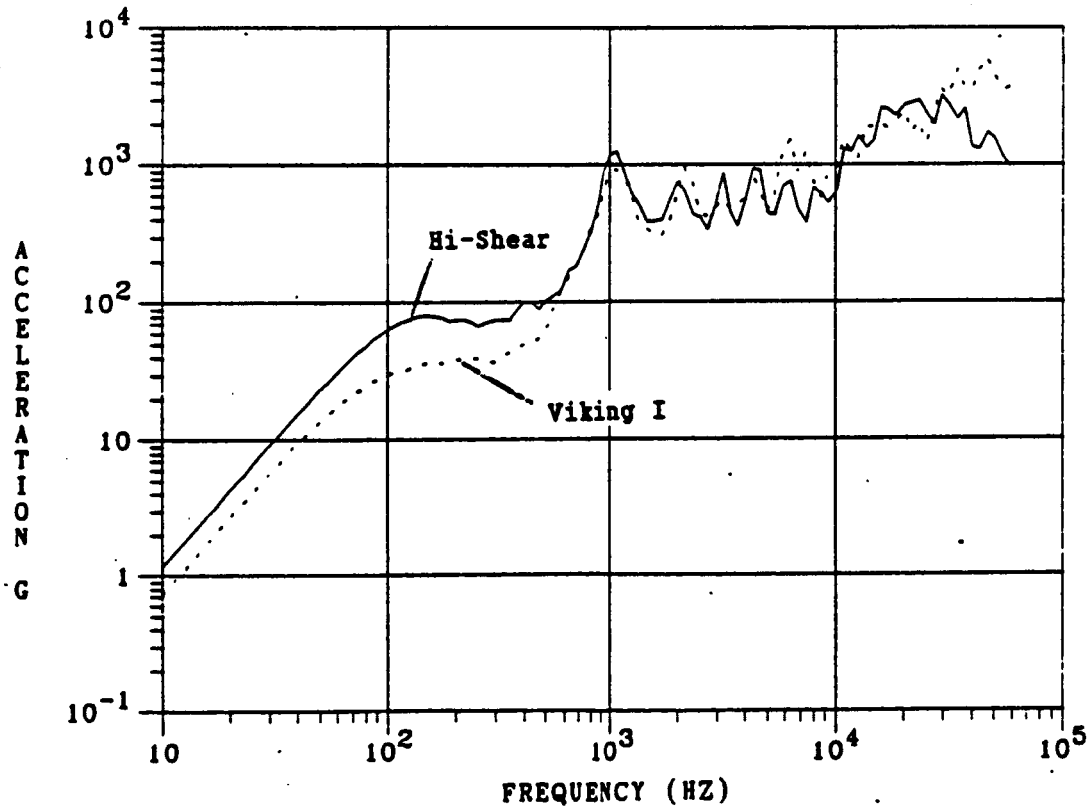

Figure 6.34 Initial shock spectra, HALOE Viking I and Hi-Shear, B&K accel.

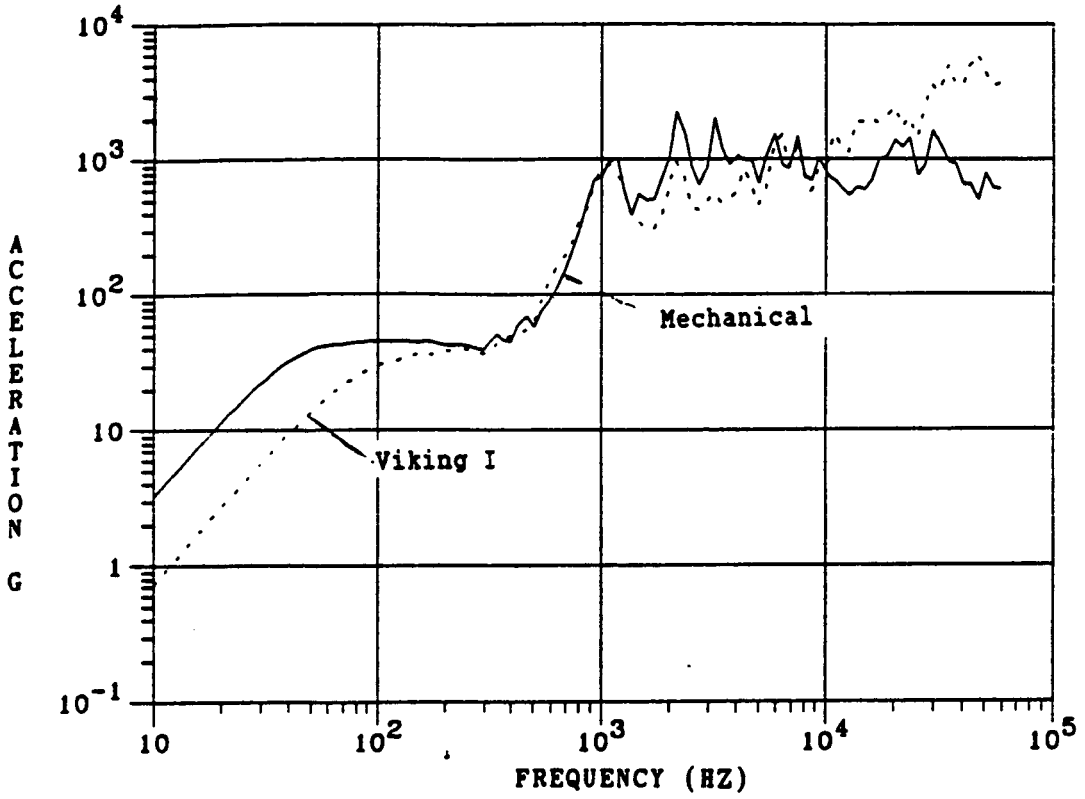

Figure 6.35 Initial shock spectra, HALOE Viking I and Mechanical, B&K accel.

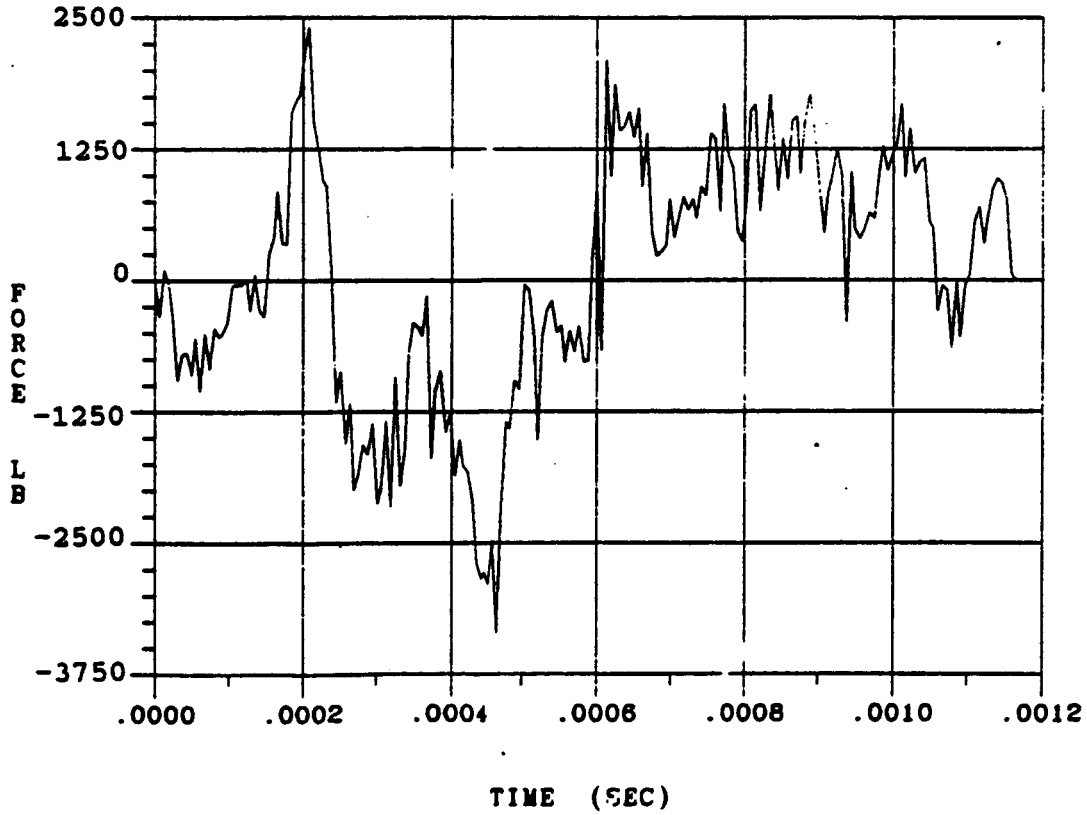

Figure 6.36 Force vs. time, separation joint test 11.

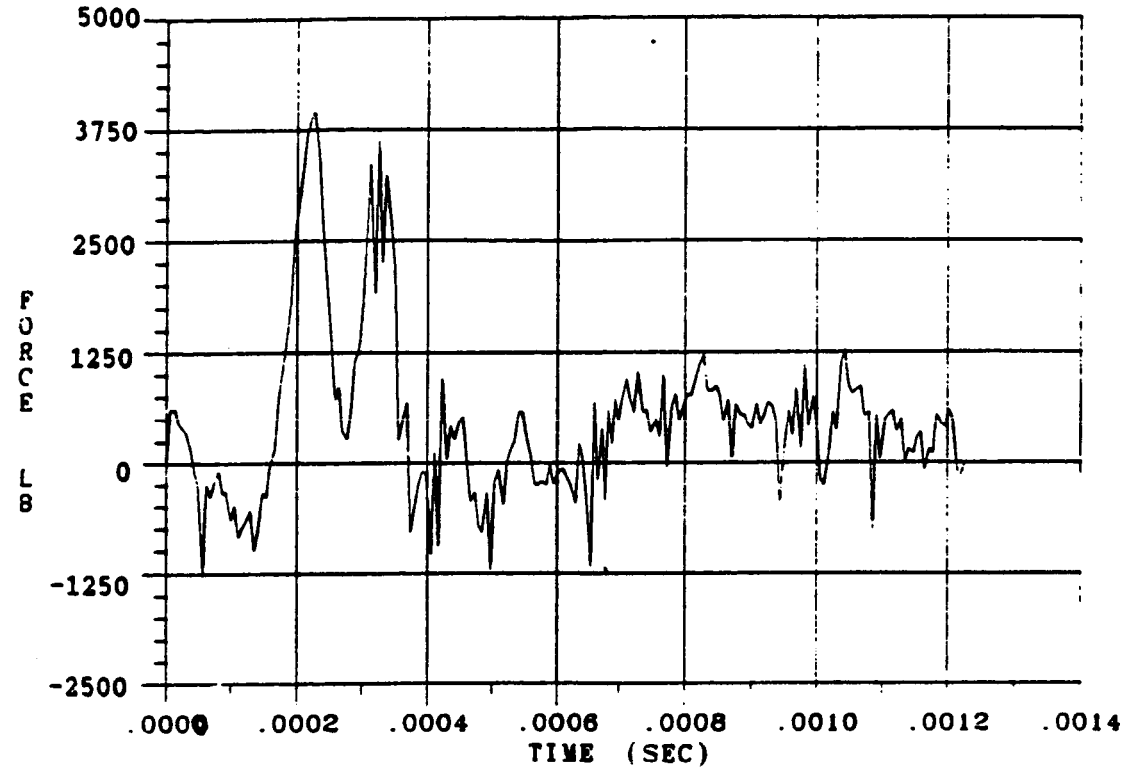

Figure 6.37 Force vs. time, separation joint test 14.

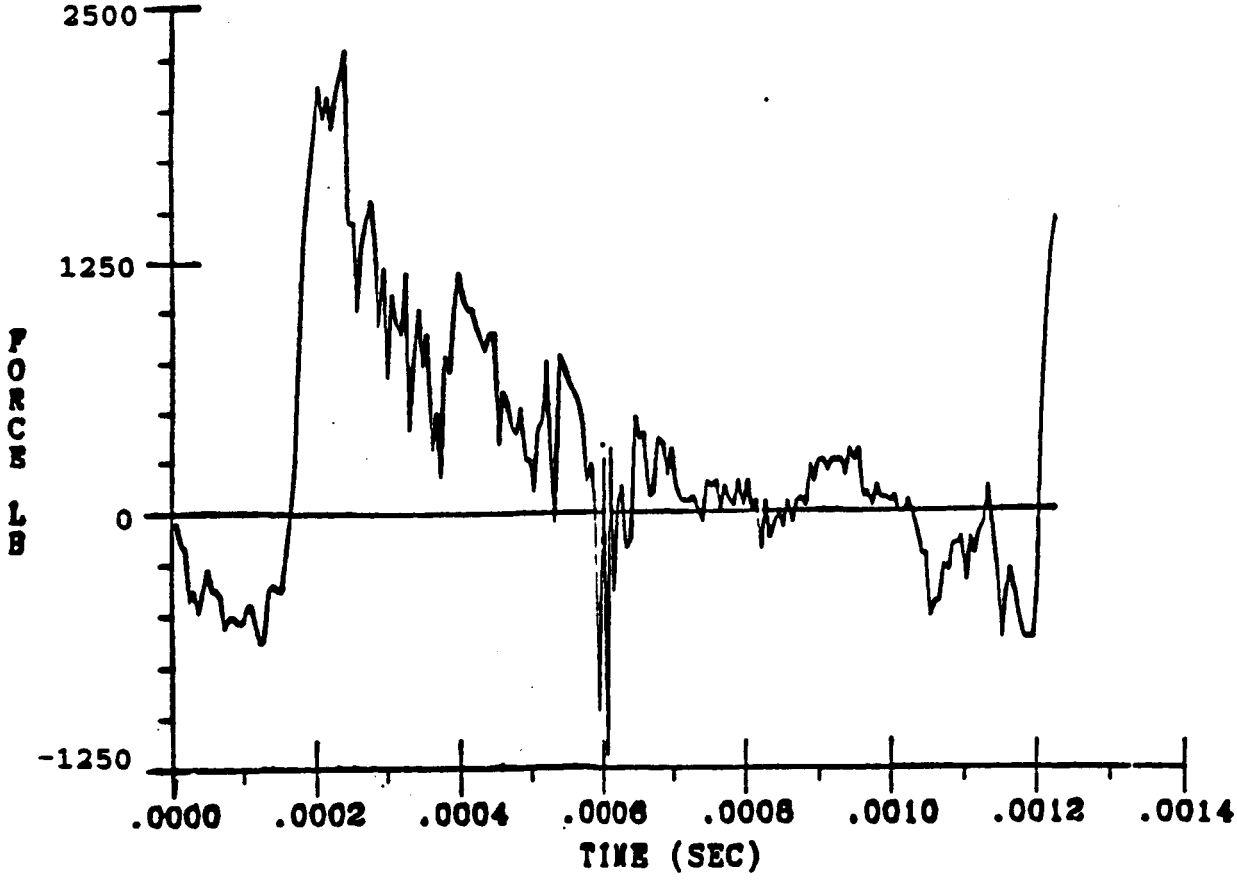

Figure 6.38 Force vs. time, separation joint test 17.

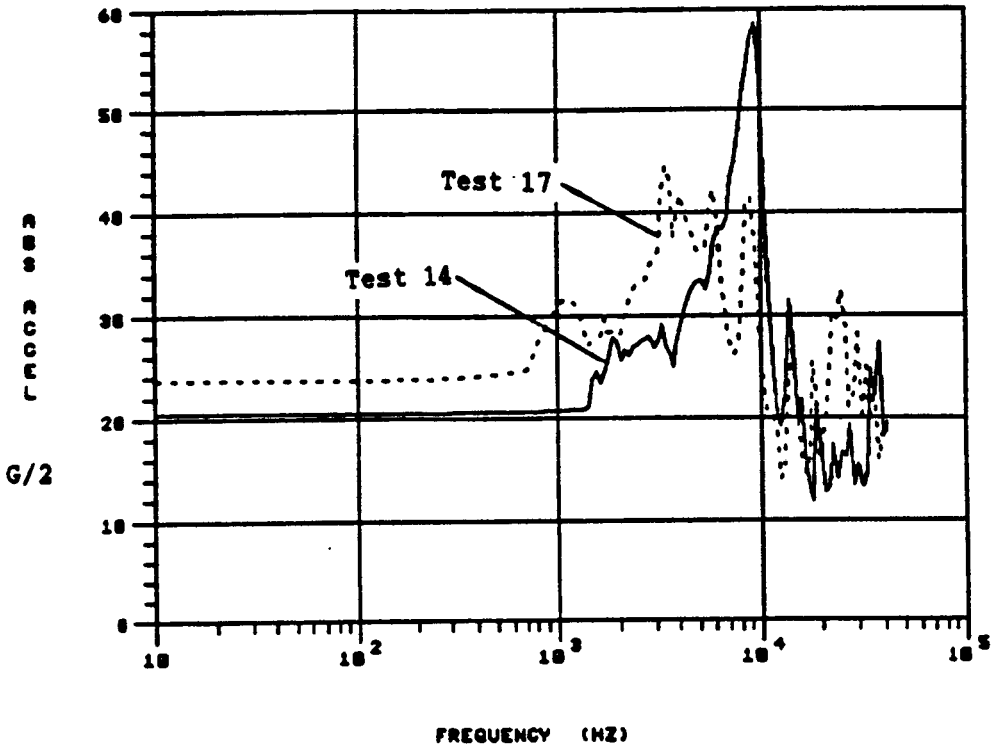

Figure 6.39 Shock spectra from forces, separation joint tests 14 and 17.

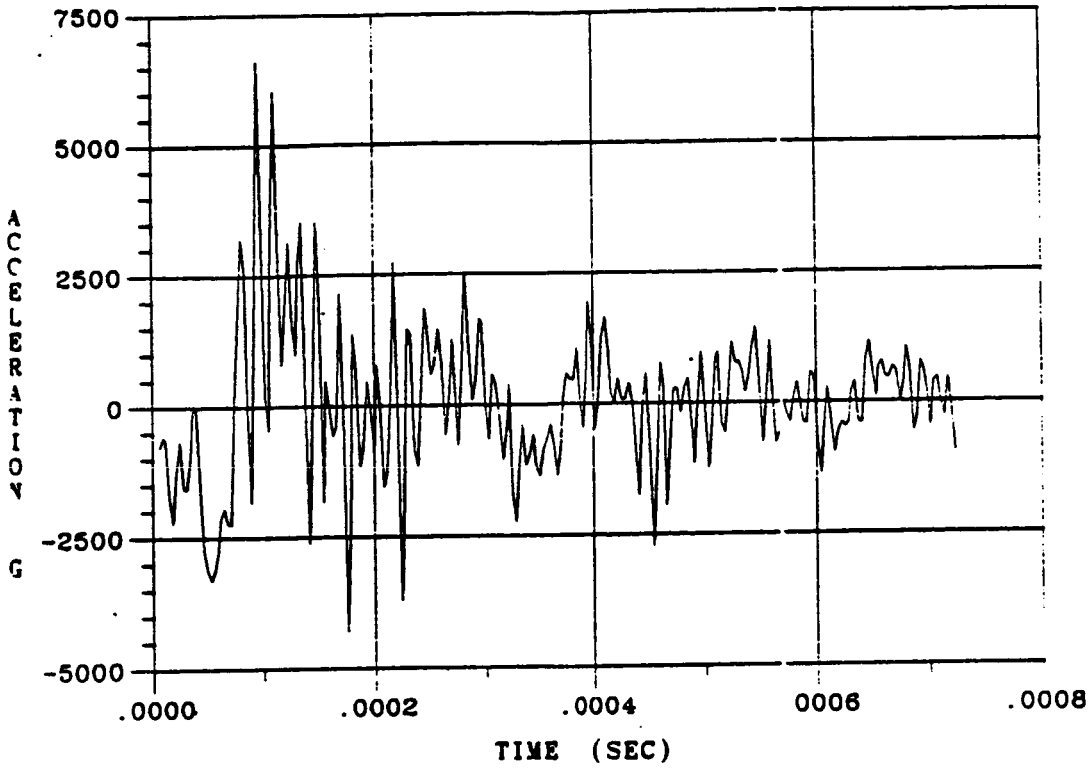

Figure 6.40 Acceleration vs. time, separation joint test 12.

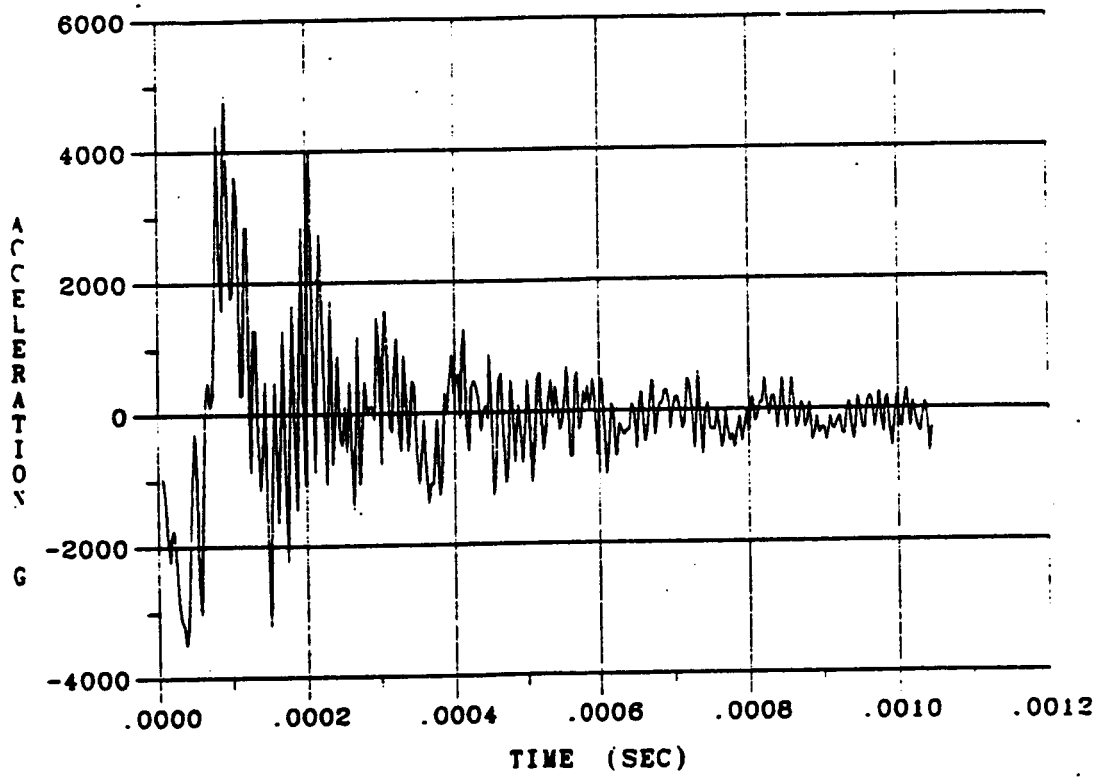

Figure 6.41 Acceleration vs. time, separation joint test 14.

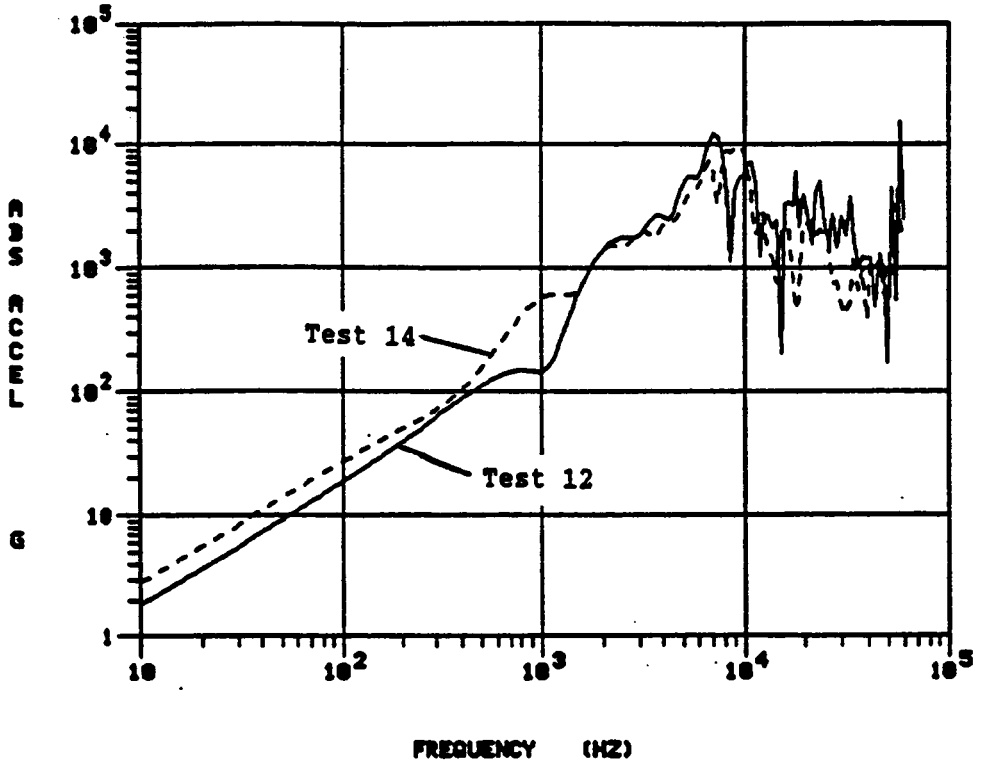

Figure 6.42 Shock spectra from acceleration, separation joint tests 12 & 14.

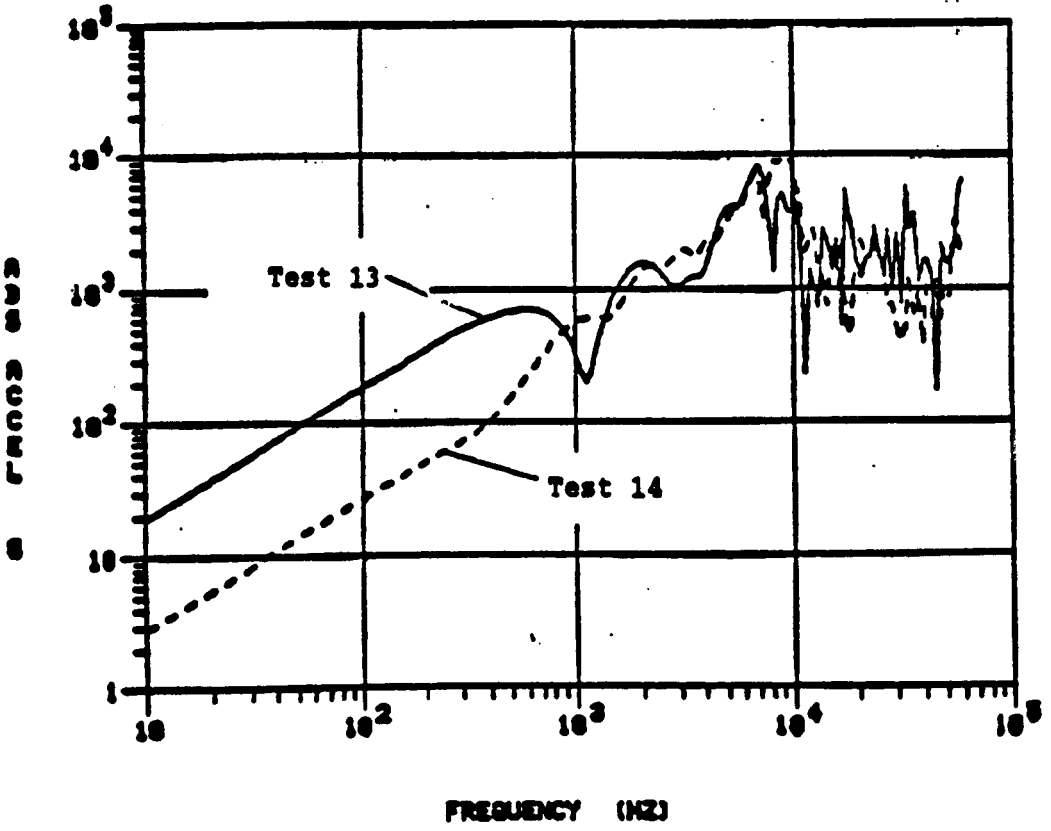

Figure 6.43 Shock spectra from acceleration, separation joint tests 13 & 14.

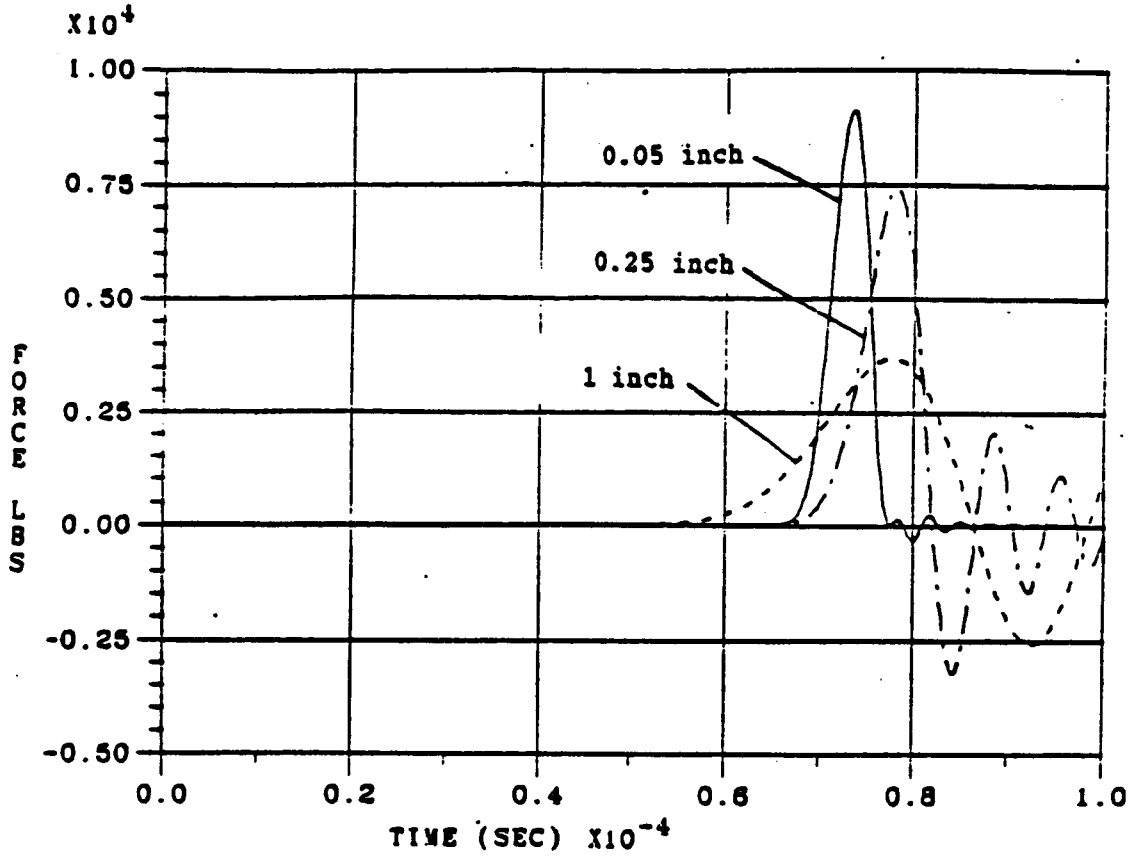

Figure 6.44 . Theoretical force vs. time, Hopkinson bar, 10,000 pound, 10 μs pulse, with grid spacing of 1 , 0.25 , and 0.05 inches.

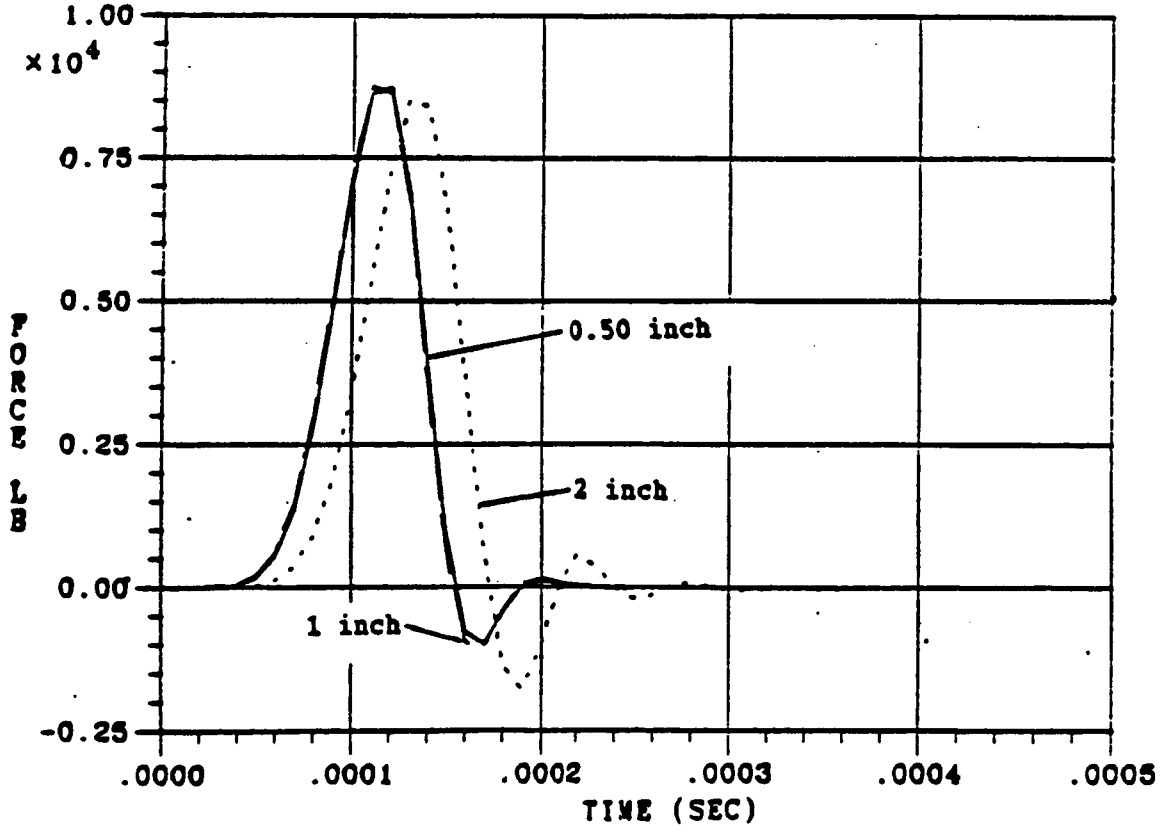

Figure 6.45 Theoretical force vs. time, Hopkinson bar, 10,000 pound, 100 μs pulse, with grid spacing of 2, 1, and 0.50 inches.

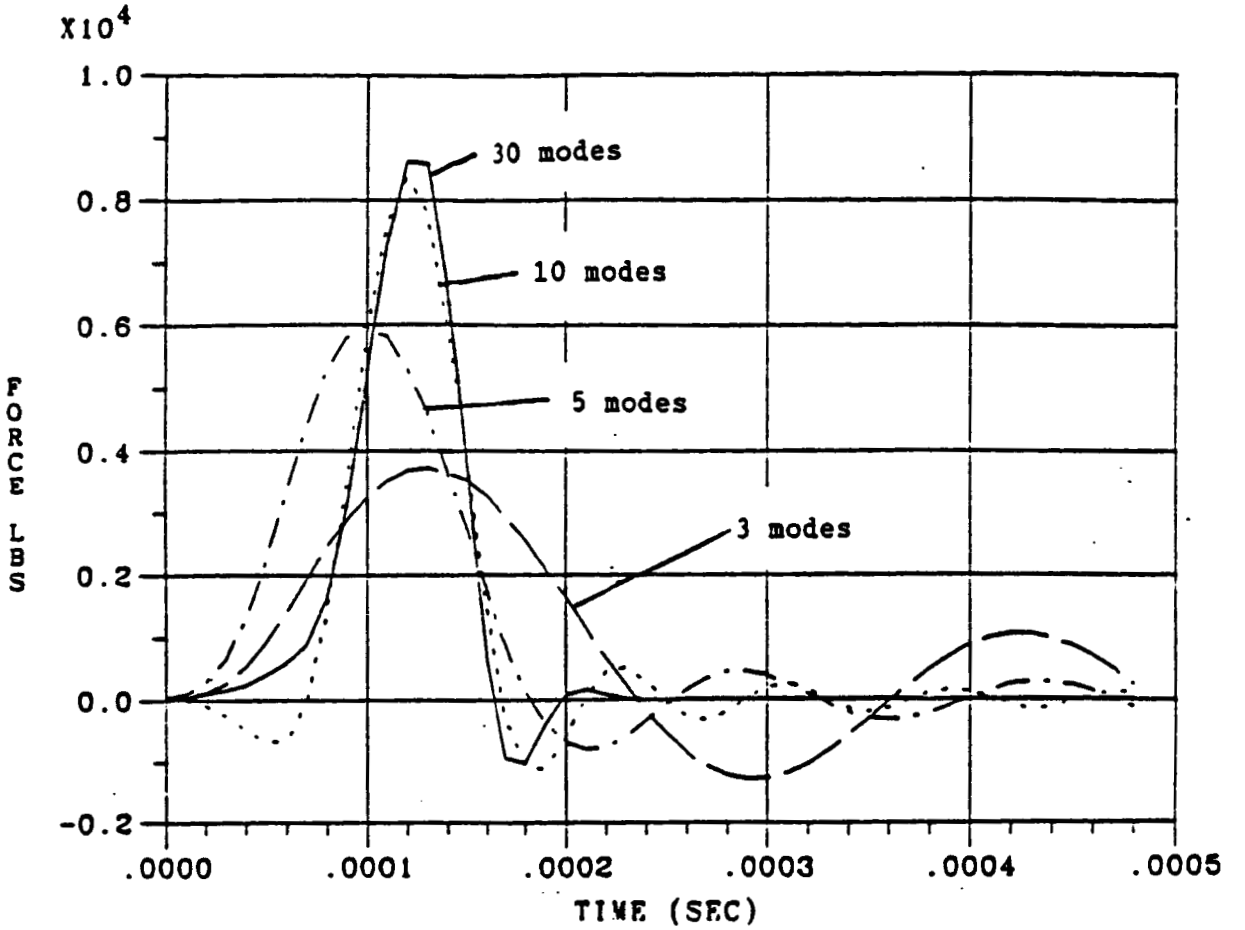

Figure 6.46 Theoretical force vs. time, Hopkinson bar, 10,000 pound, 100 μs pulse, including 3, 5, 10, and 30 modes.

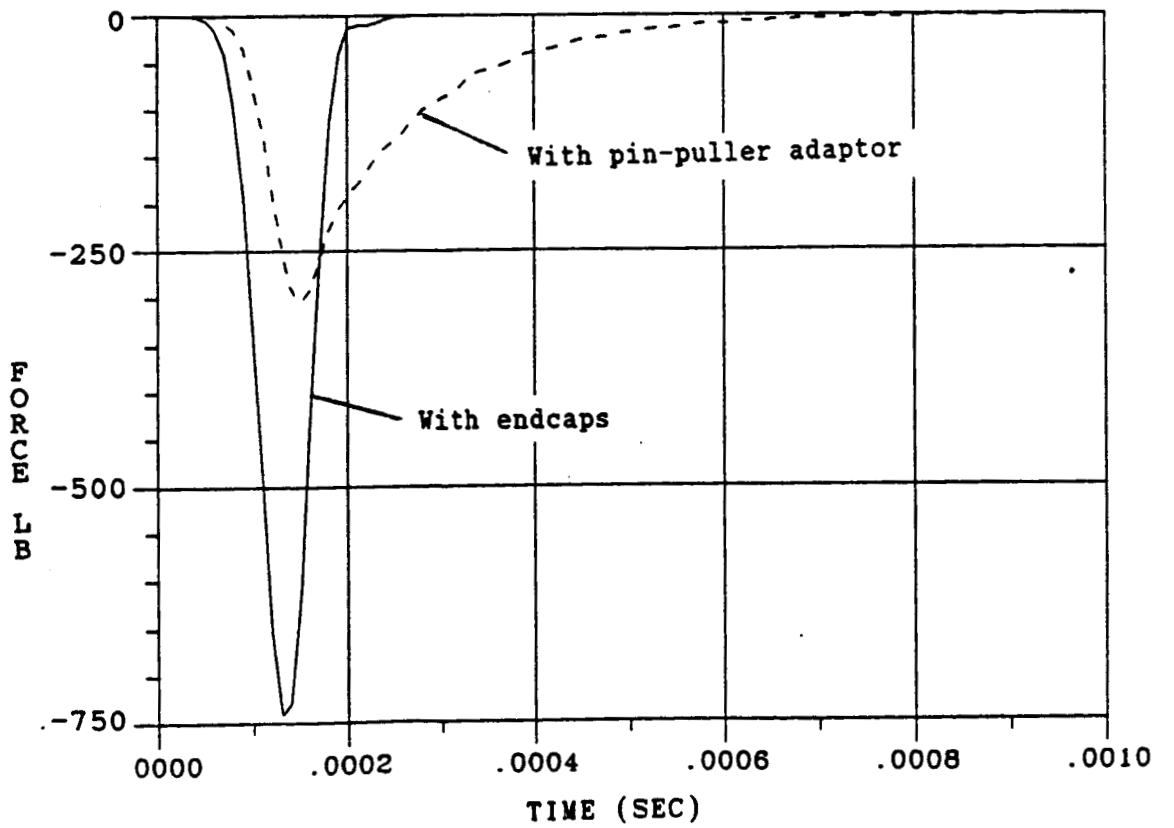

Figure 6.47 Theoretical Hopkinson bar force, with pin-puller adaptor and end-caps

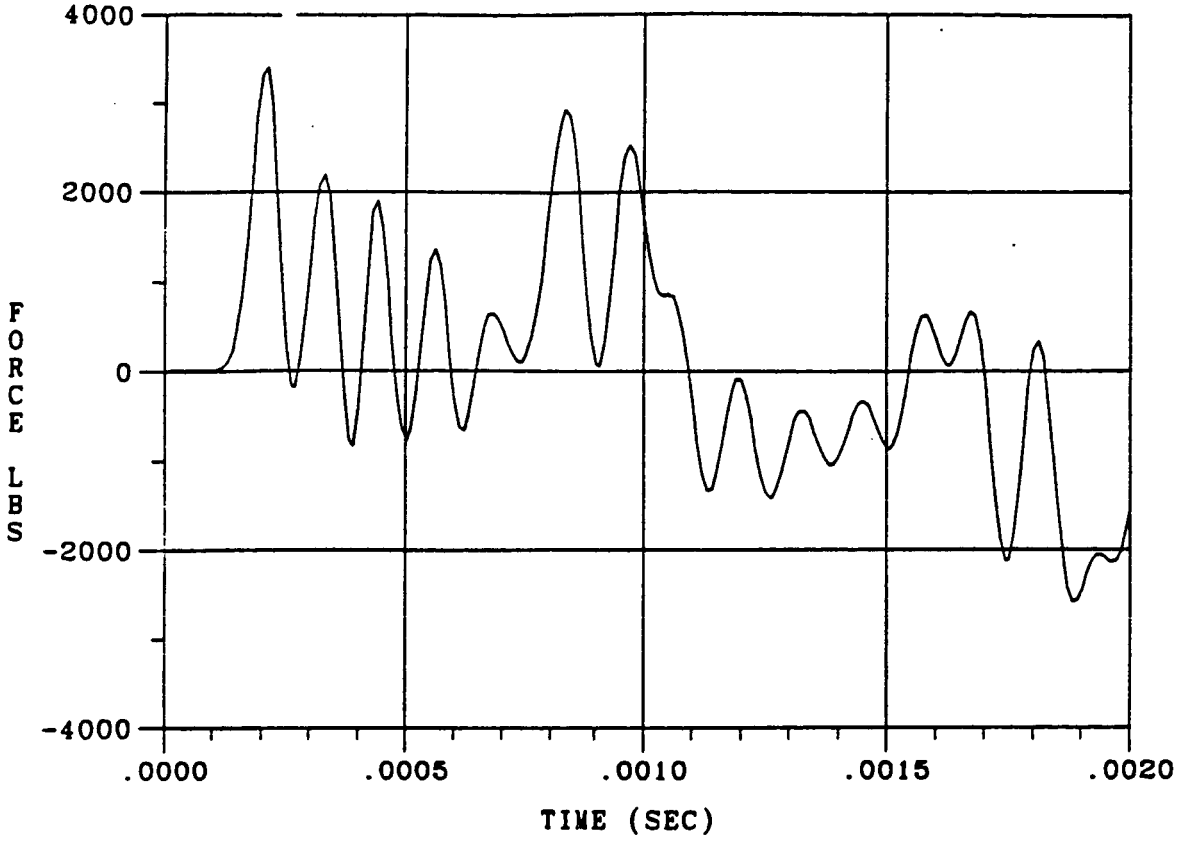

Figure 6.48 Theoretical Hopkinson bar force, tapered plate adaptor, 1/2 inch grid, 100 μs impulse.

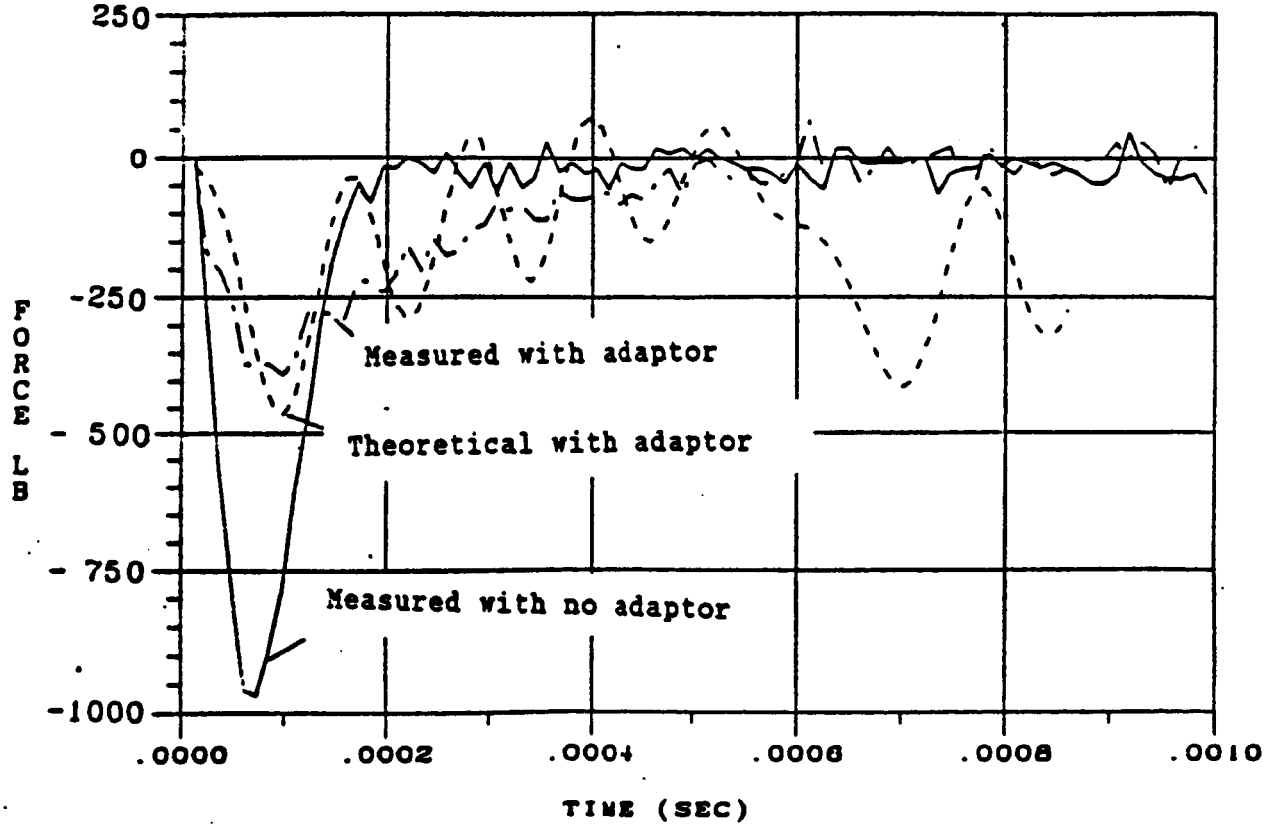

Figure 6.49 Force vs. time, Hopkinson bar with separation joint, tapered plate adaptor.

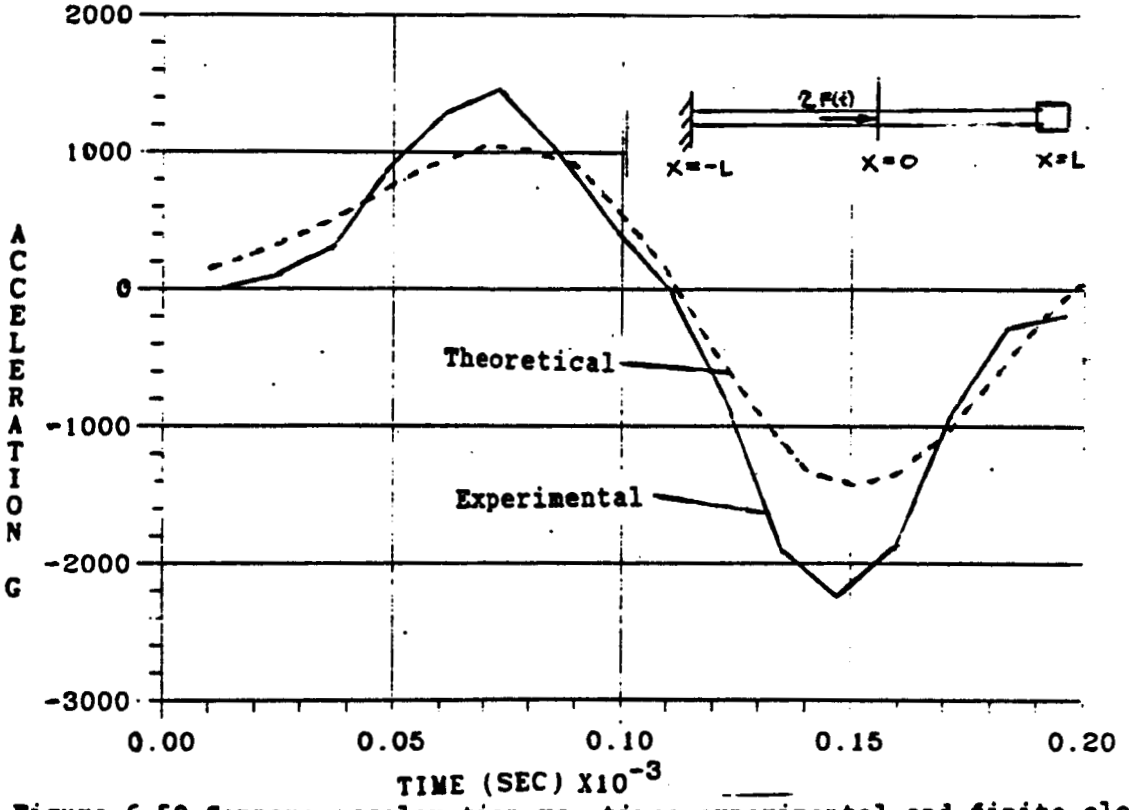

Figure 6.50 Compare acceleration vs. time: experimental and finite element solution at x=L, with endcap.

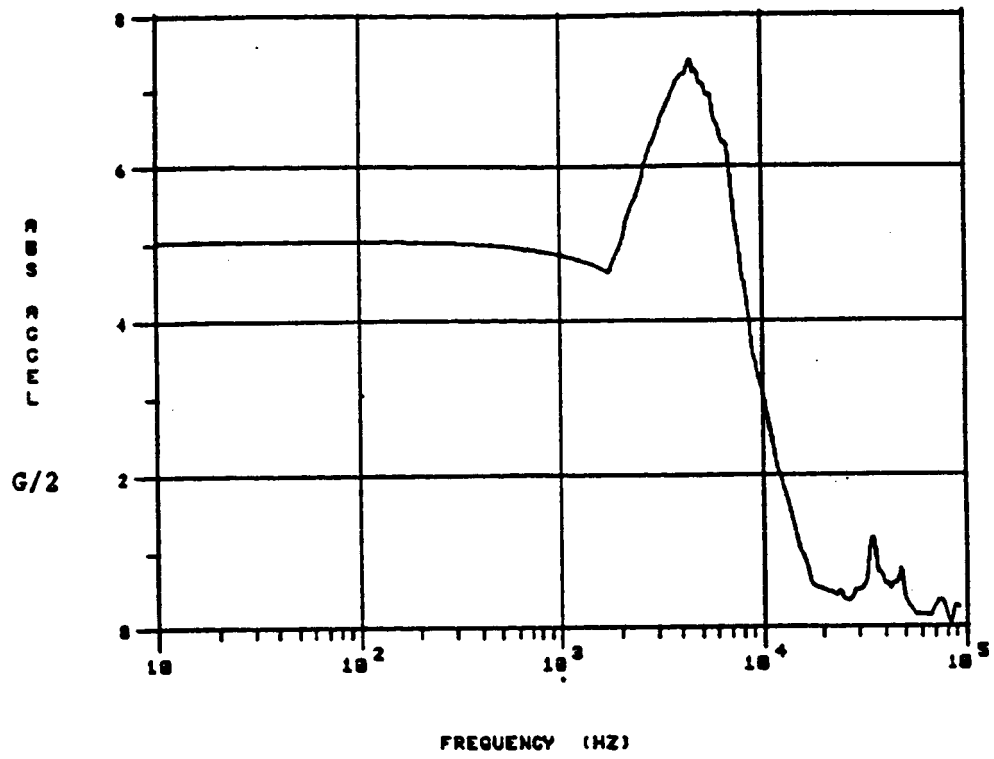

Figure 6.51 Shock spectrum from force, spherical impactor, cap on input end.

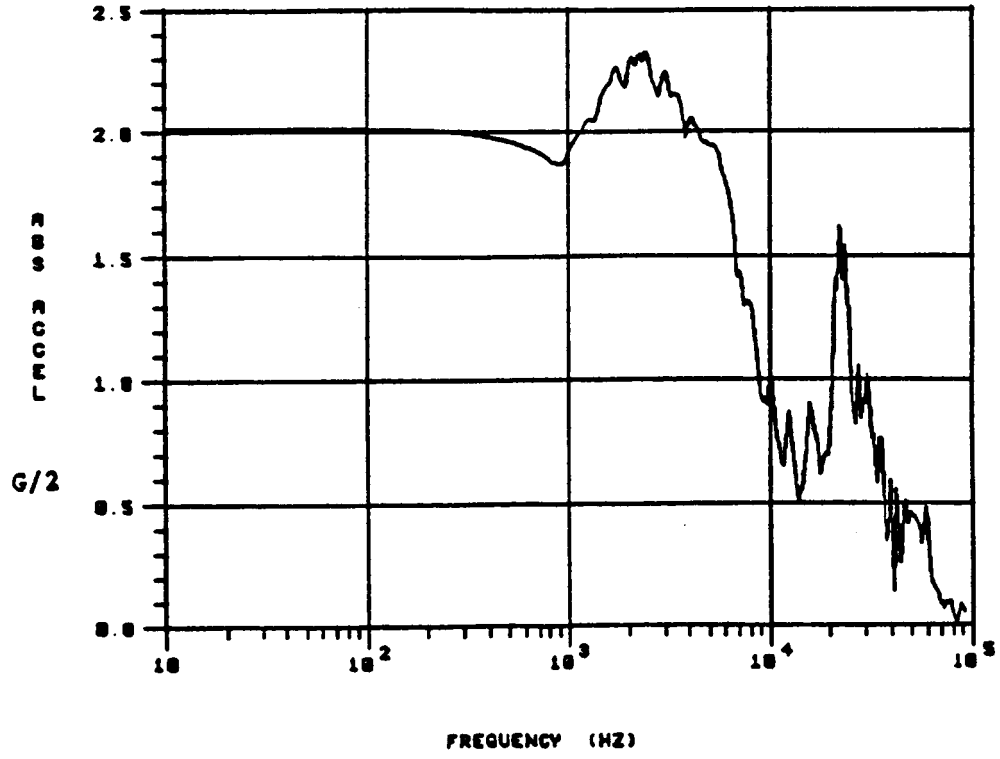

Figure 6.52 Shock spectrum from force, spherical impactor, separation joint tapered plate adaptor on input end.

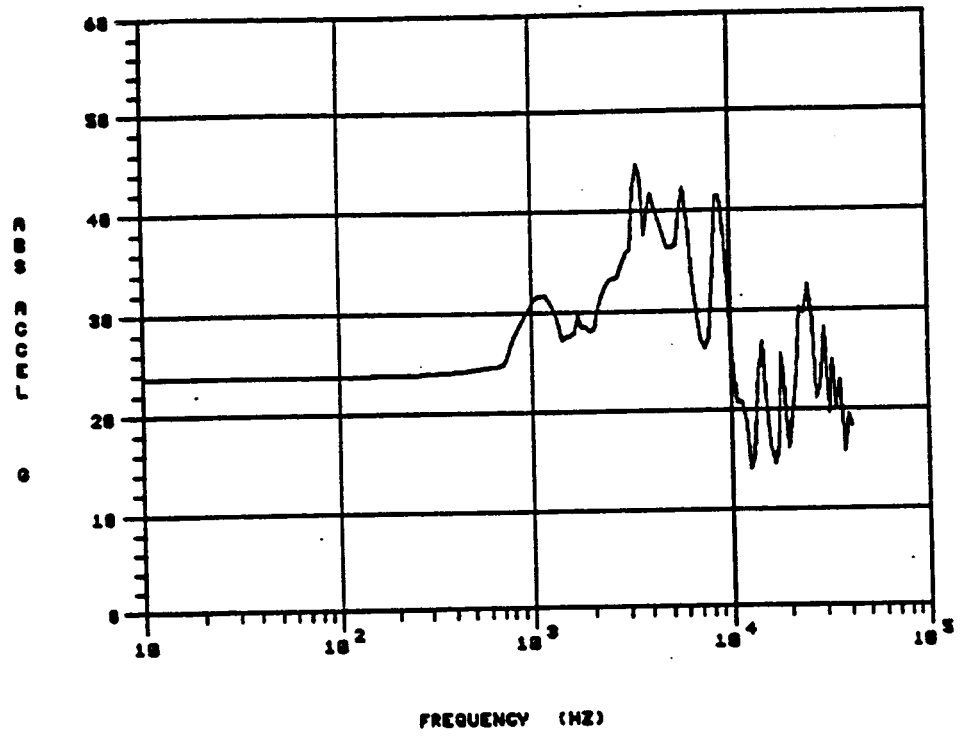

Figure 6.53 Shock spectrum from force, separation joint test 17.

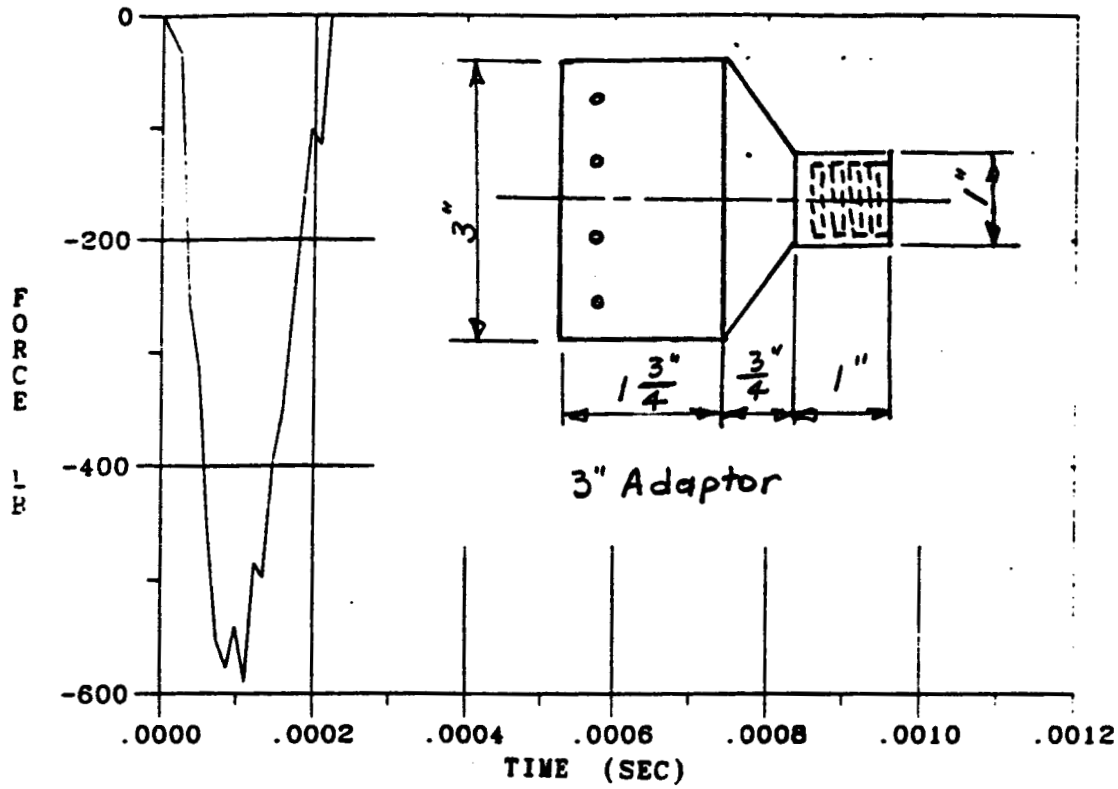

Figure 6.54 Experimental force vs. time, Hopkinson bar, spherical impactor, 15" pull-back, 3" separation joint adaptor (in inset).

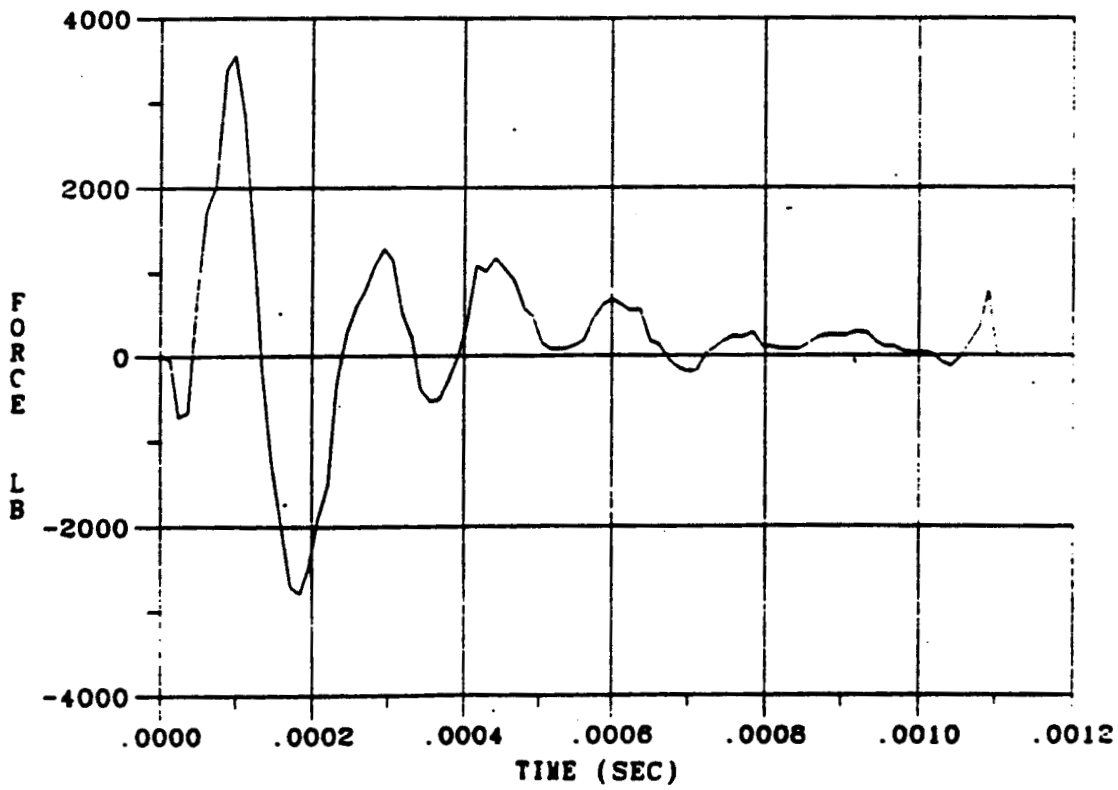

Figure 6.55 Experimental force vs. time, Hopkinson bar, 3" long separation joint with 7 grains/ft off-center.